

THE UNIVERSITY OF OKLAHOMA
GRADUATE COLLEGE

EFFECTS OF POLYMER CONCENTRATION ON THE OPTIMAL SALINITY OF
MICROEMULSIONS

A THESIS
SUBMITTED TO THE GRADUATE FACULTY
in partial fulfillment of the requirements for the
Degree of
MASTER OF SCIENCE

By
ALEXIS PENNY
Norman, Oklahoma
2020

EFFECTS OF POLYMER CONCENTRATION ON THE OPTIMAL SALINITY OF
MICROEMULSIONS

A THESIS APPROVED FOR THE
SCHOOL OF CHEMICAL, BIOLOGICAL AND MATERIALS ENGINEERING

BY THE COMMITTEE CONSISTING OF

Dr. Jeffrey Harwell, Chair

Dr. Ben Shiau

Dr. Paul Huang

© Copyright by ALEXIS PENNY 2020

All Rights Reserved.

TABLE OF CONTENTS

Table of Contents	iv
Acknowledgements	v
Abstract	vi
Chapter 1. Introduction	1
1.1. Introduction to Surfactants	1
1.2 Polymer-Surfactant Combinations	3
1.3 Study Goals and Future Efforts	5
Chapter 2. System Characterization and Determination of S*	7
2.1. Introduction	7
2.2. Materials and Methods	8
2.3. Results and Discussion	11
2.4. Conclusions	19
Chapter 3. Surfactant System Property Changes Due to Polymer (SP*).....	21
3.1. Introduction	21
3.2. Materials and Methods	23
3.3. Results and Discussion	23
3.4. Conclusions	28
Chapter 4. HLD-NAC Characterization	30
4.1. Introduction	30
4.2 Materials and Methods	31
4.3. Results and Discussion	32
4.4. Conclusions	41
Chapter 5. Conclusions and Future Work.....	43
5.1. Conclusions	43
5.2. Future Work	45
Appendices.....	47
Appendix A: Plots Determining f(P) Function for HLD Equation.....	47
Appendix B: Sample DLS Graphs (PD = Polydispersity, CR = Count Rate (kcp)).....	50
B.1. SDHS Reference Systems	50
B.2. SDHS & PDADMAC Systems	61
B.3. C ₈₋₁₀ E3.5 Reference Systems.....	95
Appendix C: DLS Sample Examples	107
References.....	108

Acknowledgements

Thank you to Dr. Jeffrey Harwell for support and help during my pursuit of a graduate degree and during a very chaotic time for the world. Thank you for pushing me and always being flexible when things didn't go as expected.

Thank you to graduate student Michael Warren for constant patience, guidance, and friendship. I am very grateful to have worked beside you.

Thank you to committee member Dr. Paul Huang for providing me with various opportunities and being a friend the past two years. I appreciate your encouragement and consistent willingness to help. Thank you to committee member Ben Shiau as well for support and flexibility towards my work.

Lastly, thank you to my family and friends for their time and support for me even when their lives were busy and stressful. Specifically, I'd like to thank Mason Klovenski "for always (sometimes) listening to me complain and providing your thoughts and help" (Klovenski, 2020).

Abstract

In this work, multiple water-soluble polymer-surfactant systems were characterized utilizing the hydrophilic lipophilic deviation (HLD) and net average curvature (HLD-NAC) concepts. Water-soluble polymers utilized in this work include polydiallyldimethylammonium chloride (PDADMAC), hydroxypropyl cellulose (HPC), and polyvinyl alcohol (PVA). Although surfactant systems are extremely dynamic, this work aims to provide further understanding of the effects caused by the addition of water-soluble polymers to the optimal salinity of Winsor III microemulsions.

The optimal salinity for each system with differing concentrations of polymer was determined using coalescence rate and interfacial tension measurements. HLD characterization values, K and C_c , were analyzed for each polymer-surfactant system to provide insight to how the polymer was interacting within each system. PDADMAC and HPC were found to induce hydrophobic shifts in the optimal salinity of reference surfactant systems, while PVA induced hydrophilic shifts. Functions, $f(P)$, corresponding to the HLD equation were found for each polymer-surfactant combination, allowing for the determination of the polymer-surfactant optimal salinity utilizing reference surfactant K and C_c values.

Changes in solution viscosity and solubilization abilities due to the addition of polymer were examined and compared with predictions from previous works based on expected charge interactions. In this study, viscosity noticeably increased only with the addition of PVA, and solubilization decreased with the addition of all polymers.

Emulsion droplet radii were found through dynamic light scattering experiments and compared to emulsion droplet radii predictions provided by the NAC model. NAC was then used to examine the hydrophilic surfactant head group area present within system middle phases.

Chapter 1. Introduction

1.1. Introduction to Surfactants

Surfactants, or surface-active agents, are organic chemicals consisting of both hydrophilic and hydrophobic groups. Surfactants are used to alter the wettability, solubilization, and emulsification properties of solution interfaces (Tadros, 2014). They are a key component in the formulation of most chemical products such as dyestuffs, paints, paper coatings, agrochemicals, pharmaceuticals, ceramics, consumer products, personal care products, etc.

Surfactants adsorb onto system surfaces or interfaces and alter the free energy resulting in changes in properties at these surfaces or interfaces. Interfacial free energy per unit area, or surface/interfacial tension (γ), can be defined as the amount of work required to expand the phase boundary (Tadros, 2014). Adsorption of surfactant molecules at the interface lowers the surface tension (γ_{AL} at the air/liquid interface or γ_{SL} at the solid/liquid interface) or interfacial tension (γ_{OW} at the oil/water interface). The more surfactant adsorbed, the lower the γ . Surfactants normally display a gradual reduction in γ until the critical micelle concentration is reached where γ will then remain constant.

Surfactants can be classified based on the charge or lack of charge of the hydrophilic portion. A surfactant may be categorized as anion, cationic, amphoteric, or nonionic as shown in Figure 1. Anionic surfactants are what is most widely used in industry, especially in detergents, due to their relatively low cost. The most common hydrophilic groups used are carboxylates, sulfates, sulfonates, and phosphates. The general formulas for these common anionic surfactants are displayed below where n is a value between 8-16 and X^+ is usually Na^+ .

Carboxylates: $C_nH_{2n+1}COO^-X^+$

Sulfates: $C_nH_{2n+1}OSO_3^-X^+$

Sulfonates: $C_nH_{2n+1}SO_3^- X^+$

Phosphates: $C_nH_{2n+1}OPO(OH)O^- X^+$

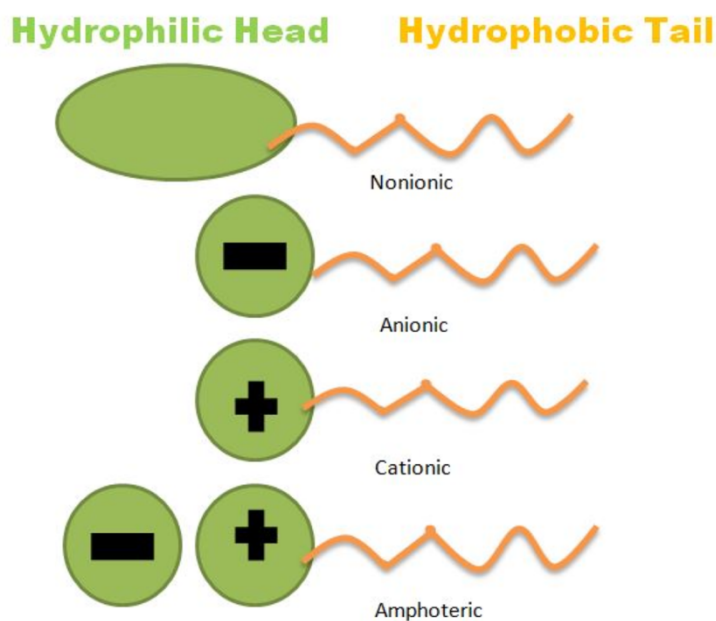
Cationic surfactants are generally incompatible with anionic surfactants but are compatible with nonionic surfactants. Cationic surfactants are used when there is a negatively charged surface present and are commonly used in anticorrosive agents for steel, flotation collectors for mineral ores, dispersants for inorganic pigments, antistatic agents, anticaking agents, and hair conditioners. Cationic surfactants also exhibit antimicrobial activity. The most common cationic surfactants consist of quaternary amines with at least one long alkyl group accompanied by a chloride ion.

Amphoteric surfactants have both positively and negatively charged groups. In acid solutions, the surfactant will behave as a cationic surfactant, while in alkaline solutions, the surfactant will behave as an anionic surfactant. They are compatible with other surfactants and soluble in water where the minimum solubility occurs at the isoelectric point. They cause little eye and skin irritations and are therefore often used in shampoos and cosmetics.

Nonionic surfactants are the second most commonly used class of surfactants (Ilenado and Neubecker, 1983). They have no charge on the headgroup and are generally nontoxic and biodegradable. They combine well with other types of surfactants and are not usually used as a single compound due to their inability to properly stabilize the air system they create (Gelardi et al., 2016). Nonionic surfactants are available at relatively low cost and are effective in wetting and spreading and commonly used in emulsifiers, foaming agents, and personal care products. The most widely used nonionic surfactants contain a polyoxyethylene group as the hydrophile, but these molecules are under increasing pressure because of the possible presence as an unwanted byproduct of a known carcinogen, dioxin, at trace levels.

Another class of surfactants classified as extended surfactants has also been of study during recent years. Extended surfactants contain intermediate polarity molecules, such as polyethylene and/or polypropylene oxide groups (EOs and POs, respectively), which are inserted between the hydrocarbon tail and hydrophilic head (Witthayapanyanon et al., 2008). Extended surfactants have a tail group that extends into the oil phase further than other surfactants while maintaining water solubility which allows for a smoother transition from the oil to the water phase (Salager et al., 2005). Uses for extended surfactants vary because of their ability to provide ultra-low interfacial tensions and solubilize bulky oil molecules. Applications widely vary from aqueous based solvent extraction, drug delivery, to bioremediation.

Figure 1: Surfactant depictions (Shapiro, 2018)



1.2 Polymer-Surfactant Combinations

Polymers are widely used in colloidal systems. When combined, polymer-surfactant combinations can significantly modify solution properties and can offer some tunability for

specific purposes such as viscosity enhancement, solubilization abilities, micro emulsion drop size, and phase behavior characteristics (Goddard et al.,1998). Polymer-surfactant combinations offer applications in a wide variety of industries such as in pharmaceutical formulations, personal care products, food products, detergents, paints and coatings, oil drilling, and enhanced oil recovery fluids (Goddard et al.,1998).

Different types of polymers can cause differing effects to a surfactant mixture. For example, polymers of low molecular weight ($5E^3 - 50E^3$), such as synthetic polymers, can be used as stabilizers (Goodwin, 2009). This occurs through the adsorption of part of the polymer to particles at the interface. The portion of the polymer left unattached to the interface can then expand away from the interface preventing other particles from close approach.

Polymers of higher molecular weight ($< 10^6$) can be used as thickeners or rheology modifiers (Goodwin, 2009). When a soluble polymer is added as a rheology modifier to a colloidal dispersion, a synergistic effect is often observed (Goodwin, 2009). A relatively great increase in viscosity of the dispersion is observed compared to the polymer solution by itself. When a polymer which does not adsorb to the dispersed phase is present, there is a weak, reversible aggregation of the disperse phase which is seen through a change in rheological behavior. However, when polymers of a molecular weight $>10^6$ are used, rheological problems can occur. For example, droplets may not break away from the bulk cleanly.

Polymers with charged groups can also be of use and are referred to as polyelectrolytes. They can be used as stabilizing agents or to induce aggregation depending on their charge.

This work will focus on water soluble polymers, which can be classified as either natural or synthetic. Water-soluble polymers dissolve, disperse, or swell in water and, thus, modify the physical properties of aqueous systems in the form of gelation, thickening or

emulsification/stabilization (Kadajji & Betageri, 2011). These polymers usually have repeating units or blocks of units; the polymer chains contain hydrophilic groups that are substituents or are incorporated into the backbone. The hydrophilic groups may be nonionic, anionic, cationic or amphoteric (Will et al., 2007). In this work, synthetic water-soluble polymers polyvinyl alcohol (PVA) and polydiallyldimethylammonium chloride (PDADMAC) are of focus. PVA is soluble in highly polar, hydrophilic solvents and is used as a stabilizer of emulsions and a viscosity increasing agent (Kadajji & Betageri, 2011). PDADMAC is a cationic polyelectrolyte with high charge density. It is well suited for flocculation and can neutralize negatively charged colloidal material. Natural polymer, hydroxypropyl cellulose (HPC), is a nonionic water-soluble polymer which is commonly used as a thickening agent and for other uses within the drug delivery industry (Kadajji & Betageri, 2011). HPC is an ether of cellulose in which some of the hydroxyl groups in the repeating glucose units have been hydroxypropylated forming $-OCH_2CH(OH)CH_3$ groups using propylene oxide.

1.3 Study Goals and Future Efforts

The goal of this work is to provide further understanding of the effects of these three different water-soluble polymers on multiple surfactant reference systems. To achieve this, phase behavior studies were conducted using the hydrophilic-lipophilic difference (HLD) concept and HLD net average curvature (NAC) concept. Using these methods and previous knowledge of polymer-surfactant interactions, each system was analyzed in order to distinguish possible reasons why the interactions between polymer and surfactant occurred.

Future efforts should include more in-depth analysis of the cause for some of the trends seen. Rheology should also be studied quantitatively, and a broader range of polymer

concentrations should be examined. These findings could then be applied to specific industries to accommodate needs such as HLD value, viscosity, solubility, or emulsion drop size.

Chapter 2. System Characterization and Determination of S*

2.1. Introduction

The systems studied in this paper include an anionic surfactant and a nonionic surfactant paired with a nonionic polymer and a cationic polyelectrolyte each separately and another extended anionic surfactant paired with a nonionic surfactant. To begin studying the effects of the polymers on the surfactant systems, phase behavior analysis using the hydrophilic-lipophilic difference (HLD) must be conducted.

HLD is an empirical, thermodynamic model that describes the amphiphilic behavior of surfactants and other active solutes on the interface within biphasic systems (Warren, 2020). The HLD relation, displayed as Equation 1 and 2, was first developed by Salager and later extended by Acosta to describe microemulsions and the phase inversion point:

$$(1) \quad HLD_{Ionic\ Surfactant} = \ln(S) + f(A) - \alpha_T(\Delta T) - K(EACN) + Cc$$

$$(2) \quad HLD_{NonIonic\ Surfactant} = b(S) + f(A) - c_T(\Delta T) - K(EACN) + Cc$$

where S is the aqueous phase salinity (g NaCl/100 mL), f(A) is a function of alcohol or cosolvent concentration, a_T and c_T are the surfactant temperature coefficients, ΔT is the temperature difference from 25°C, K and EACN reflect the lipophilic interactions between the hydrophobic tail of the surfactant and the oil, and Cc is the characteristic curvature. a_T and c_T are typically $\sim 0.01\text{ K}^{-1}$ for most surfactants (Broze, 1999; Hammond and Acosta, 2011; Salager et al., 1979), and K ranges from approximately 0.004 - 0.17 (Acosta et al., 2008; Hammond and Acosta, 2011; Salager et al., 1979; Velásquez et al., 2009; Witthayapanyanon et al., 2008). EACN is determined by the hydrophobicity of the oil in use. For alkanes, the EACN is equal to the number of carbon atoms present in the molecule. The Cc value describes the degree to which a surfactant is more hydrophilic or hydrophobic. A negative Cc value corresponds to a hydrophilic surfactant while a

positive C_c value corresponds to a hydrophobic surfactant. Acosta coined the term Characteristic Curvature, C_c , to describe the surfactant's tendency to cause the interface to curve away from the aqueous phase (hydrophilic surfactant) or away from the oil phase (hydrophobic surfactant) in order to maximize the interaction with the preferred phase.

The value of HLD describes the deviation of a formulation from optimum conditions. By definition, $HLD = 0$ for a Winsor Type III microemulsion with equal volumes of oil and water in the middle phase. A negative HLD value corresponds to a Winsor Type I microemulsion while a positive HLD value corresponds to a Winsor Type II microemulsion. A Winsor Type I microemulsion consists of oil solubilized in normal micelles in the water phase, while a Winsor Type II microemulsion consists of surfactant-solubilized water in reverse micelles in the oil phase. A Winsor Type III microemulsion consists of water, oil, and surfactant all in equilibrium with each other. The phase inversion point occurs when HLD transitions from negative to positive. In characterizing a microemulsion, it is generally assumed that all the surfactant is present in the middle phase, along with some oil and some water. For an optimum Winsor III microemulsion, the volume of oil equals the volume of water in the middle phase.

Optimum conditions are said to occur at Winsor Type III microemulsion with an HLD value of zero where S is defined as the optimal salinity, or S^* . At these conditions, the minimum interfacial tension (IFT) and coalescence rate occurs, and the solubilization capacity (SP) is at a maximum for a given system.

2.2. Materials and Methods

Materials

Three reference surfactants were utilized in this study. The anionic surfactants used, extended C₁₂₋₁₃ alkyl ethoxy sulfate Isalchem 123-2 (508.56gmol⁻¹/ 70.18%) and SDHS MM80 (388gmol⁻¹/80%), were received from Sasol North America and Croda, respectively. Nonionic surfactant, C₈₋₁₀E3.5 (molecular weight 334 gmol⁻¹/100%) was purchased from Sasol North America. Water soluble polymers, poly(diallyldimethylammonium) chloride (PDADMAC) (molecular weight 80,000 g mol⁻¹), Hydroxypropyl cellulose (HPC) (molecular weight 100,000 g mol⁻¹), and polyvinyl alcohol (PVA) (molecular weight 90,000 g mol⁻¹) were purchased from VHR and Sigma Aldrich. For phase behavior experiments, sodium chloride (99%) purchased from Sigma Aldrich was added to deionized filtered water. Linear alkanes, hexane (98%, EACN=6), heptane (98%, EACN=7), and octane (99%, EACN=8) were purchased from VWR. Before utilizing HPC in phase behavior studies, existing water was removed by placing the HPC powder in the oven at 50°C for 30 minutes. All materials were used without further purification. The chemical structures of the surfactants and polymers are presented below.

Table 1: Surfactant Structures

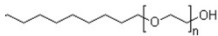
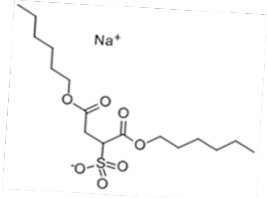
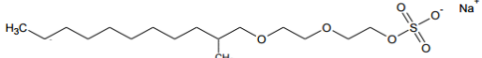
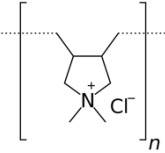
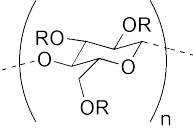
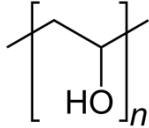
Surfactant Structures			
	C ₈₋₁₀ E3.5	SDHS	C ₁₂₋₁₃ Alkyl Ethoxy Sulfate
Molecular structure			
	C ₈ H ₁₇ -(EO)-OH	NaC ₁₂ H ₂₅ -(EO) ₂ -SO ₄	C ₁₂ H ₂₆ -(EO) ₂ -SO ₄ Na

Table 2: Polymer Structures

Polymer Structures			
	PDADMAC	HPC	PVA
Molecular structure		 R = H or CH ₂ CH(OH)CH ₃	
	(C ₈ H ₁₆ NCl) _n	C ₃₆ H ₇₀ O ₁₉	(C ₂ H ₄ O) _n

Phase Behavior Studies

Phase behavior studies were conducted for each surfactant polymer combination with each of the three oils at varying salinities. Studies were performed in 15 mL flat-bottom vials with Teflon-lined caps. Vials contained consistent amounts of surfactant in 5 mL aqueous phase and 5 mL of the studied oil, thus, the ratio of aqueous solution to oil remained unity. Vials were mixed routinely by hand and formulation coalescence rates were recorded at 25°C. Coalescence rates were then modeled using an Akima spline interpolation method which determined the optimal salinity (S*) (Warren, 2020). The Akima spline model was chosen because it underestimates the least among all other interpolation models and was seen to produce the most natural results. Seemingly accurate data was obtained; however, the model is not perfect, and, in few cases raw coalescence data was used to determine S* instead of using the spline approximation. S* was said to be the formulation with the fastest coalescence rate.

Interfacial Tension Measurements

The oil-water interfacial tension (IFT) was measured using a spinning drop tensiometer (M6500 Grace Instrument, Houston, Texas) in order to confirm that coalescence rate measurements provided the correct S^* . The salinity of the formulation with the lowest IFT was considered S^* . Three μL of the studied oil was placed into a 300 μL capillary tube containing studied aqueous solution. All IFT tests were repeated five times by recording the diameter of the oil droplet and the rotational velocity (rpm) at 25°C. The formula for calculating the interfacial tension is presented below

$$(3) \quad \gamma = 1.45 * 10^{-7} \Delta\rho D^3 \omega^2$$

where γ is the interfacial tension (mN m^{-1}), $\Delta\rho$ is the difference between the water and oil phase densities (g cm^{-3}), D is the oil droplet diameter (mm), and ω is the rotational velocity (rpm).

2.3. Results and Discussion

*Determination and Comparison of S^**

Coalescence rates as well as IFT values were recorded for C₈₋₁₀E3.5 and SDHS reference surfactant systems in order to determine S^* . It is seen in Figures 2 and 3 that both methods produced very similar results regarding the optimal salinity, therefore, coalescence rates were used, subsequently, as the primary method for selecting the optimal salinity in all other C₈₋₁₀E3.5 and SDHS surfactant systems due to the method's reproducibility and low time commitment. It is seen that S^* for SDHS reference can vary between SDHS batches, therefore, the coalescence data presented in Figure 3 is an average of two experimental sets. IFT measurements were used to determine S^* for C₁₂₋₁₃ alkyl ethoxy sulfate surfactant systems because coalescence rates were very slow for the extended surfactant and the Type III windows were very small, making the

Akima spline method difficult to use. The IFT measurements are displayed for the salinities producing Type III microemulsions for 123-2S surfactant system in Table 3.

As EACN increased, the optimal salinity increased, which was expected due to the relationship between S^* and HLD shown in Equations 1 and 2. Interfacial tension can be defined as the amount of energy required to increase interfacial area, therefore, it is reasonable to predict that as lipophilic chain length increases, interfacial tension will increase. This prediction supports the experimental data below and in previous studies where minimum IFT increased as EACN increased for all systems (Huh, 1979).

Figure 2: $C_{8-10}E3.5$ Relationship between coalescence rate and IFT values

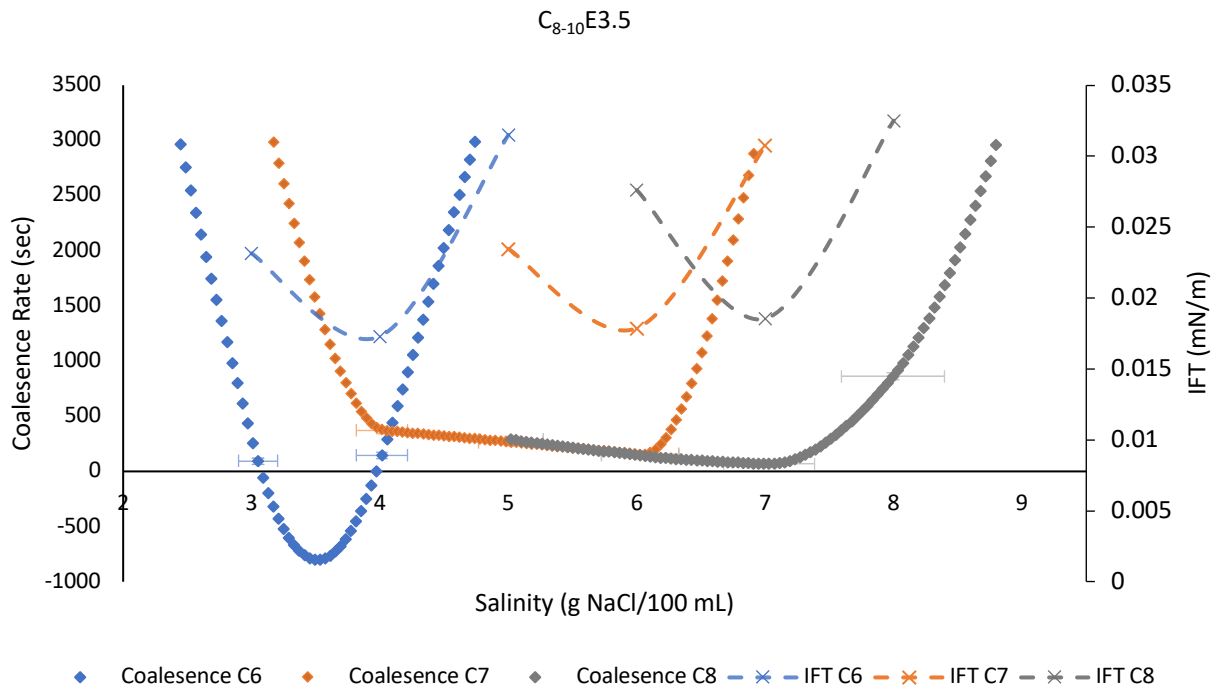


Figure 3: SDHS Relationship between coalescence rate and IFT values

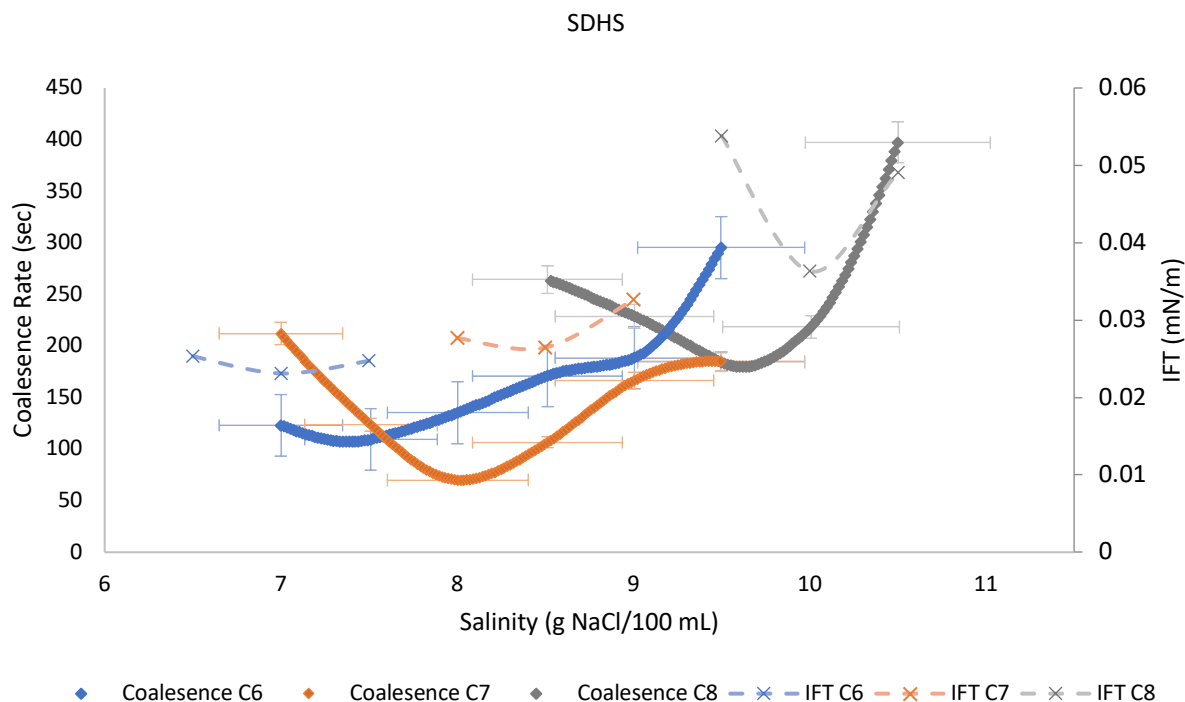


Table 3: C₁₂₋₁₃ Alkyl ethoxy sulfate IFT values

	C ₆		C ₇		C ₈	
Salinity (g NaCl/mL) ±5%	14	14.5	15.5	16	16.5	17
IFT (mNm ⁻¹)	0.0036	0.0094	0.0071	0.0066	0.0081	0.0040

K & C_c Values

K and C_c values were found by plotting a function of S* against EACN. According to Equations 1 and 2, the K value is the slope and the C_c value is the y-intercept of the linear plot. K and C_c values are displayed in Figures 4-8 for all surfactant-polymer combinations.

The K values for C₈₋₁₀E3.5 and SDHS surfactants remained relatively constant with the addition of PDADMAC while the C_c values generally increased with increasing PDADMAC

concentration, indicating a hydrophobic shift. Although PDADMAC is a hydrophilic polymer, the hydrophobic shift is thought to be due to the polymer acting as a salt, as the polymer is a polycation. As a cation, the van't Hoff factor is greater than 1, meaning that the polymer dissociated in solution. It was seen that the PDADMAC eventually stopped shifting S^* of the surfactant solutions at the highest concentration used. This is speculated to be due to the polymer falling out of the linear structure and no longer interacting with the surfactant as more polymer was added. At high polymer concentrations, it is not unusual for a polymer to self-associate or complex with surfactant and become ineffective in shifting the salinity of the formulations at a given temperature. The aqueous phase in Type I emulsions became cloudy as polymer concentration was increased, further justifying the conclusion of complexation.

Figure 4: Relationship between $C_{8-10}E3.5$ & PDADMAC K and C_c values

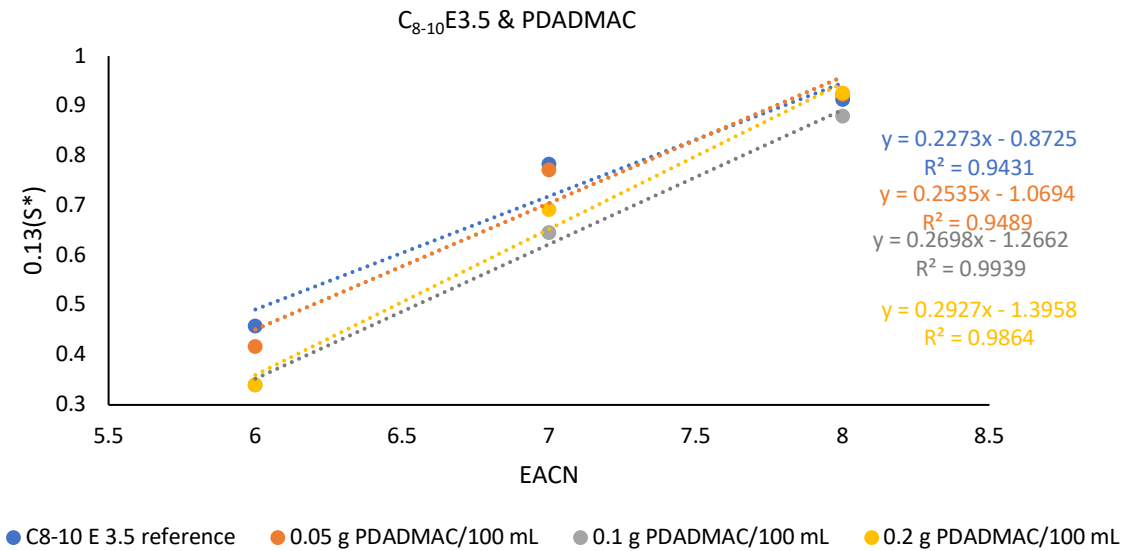
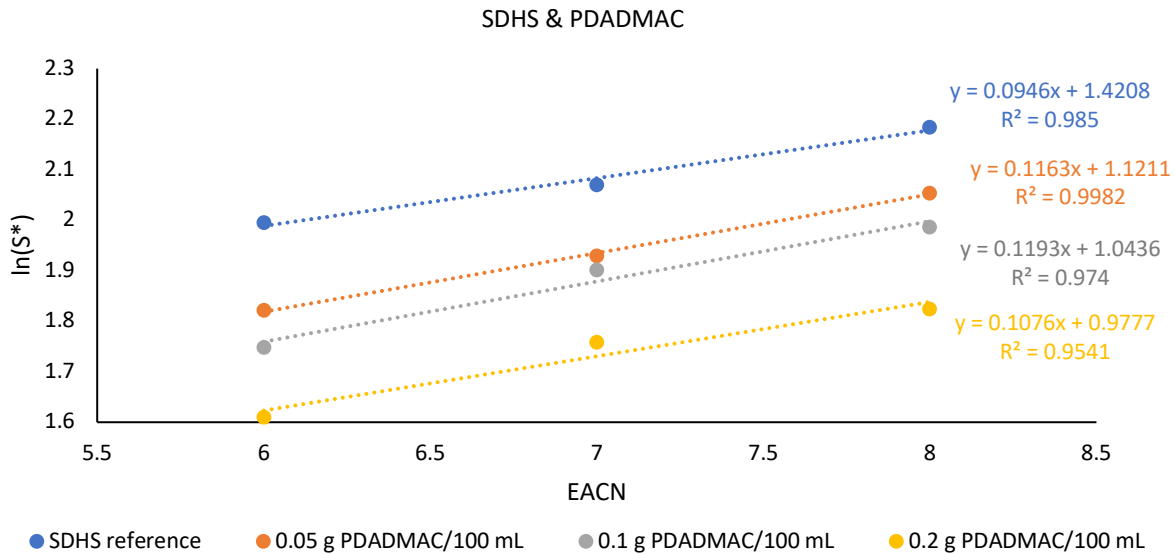


Figure 5: Relationship between SDHS & PDADMAC K and C_c values



The K values remained relatively constant for C₈₋₁₀E3.5, while K values for SDHS increased with the addition of HPC. The C_c values increased for both surfactant systems. Regardless, as HPC concentration was increased, the formulations became more hydrophobic until the highest HPC concentration was reached where formulation S* remained consistent. The differing trends in the K value for each system was because HPC interacted with the surfactant structures differently. HPC should have a van't Hoff factor less than 1, meaning that polymer particles associated in solution. HPC was speculated to mainly interact with the head groups of the C₈₋₁₀E3.5 system, while HPC interacted with both the head groups and the tail groups more equally in the SDHS system. Because HPC has both hydrophilic and hydrophobic groups, this result was expected because it can interact with the palisade layer more than hydrophilic PDADMAC which interacts more with only the aqueous phase. The hydrophobic effect also supports why SDHS would interact more strongly with HPC, resulting in more opportunities for hydrogen bonding.

Figure 6: Relationship between C₈₋₁₀E3.5 & HPC K and C_c values

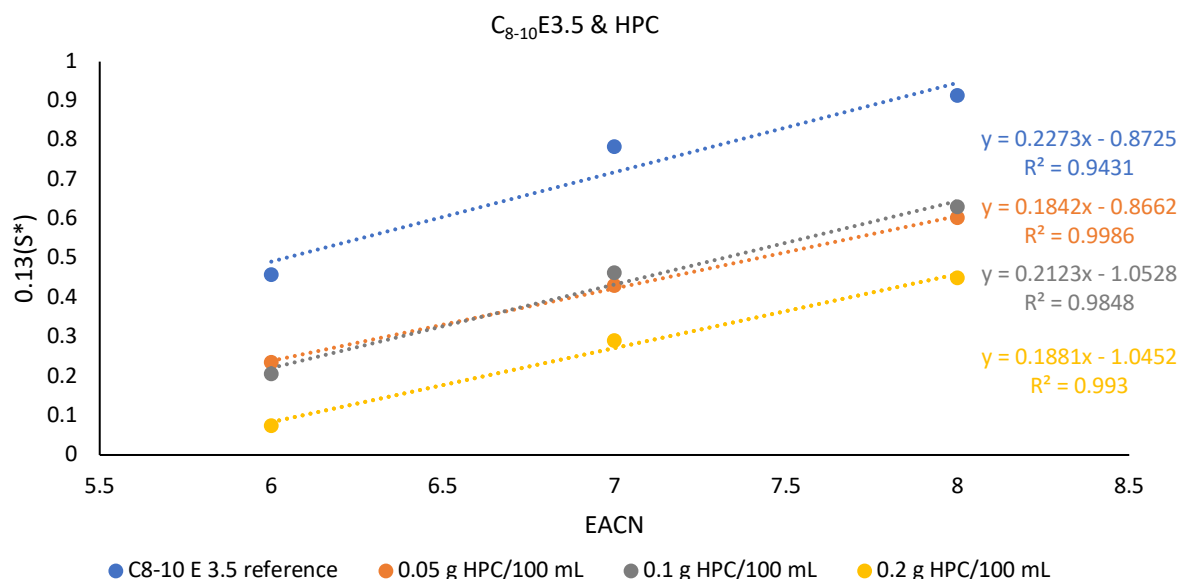
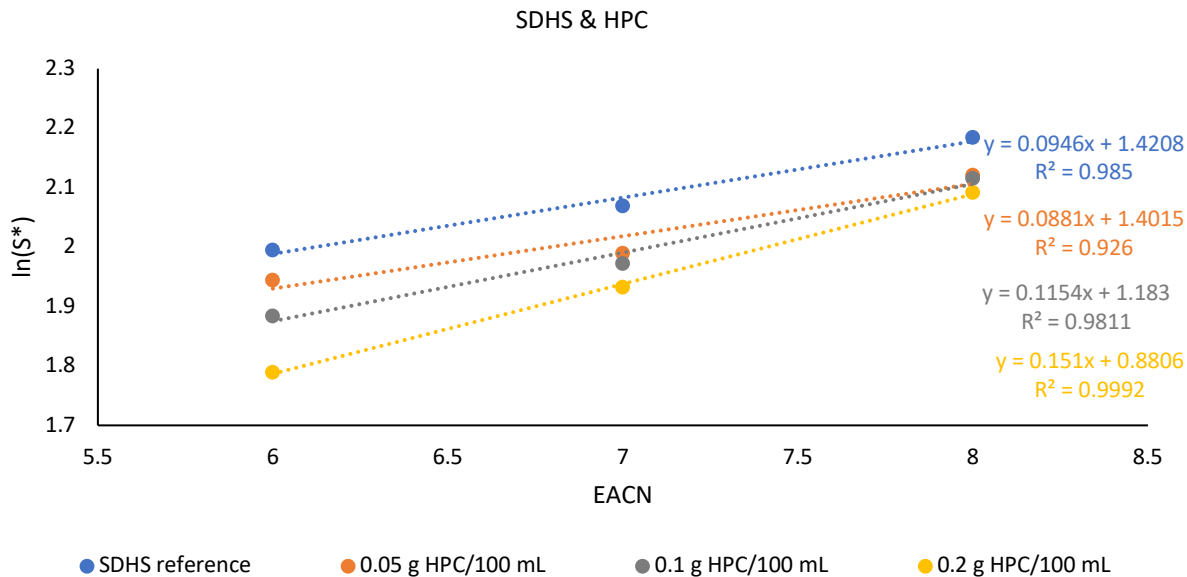


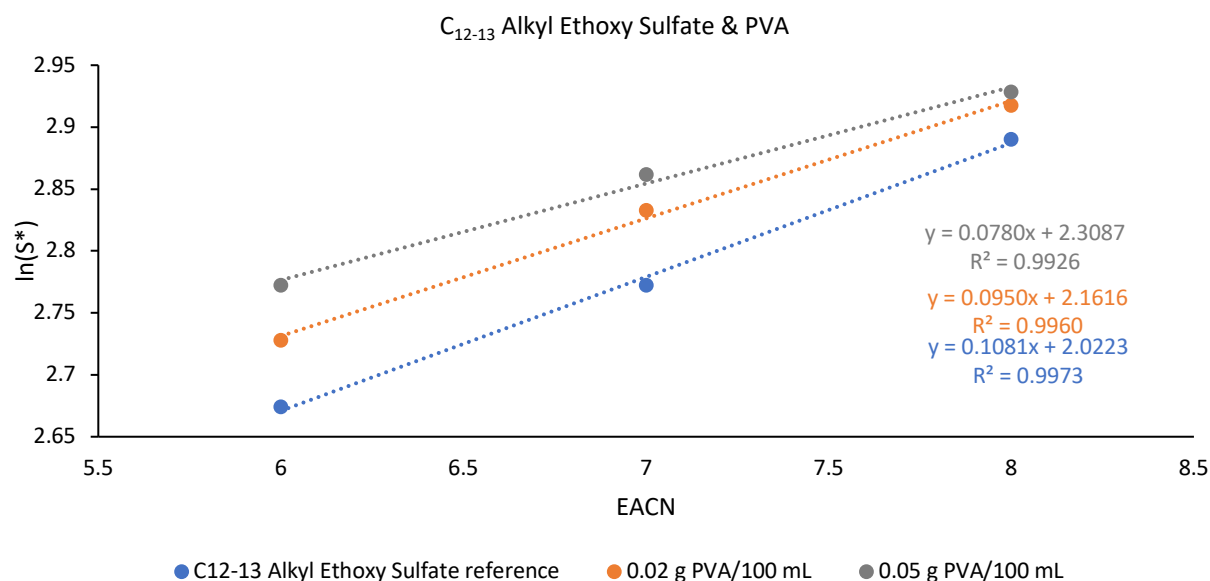
Figure 7: Relationship between SDHS & HPC K and C_c values



The K values for C₁₂₋₁₃ alkyl ethoxy sulfate extended surfactant remained relatively constant with the addition of PVA while the C_c values decreased with increasing PVA concentration indicating a hydrophilic shift due to changes in surfactant head group interactions.

It was expected that PVA would induce a hydrophilic shift in the extended surfactant formulations since PVA is considered a hydrophilic polymer. 0.1g PVA/100 mL was also tested, however the polymer seemed to no longer be effective and to phase separate due to self-association. The PVA was believed to form a water rich PVA coacervate phase. Because the polymer is relatively large and there is a limited amount of space in the palisade layer, the polymer was bound to exhibit limited solubility.

Figure 8: Relationship between C₁₂₋₁₃ alkyl ethoxy sulfate & PVA K and C_c values



Determination of f(P) Function for the Addition of Polymer

A function, $f(P)$, was found for each polymer-surfactant pair at each oil used so that one could use only the surfactant reference K and C_c values in the HLD equation to predict S* with the addition of polymer. The $f(P)$ values were found by plotting a function of the difference between S* with polymer and S* without polymer against the natural log of the polymer concentration used. The function of the difference between S* with and without polymer depended on the surfactant charge, and the log of the polymer concentration was used because it is

proportional to the polymer activity, or effective concentration. Supporting plots are displayed in Appendix A and $f(P)$ functions are presented in Tables 4-8.

The model provided relatively good estimates for S^* with the addition of polymer. Although the percent error is large in some cases and the model generally overestimates, the S^* approximation was never above ± 3 g NaCl/100 mL, allowing for simpler formulation work.

Table 4: $f(P)$ functions for the HLD equation for C₈₋₁₀E3.5 & PDADMAC

C ₈₋₁₀ E3.5 & PDADMAC						
	f(P)			% Error		
	Polymer Concentration (g/100 mL)			Polymer Concentration (g/100 mL)		
	<u>0.05</u>	<u>0.1</u>	<u>0.2</u>	<u>0.05</u>	<u>0.1</u>	<u>0.2</u>
C ₆	-1.281	-0.985	-0.688	29.886	2.683	8.641
C ₇	-1.336	-1.027	-0.718	21.118	0.473	0.360
C ₈	-0.261	-0.201	-0.140	4.800	0.898	3.239

Table 5: $f(P)$ functions for the HLD equation for SDHS & PDADMAC

SDHS & PDADMAC						
	f(P)			% Error		
	Polymer Concentration (g/100 mL)			Polymer Concentration (g/100 mL)		
	<u>0.05</u>	<u>0.1</u>	<u>0.2</u>	<u>0.05</u>	<u>0.1</u>	<u>0.2</u>
C ₆	-0.641	-0.493	-0.344	9.145	20.034	40.854
C ₇	-0.629	-0.484	-0.338	7.358	12.596	32.450
C ₈	-0.591	-0.455	-0.318	15.774	25.710	50.047

Table 6: $f(P)$ functions for the HLD equation for C₈₋₁₀E3.5 & HPC

C ₈₋₁₀ E3.5 & HPC						
	f(P)			% Error		
	Polymer Concentration (g/100 mL)			Polymer Concentration (g/100 mL)		
	<u>0.05</u>	<u>0.1</u>	<u>0.2</u>	<u>0.05</u>	<u>0.1</u>	<u>0.2</u>
C ₆	-2.671	-2.053	-1.435	52.385	6.536	266.147
C ₇	-2.346	-1.803	-1.260	10.942	18.341	113.564

C ₈	-2.541	-1.953	-1.365	3.318	4.699	63.383
----------------	--------	--------	--------	-------	-------	--------

Table 7: f(P) functions for the HLD equation for SDHS & HPC

SDHS & HPC						
	f(P)			% Error		
	Polymer Concentration (g/100 mL)			Polymer Concentration (g/100 mL)		
	<u>0.05</u>	<u>0.1</u>	<u>0.2</u>	<u>0.05</u>	<u>0.1</u>	<u>0.2</u>
C ₆	-1.184	-0.910	-0.636	11.262	1.613	12.795
C ₇	-0.422	-0.324	-0.227	3.923	7.097	12.793
C ₈	-0.161	-0.124	-0.087	13.464	14.533	17.768

Table 8: f(P) functions for the HLD equation for C₁₂₋₁₃ Alkyl ethoxy sulfate & PVA

C ₁₂₋₁₃ alkyl ethoxy sulfate & PVA				
	f(P)		% Error	
	Polymer Concentration (g/100 mL)		Polymer Concentration (g/100 mL)	
	<u>0.02</u>	<u>0.05</u>	<u>0.02</u>	<u>0.05</u>
C ₆	1.165	0.892	2.388	3.797
C ₇	0.752	0.576	1.459	5.281
C ₈	0.624	0.478	0.670	1.188

2.4. Conclusions

The measuring of coalescence rates was shown to be a valid method of determining S* based on measured IFT values. K and C_c values were found for each polymer-surfactant system to achieve a greater understanding of how the polymer interacted with each system. Even though the surfactants used may have well-known reference K and C_c values, potential batch to batch composition differences require a formulator to preform phase behavior experiments on each reference surfactant (Warren, 2020).

Differing effects were seen for the studied systems based on surfactant and polymer structures. PDADMAC was assumed to act as a cation and mostly interact with the aqueous phase

instead of the palisade layer. HPC and PVA were assumed to interact mostly with the aqueous phase as well, but also interact with the palisade layer more than PDADMAC. PVA was deemed difficult to work with because of the size of the polymer.

Functions, $f(P)$, corresponding to the HLD equation were determined for each surfactant/polymer combination using each studied oil. Utilizing the model allows for the determination of S^* with the addition of polymer using reference surfactant K and C_c values. The model is very specific to this study and requires much more work for application to other systems.

Chapter 3. Surfactant System Property Changes Due to Polymer (SP*)

3.1. Introduction

The effects on viscosity and solubilization abilities seen by adding polymers to surfactant solutions is dependent on the structures involved and the nature of the interaction forces between the surfactant, polymer, and solvent in use.

First, it is possible that weak or no polymer-surfactant association occurs and is displayed in Figure 9. This situation could happen if both the polymer and surfactant carry the same type of ionic charge, if the polymer is relatively rigid and for steric reasons does not interact with ionic or nonionic surfactants, or if the polymer and the surfactant are uncharged and no attractive interactions exist between them (Nagarajan, 2001). It has also been concluded that interactions between nonionic surfactants and polymers are usually relatively weak (Lindman et al., 2018).

Strong interactions between polymer and surfactant have been found to occur within the combination of a nonionic polymer with an ionic surfactant and a polyelectrolyte with an oppositely charged surfactant (Lindman et al., 2018). Anionic surfactants usually have a strong interaction with nonionic hydrophilic polymers while cationic surfactants do not. These systems are explained in depth by Goddard's two-part review (2018).

Figure 10 displays a system where the polymer and surfactant have opposite attracting electrical charges and single surfactant molecules are bound linearly along the length of the polymer molecules. This situation causes the creation of complexes with reduced charge and reduced hydrophilicity leading to the precipitation of these complexes from solution (Nagarajan, 2001).

Relations shown in Figure 11 occur in systems containing surfactant and polymer possessing opposite charges where a single surfactant molecule binds at multiple sites on a single

polymer molecule or to more than one polymer resulting in intramolecular bridging (Nagarajan, 2001).

Figure 9:

No polymer-surfactant association

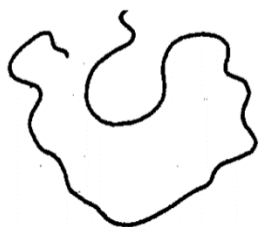


Figure 10:

Polymer and surfactant with opposite attracting electrical charges, single surfactant molecules are bound linearly along the length of the polymer molecules

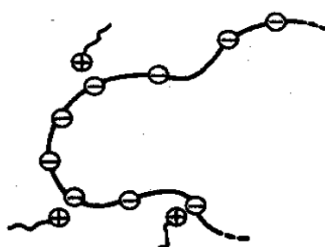
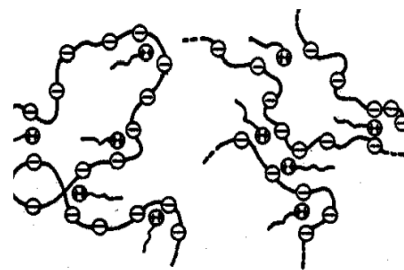


Figure 11:

Polymer and surfactant have opposite charges, a single surfactant molecule binds at multiple sites on a single polymer molecule or to more than one polymer resulting in intramolecular bridging



(Nagarajan, 2001)

For systems with strong interactions between polymers and surfactants, viscosity has been seen to increase significantly at certain polymer/surfactant concentrations (Goddard et al., 1998). Gel formation also has been found to occur for systems with strong interactions, however, this is most likely caused by chain entanglement between surfactant and polymer. On the other hand, it was shown that a viscosity reduction is possible if there is competition between the surfactants, polymers, or salts. An example of this occurred when a water-soluble polymer polypropyleneoxide (PPO) was combined with a cationic surfactant (CTAB) where competition between the polymer and salicylate produced a structural reorganization facilitating a thinning process (Brackman and Engberts, 1993).

In addition, it is known that surfactants can increase solubilization effects of polymers and vice-versa. Generally, the addition of a polymer to a surfactant solution increases solubilization

abilities if there are strong interactions present due to polymer/surfactant complexes decreasing the critical aggregation concentration of the surfactant (Goddard et al., 1998). The degree of solubilization falls however, when the concentration of surfactant reaches the precipitation zone.

3.2. Materials and Methods

Materials

The materials were used as stated in section 2.2.

Solubilization Capacity

Solubilization capacity (mL of oil in the middle phase/g surfactant) for a given system can be calculated from the following relation.

$$(4) \quad SP = 0.1457 * x + 0.0401$$

where x is the height of the middle phase (mm). SP was calculated for S^* of each system in this work.

3.3. Results and Discussion

The only system which noticeably became more viscous with the addition of polymer is that of C₁₂₋₁₃ alkyl ethoxy sulfate and PVA, which is thought to be due to complexation of the extended polymer with surfactant and itself as predicted by literature. At higher polymer concentrations in systems with strong interactions, it was expected that solutions would become more viscous due to binding between surfactant and polymer resulting in configurational changes (Saito, 1979). Rheology tests were not performed, so it is possible that there was a slight increase in viscosity for other systems, and this should be evaluated in future studies.

In every surfactant system at all polymer concentrations, solubilization abilities were shown to decrease with increasing EACN. Huh studied the relationship between minimum interfacial tension and solubilization of oil and aqueous phase in the middle phase (1979). He concluded that interfacial tension of oil microemulsions and aqueous phase microemulsions are almost symmetric with respect to oil volume per surfactant volume in microemulsions and aqueous volume per surfactant volume in microemulsions. He also found that interfacial tension of oil microemulsions is approximately equal to the interfacial tension of aqueous microemulsions when oil volume per surfactant volume in microemulsions is equal to aqueous volume per surfactant volume in microemulsions. Based on Huh's findings and given that minimum IFT values increased with increasing EACN, it was expected that solubilization abilities would decrease with increasing EACN.

Because there are weak interactions between surfactant and polymer for nonionic C₈₋₁₀E3.5 systems, the addition of HPC and PDADMAC was expected to decrease solubilization abilities in these systems. Evidence supporting a decrease in solubilization abilities between systems with weak charge interactions can be found throughout many studies (Zhang et al., 2015 a). It is seen in Figures 12 and 14 that solubilization abilities were decreased with the addition of polymer for all concentrations besides 0.2 g HPC/100 mL, which increased solubilization above that of the reference surfactant. The reason for this abnormal occurrence is not known and is beyond the scope of this thesis.

The addition of HPC, PDADMAC, and PVA was, however, expected to increase the solubilization abilities of SDHS and the C₁₂₋₁₃ alkyl ethoxy sulfate. For all three systems, solubilization abilities decreased with the addition of polymer, which is displayed in Figures 13, 15, and 16. SP* calculations were not done for the C₁₂₋₁₃ alkyl ethoxy sulfate systems; however,

the decrease in solubility can be seen by simply viewing the decrease in middle phase volume of stabilized samples in Figure 16. The decrease in solubility for these systems with strong interactions goes against what was expected from literature and many previous experimental studies (Zhang et al., 2015 a,b).

However, a study by Saito found that a combination of an anionic surfactant and nonionic polymer, much like the SDHS and HPC combination presented in this work, displayed a decrease followed by the leveling off in solubilization of hydrocarbons (Saito, 1967). He attributed this to that when surfactant molecules are effectively bound to polymers and a solubilize has a structure fitting to the polymers, the solubilization power of the surfactant solution may be synergistic with the polymer. The reverse is the case when a solubilize does not fit to the structure of polymers in the complexes. This occurrence could be the cause for the systems with strong charge interactions in this work as well as competition for water molecules at the interfaces (Warren, 2020), or competition for open area at the interface due to the large polymer size, all resulting in loss of interaction at the palisade layer.

Additionally, another study found that addition of salts increases the solubilization of hydrophobic compounds, since they may shield the charges of the polar head group of the surfactant, leading to a transition from more spherical to more elongated micelles, which lowers the critical micelle concentration (Zhang et al., 2016). Because both PDADMC and HPC caused hydrophobic shifts in systems, less salt was added to solutions of higher polymer concentrations to maintain an HLD of zero, supporting the decrease in solubilization of oil.

From Table 9, it is seen that HPC caused much more drastic drops in solubilization abilities than PDADMAC on SDHS systems. This is could be due to the idea that PDADMAC interacted

with the aqueous phase more than the palisade layer, and it is possible that both systems could later experience proportional increases in solubility at higher polymer concentrations.

Figure 12: C₈₋₁₀E3.5 & PDADMAC SP*

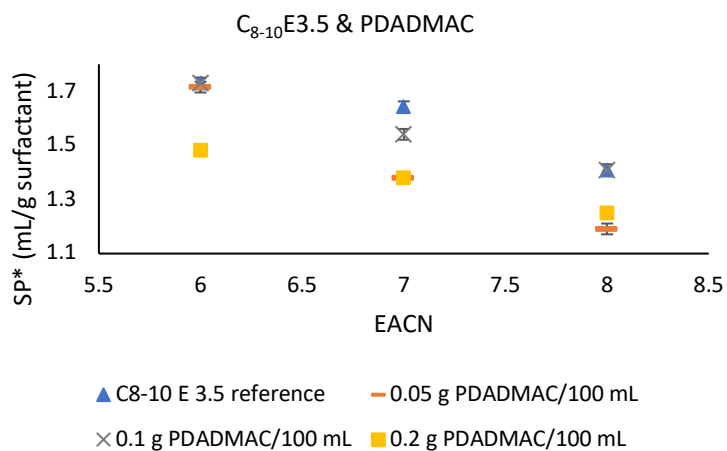


Figure 13: SDHS & PDADMAC SP*

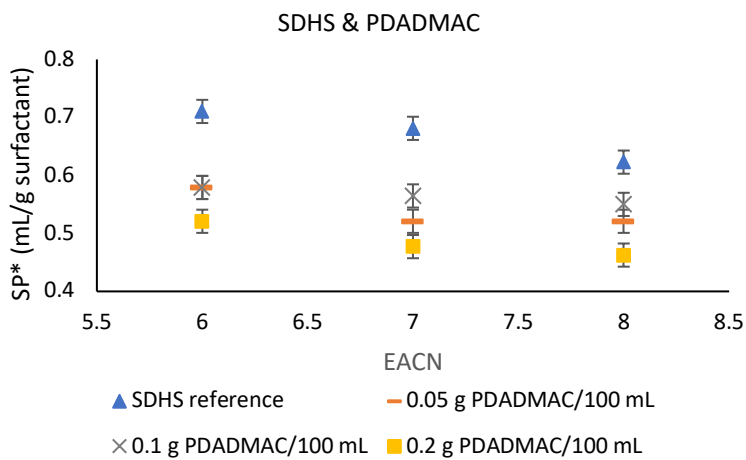


Figure 14: C₈₋₁₀E3.5 & HPC SP*

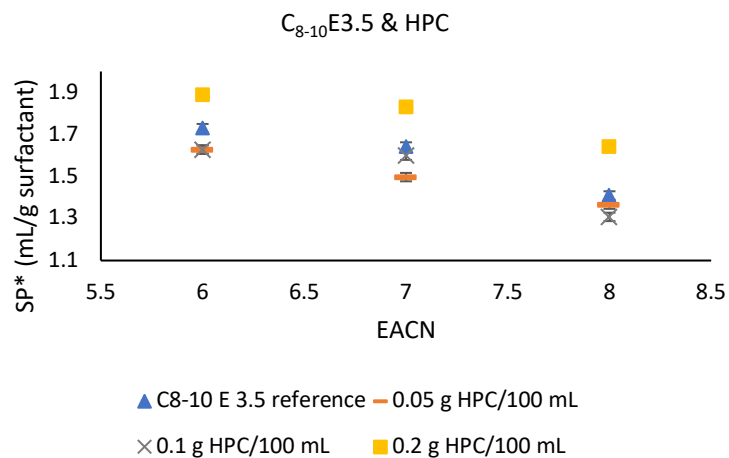


Figure 15: SDHS & HPC SP*

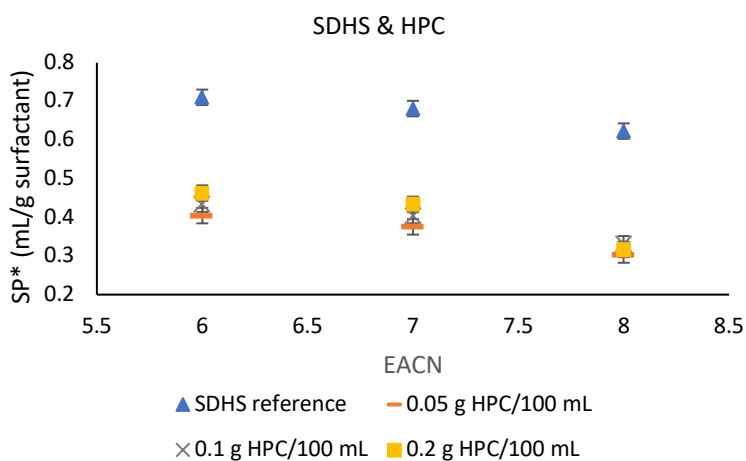
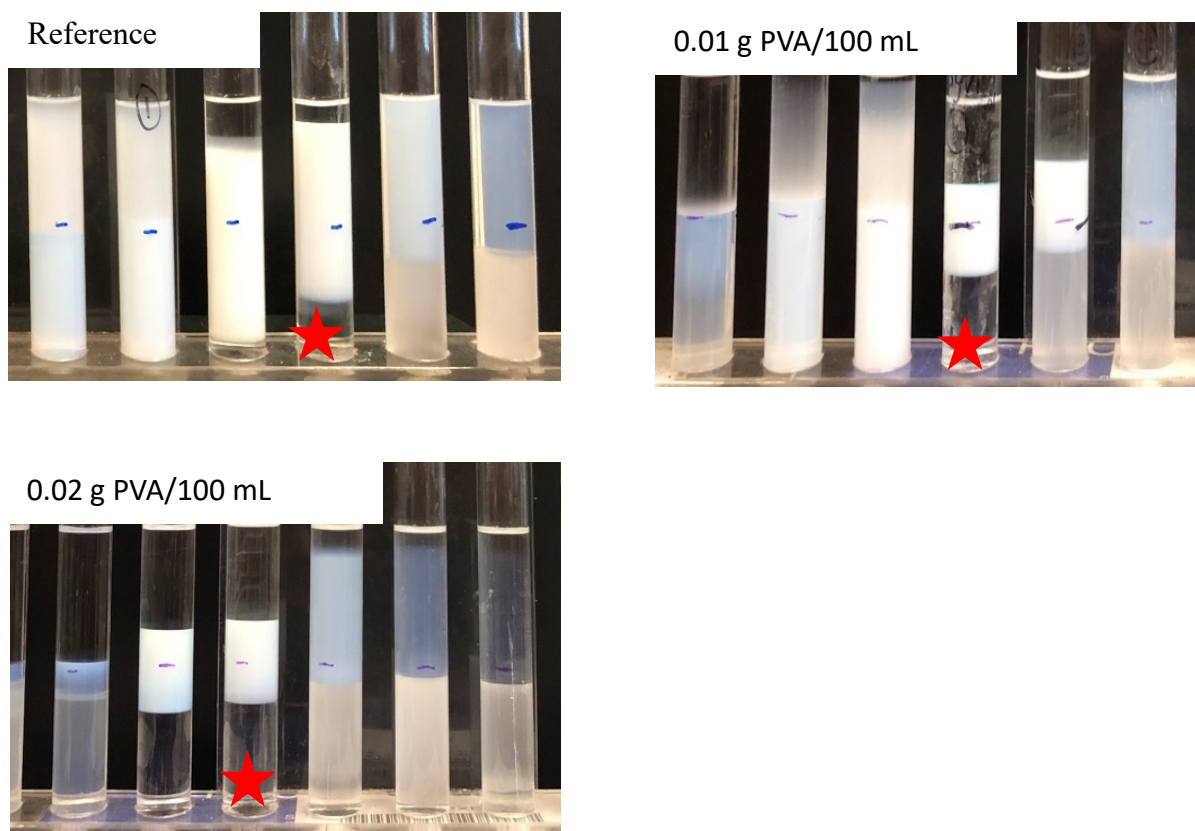


Table 9: Δ SP* from reference

	0.05 g/100 mL	0.1 g/100 mL	0.2 g/100 mL	
Δ SP* from reference (mL/g surfactant)	C ₈₋₁₀ E3.5 & PDADMAC			
	C ₆	-0.01	0.00	-0.25
	C ₇	-0.26	-0.10	-0.26
	C ₈	-0.22	0.00	-0.16
	SDHS & PDADMAC			
	C ₆	-0.13	-0.13	-0.19
	C ₇	-0.16	-0.12	-0.20
	C ₈	-0.10	-0.07	-0.16

C ₈₋₁₀ E3.5 & HPC			
C ₆	-0.10	-0.10	0.16
C ₇	-0.15	-0.04	0.19
C ₈	-0.04	-0.10	0.23
SDHS & HPC			
C ₆	-0.31	-0.28	-0.25
C ₇	-0.31	-0.28	-0.25
C ₈	-0.32	-0.29	-0.31

Figure 16: C₁₂₋₁₃ alkyl ethoxy sulfate wide scans where the star represents S*



3.4. Conclusions

Although the rheology of the systems was not quantitatively studied, the C₁₂₋₁₃ alkyl ethoxy sulfate and PVA system noticeably became more viscous with the addition of polymer. This is

believed to be due to complexation of the extended polymer with itself, based on theories in literature.

For all polymer-surfactant systems, solubilization abilities decreased with increasing EACN as predicted by Huh (1979). Based on previous studies, solubilization abilities were expected to decrease for systems with weak charge interactions between surfactant and polymer. This trend was generally seen for nonionic C₈₋₁₀E3.5 systems with the addition of HPC and PDADMAC. One exception to this prediction was presented in the data, however, the reason for the occurrence is unknown and was not analyzed in this work.

Solubilization abilities were expected to increase with the addition of polymer in systems with strong charge interactions between polymer and surfactant based on most works in literature. However, in this study, the opposite trend was found to occur for the addition of PDADMAC, HPC, and PVA to SDHS and C₁₂₋₁₃ alkyl ethoxy sulfate systems. Based on other studies where similar instances occurred, the decrease in solubilization abilities was attributed to possible structural incompatibility, competition for water molecules at the interfaces, competition for open area at the interface due to relatively large polymer size, and lack of salt due to the PDADMAC and HPC inducing a hydrophobic shift.

It was also noted that HPC caused more drastic drops in solubilization abilities than PDADMAC on SDHS systems with strong polymer-surfactant interactions, further supporting the claim that HPC interacted with the palisade layer more than the PDADMAC.

Chapter 4. HLD-NAC Characterization

4.1. Introduction

HLD is a very useful tool to determine which type of emulsion will be formed; however, to obtain more information regarding physical properties such as droplet radius, density, viscosity, and interfacial tension, another method is needed. Using HLD values, Net Average Curvature (NAC) equations can be utilized to determine the listed properties. In this study, the purpose of using NAC is to determine whether the model provides an accurate prediction of drop sizes and consistent results regarding interactions between polymer and surfactant as found in phase behavior studies.

The key NAC equations can be summarized as below (Acosta et al., 2003)

$$(5) \quad H_n = -\frac{HLD}{2L} = \frac{1}{2} \left(\frac{1}{r_o^{\mu E}} - \frac{1}{r_w^{\mu E}} \right)$$

$$(6) \quad H_a = \frac{1}{2} \left(\frac{1}{r_o^{\mu E}} + \frac{1}{r_w^{\mu E}} \right) = 1/\xi$$

where H_n and H_a are the net and average curvatures of the surfactant, L represents the extended length of the surfactant tail and is representative of the solubilization capacity of the surfactant using the Tanford Equation (Tanford, 1980), $r_o^{\mu E}$ and $r_w^{\mu E}$ are the sphere equivalent radii of oil and water droplets, and $1/\xi$ is a sort of order parameter called Gennes Coherence Length, which is dependent on the oil used and measured through neutron scattering or by measuring phase volumes of the formulations at optimal salinity. The net average curvature equation implies there is infinite mutual solubility at an HLD value of zero, which is impossible. Average curvature is always finite, so solubilities are always finite. Therefore, calculations must take both equations into account, allowing the theory to be named net average curvature. It should be noted that NAC assumes

chemical symmetry. This is not the case in reality and is based on structure, thus, it is likely to see deviations in either Type I or Type II domains.

4.2. Materials and Methods

Materials

The materials were used as stated in section 2.2.

Particle Size Analysis (DLS)

DLS measurements were taken using a Brookhaven Instruments NanoBrook 90Plus PALS (Particle Size & Zeta Potential using Phase Analysis Light Scattering) instrument and analyzed using Brookhaven's Particle Solutions software (v. 3.5). All data was collected using a 90° scattering angle. Approximately 2 mL of each solution was filtered and put into glass cuvettes which were ensured to be free of dust by rinsing with filtered water beforehand. Measurements were performed after appropriate dilution of Type I microemulsions if needed. Solutions were set aside to stabilize for 30 minutes before running three 60 second DLS analysis trials. DLS data was considered valid if data was reproducible-the correlation function for each trial was very similar, and each sample was stabilized. Intensity and number DLS measurements seemed very reasonable and are displayed in Appendix A.

HLD-NAC Calculations

When performing NAC calculations, a constant adjustable length parameter, which was shown to be proportional to the extended length of the surfactant hydrophobic tail, was used for C₈₋₁₀E3.5 and for SDHS. Experimental droplet radius was found using DLS intensity

measurements because intensity is the purest form of light scattering data obtainable. The characteristic length parameter was kept constant for each surfactant for each oil and was determined by fitting the reference surfactant's Type III window and approximate range of experimental drop sizes. This term, ξ , is known to decrease with increasing EACN because a surfactant has more control over a small oil molecule than a larger one. It was found that ξ in this study followed this trend, further verifying the decrease in oil solubilization in the middle phase with increasing EACN. Surfactant head group area was changed for each surfactant-polymer system so that the NAC predicted middle phase volume was approximately equal to the experimental middle phase volume.

4.3. Results and Discussion

First, the experimental emulsion drop sizes were plotted against the NAC predicted emulsion drop sizes. The model provided a relatively good estimation for droplet radii, as most experimental radii were within 10 nm of the model. For most systems, it was seen that the NAC model provided better predictions for samples of an HLD value above zero than below zero. This could be the case for multiple reasons. As mentioned previously, NAC assumes chemical symmetry, which is not a true assumption. Either the surfactant head or tail group will be dominant over the other in most cases. The model also assumes emulsions are spherical pure water or oil drops where the size of the water droplets is predicted based on the surfactant concentration, so the oil droplet size is mirrored.

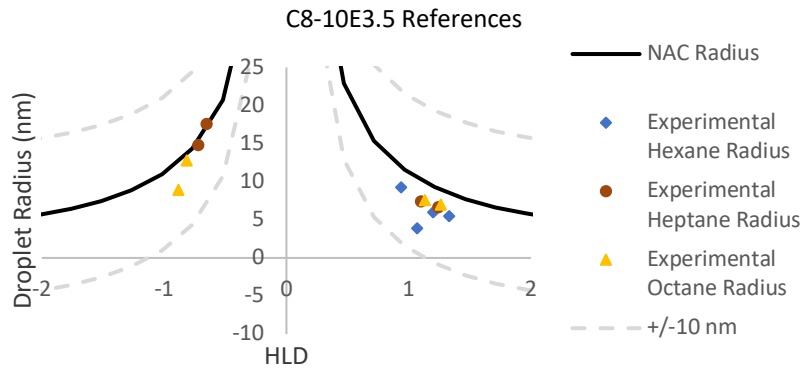
This occurrence was also thought to be due to the polymer having difficulties solubilizing in the oil phase. Because the aqueous phase was more dynamic than the oil phase, the oil emulsions in Type I microemulsions might be hypothesized to fit the model better given that the surfactant,

polymer, and salt all mostly reside in the aqueous phase instead of the oil phase. However, based on the data, it is now believed that polymer could not get in the water droplet emulsions because it was not able to solubilize in the oil phase. Therefore, the water droplets in the oil phase were more ideal. Additionally, systems at higher polymer concentration resulted in more accurate drop size fittings, which may mean that polymer solubilization in the oil phase decreased as polymer concentration is increased. This is reasonable considering the aqueous phase density is most likely changing.

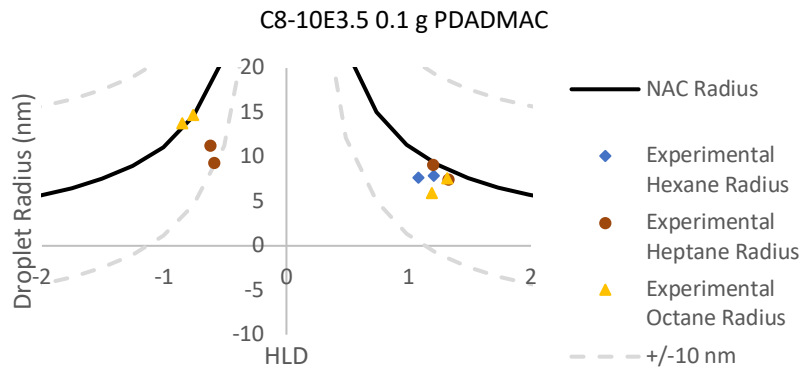
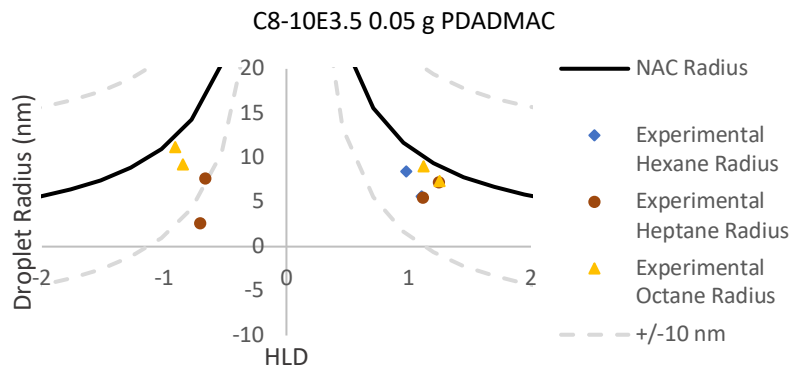
Another general trend is that the model provided more accurate predictions as an HLD value of zero was approached. This was expected since the model's parameters were derived from systems with HLD values very close to zero. The NAC model should be assumed to have greater error at HLD values not close to zero. It should also be noted that the NAC model will not provide relatively accurate predictions if a system's K and C_c values are not correct.

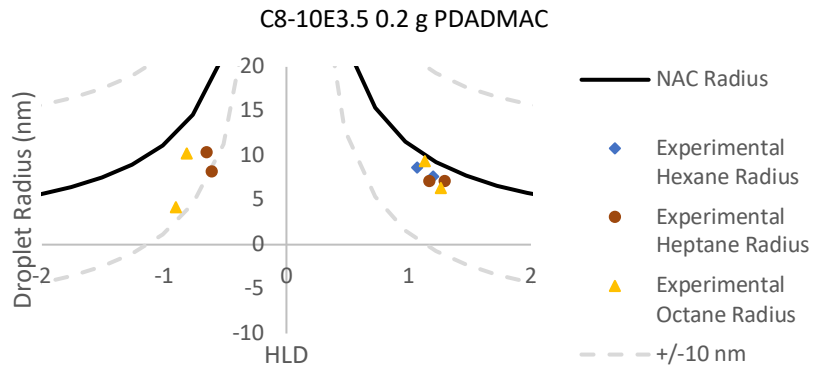
Lastly, the polydispersity of DLS samples was analyzed. The Type I DLS samples were much more polydisperse than the Type II samples indicating that the polymer resided in the aqueous phase instead of in the middle or oil phases, thus confirming the findings of prior phase behavior studies.

Figure 17: Comparison between C₈₋₁₀E3.5 exp. and NAC emulsion drop radius

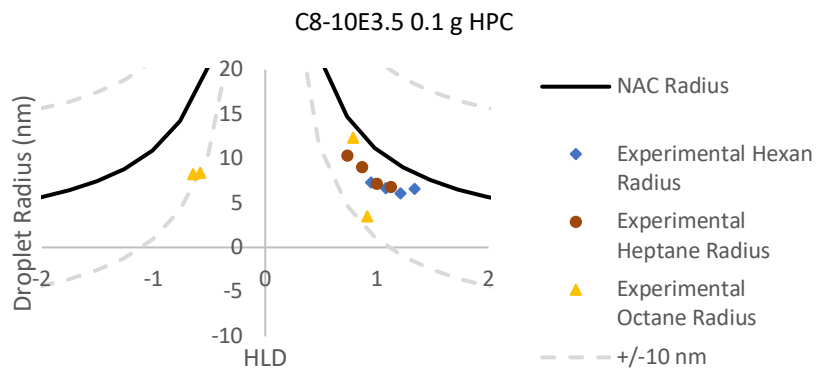
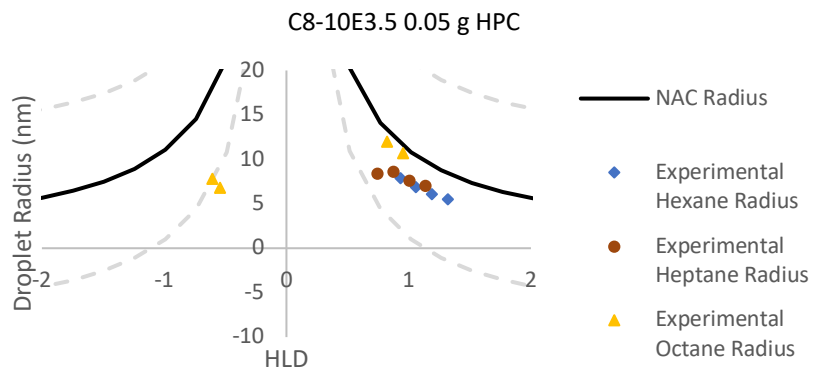


Figures 18-20: Comparison between C₈₋₁₀E3.5 & PDADMAC exp. and NAC emulsion drop radius





Figures 21-23: Comparison between C₈₋₁₀E3.5 & HPC exp. and NAC emulsion drop radius



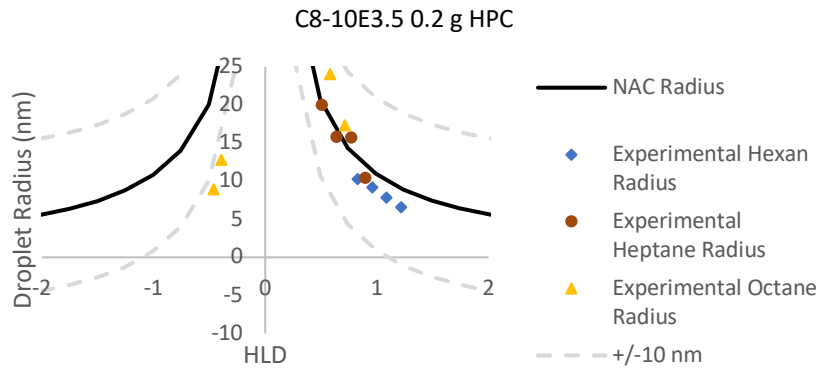
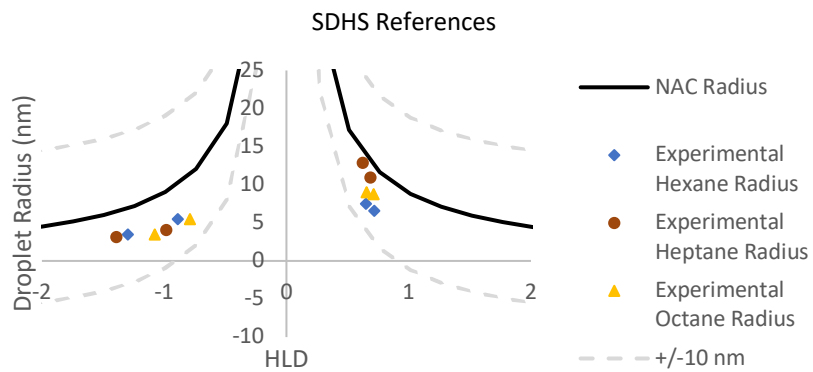
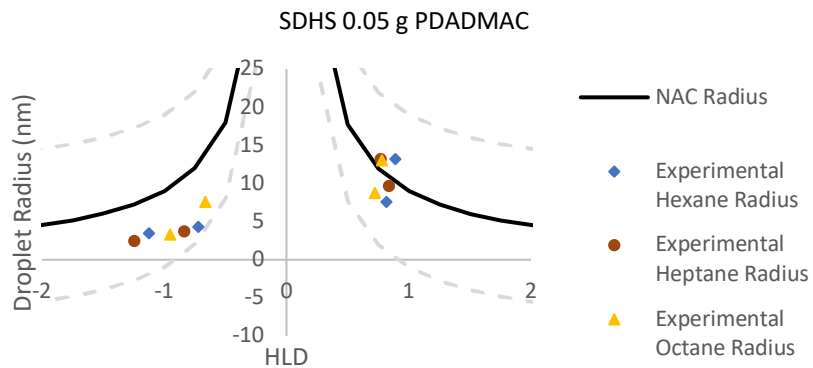
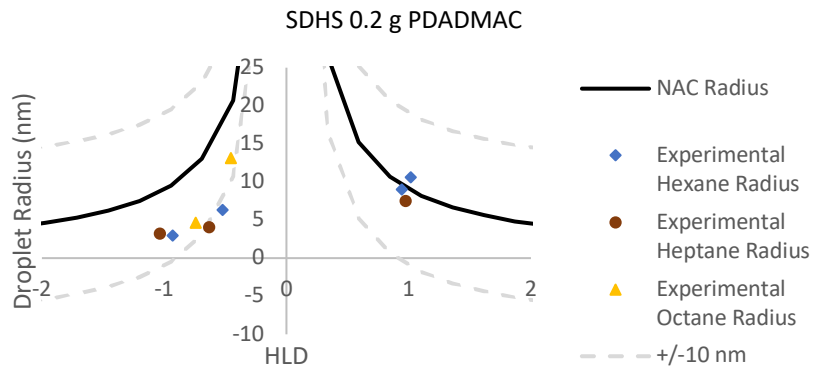
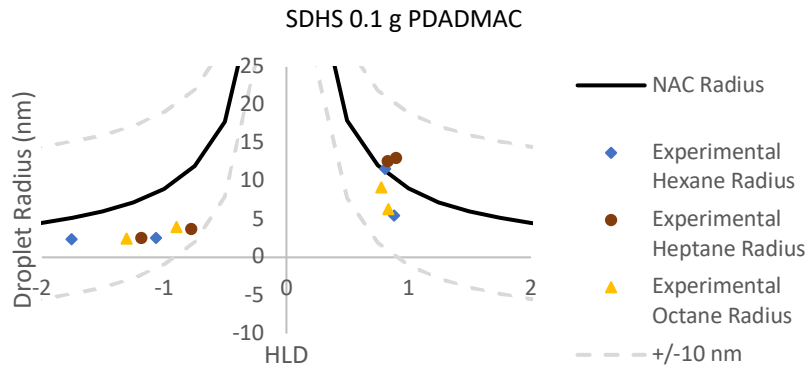


Figure 24: Comparison between SDHS exp. and NAC emulsion drop radius

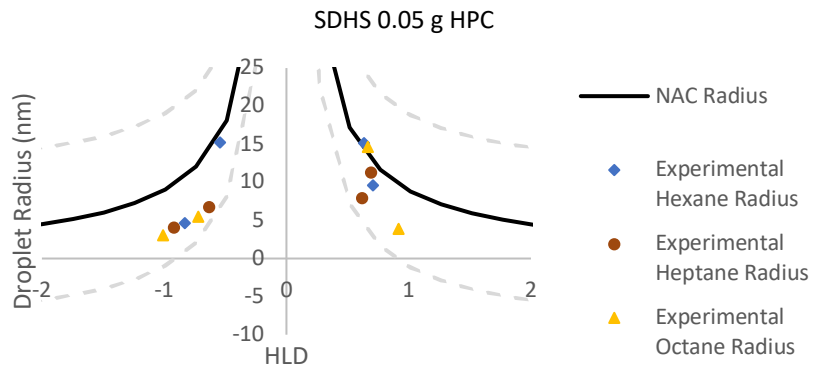


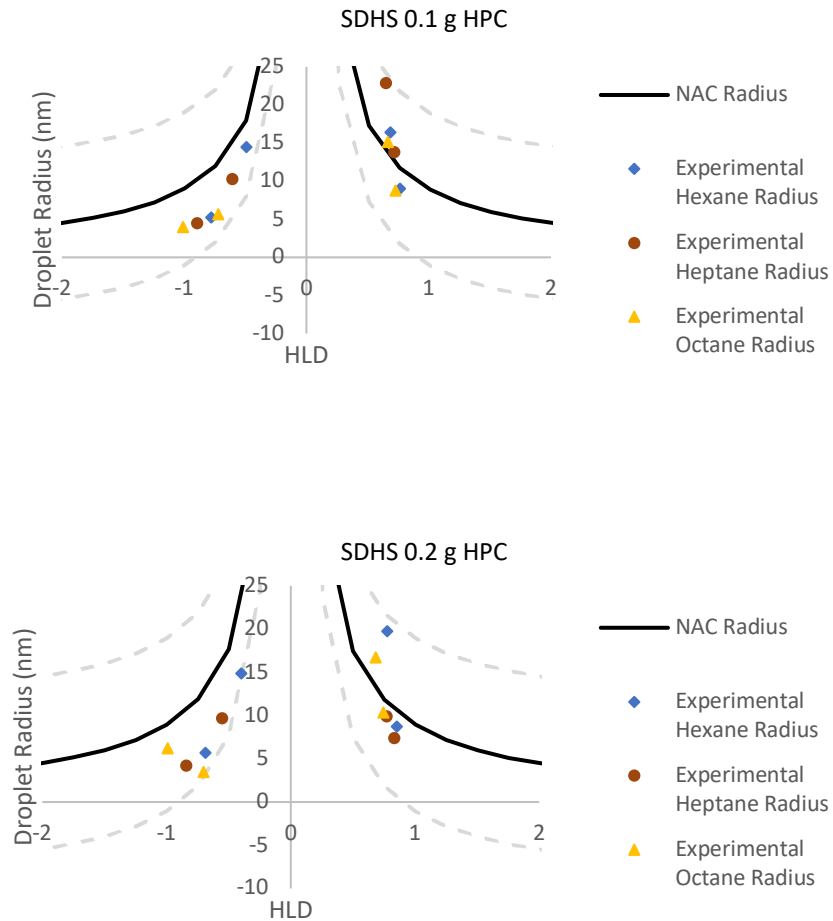
Figures 25-27: Comparison between SDHS & PDADMAC exp. and NAC emulsion drop radius





Figures 28-30: Comparison between SDHS & HPC exp. and NAC emulsion drop radius





HLD-NAC was then utilized to quantify system properties such as surfactant head group area (\AA^2). The surfactant head group area used by NAC is displayed in Figures 31-34. Head group area was usually seen to decrease with increasing EACN for a given PDADMAC or HPC concentration. This was expected given that at an interface, as the length of present hydrophobic chains increase, the surfactant head groups pack more closely together to maintain as much distance as possible from the hydrophobic groups the surfactant tail attracts. There are cases where this trend was not seen such as in the SDHS and PDADMAC system. The model is not perfect; however, it can provide some useful insight to general ranges for properties. In reality, ξ , surfactant head group area and L are all dependent on each other. Therefore, results cannot be fully accurate when only one variable was varied for each system.

The addition of PDADMAC to C₈₋₁₀E3.5 and SDHS seemed to decrease the surfactant head group area with increasing polymer concentration. The decrease in head group area caused by PDADMAC is reasonable considering the conclusion that the polymer is acting as a cation. As higher concentrations of PDADMAC were utilized, the systems became more hydrophobic, much like they would if EACN was increased. Also, the Type III window made in Windsor wide scans became smaller with the addition of polymer, further supporting the decrease in area.

The addition of HPC to C₈₋₁₀E3.5 and SDHS initially decreased the surfactant head group area, but then increased the head group area at the highest HPC concentration. It was discovered previously that the addition of HPC caused C₈₋₁₀E3.5 and SDHS to become more hydrophobic, which would explain the initial decrease in surfactant head group area to provide space for hydrophobic groups. However, the increase in surfactant head group area could possibly imply that the tail groups of the HPC interact less with the palisade layer at higher concentrations, thus making space for the head groups to then begin spreading out. Because the Van't Hoff factor is less than 1 for HPC, this is a reasonable conclusion. The HPC may have associated in the aqueous phase as concentration was increased.

Figure 31: C₈₋₁₀E 3.5 & PDADMAC changes in surfactant head group area

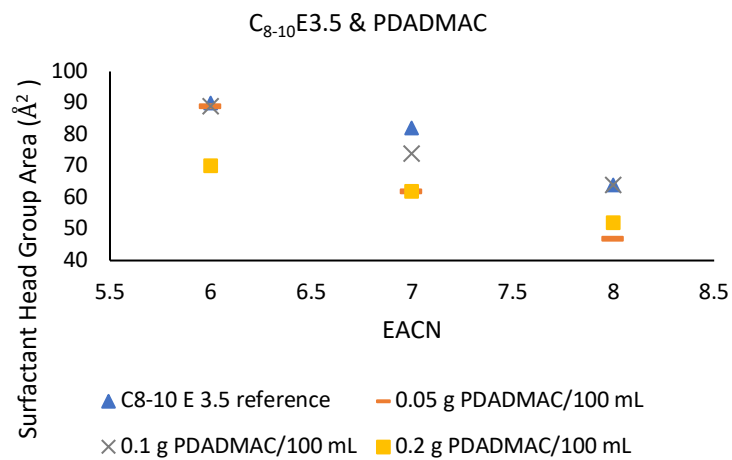


Figure 32: SDHS & PDADMAC changes in surfactant head group area

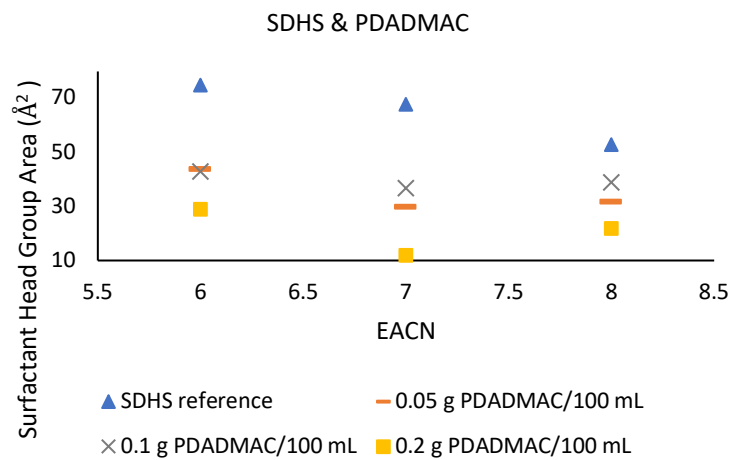


Figure 33: C₈₋₁₀E3.5 & HPC changes in surfactant head group area

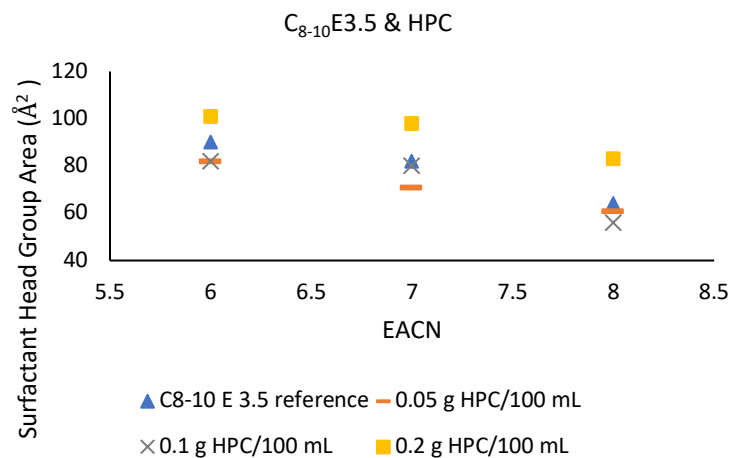
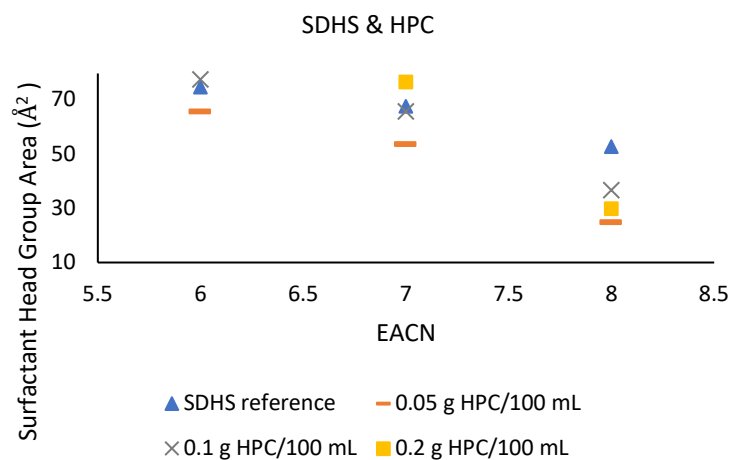


Figure 34: SDHS & HPC changes in surfactant head group area



4.4. Conclusions

The ξ parameter was first seen to decrease with increasing EACN, which further proves that the solubilization of oil in the middle phase decreased with increasing EACN.

The NAC model provided a relatively good estimation for droplet radii, as most experimental droplet radii were within 10 nm of the model. For all systems, it was seen that the NAC model provided better predictions for samples of an HLD value above zero than below zero.

This is thought to be due to the limitations of the model and the solubilization limits of the polymer in the oil phase. It was also seen that the model provided more accurate predictions as an HLD value of zero was approached. This was expected since the model's parameters were derived from systems with HLD values very close to zero.

Surfactant head group area was observed generally to decrease with increasing EACN for a given PDADMAC or HPC concentration. This trend was expected, but it should be noted that the NAC model should not be taken to be always accurate due to ξ , surfactant head group area and L being dependent on each other. It was not possible in this study to change more than one variable for each system as they would change in reality.

The decrease in surfactant head group area with the addition of PDADMAC to C₈₋₁₀E3.5 and SDHS systems was reasonable considering PDADMAC acts as a cation, causing solutions to become hydrophobic.

The addition of HPC to C₈₋₁₀E3.5 and SDHS systems was also expected to decrease surfactant head group area because of the induced hydrophobic shift. While the addition of HPC initially caused a decrease in head group area, an eventual increase was also observed. This is speculated to be due to HPC tail groups interacting less with the surfactant tail groups at higher concentrations due to association.

Because of the many assumptions one makes when utilizing NAC, it is probably not well suited for industry applications at this time, however, the model is effective in providing a quick method to quantify system changes at the head group level.

Chapter 5. Conclusions and Future Work

5.1. Conclusions

The purpose of this study was to contribute to the understanding of the effects of water-soluble polymers on reference surfactant systems through HLD-NAC phase behavior characterization. Specifically, shifts on system optimal salinity, deviations from reference K and Cc values, changes of the solubilization parameter, and changes in microemulsion droplet radius were studied as polymer was introduced to reference surfactant systems.

Characterization behavior among reference surfactants as well as polymer-surfactant interactions have been extensively studied in prior works. However, due to how dynamic surfactant-polymer systems are, the predicted outcomes and characterization values with the addition of polymer may not always be reality. Composition differences between batches of surfactant create the need for consistent evaluation. The strength of general interactions between differently charged polymers and surfactants are known, however, the systems are sensitive to structural hinderances and competition at the interface, making formulation work imperative to gain understanding of the systems.

The three polymers used in this study were PDADMAC, HPC, and PVA. PDADMAC and HPC induced hydrophobic shifts, decreasing the optimal salinity of C₈₋₁₀E3.5 and SDHS systems, while PVA induced a hydrophilic shift, increasing the optimal salinity of C₁₂₋₁₃ alkyl ethoxy sulfate systems. K and Cc values were first found for surfactant-only systems, then new K and Cc values were found for each concentration of polymer for polymer-surfactant systems through formulation work. A function, f(P), was found for each polymer concentration and oil to account for the addition of polymer to surfactant systems so that reference surfactant K and Cc values could predict the optimal salinity of systems with polymer using the HLD equation. These functions are

displayed in Tables 4-8. Overall, it was concluded that PDADMAC acted as a cation and mostly interacted with the aqueous phase instead of the palisade layer. HPC and PVA mostly interacted with the aqueous phase as well but were able to interact with the palisade layer more than PDADMAC. This conclusion was further confirmed through examination of the polydispersity of DLS samples.

Although the rheology of the systems was not quantitatively studied, the C₁₂₋₁₃ alkyl ethoxy sulfate and PVA system noticeably became more viscous with the addition of polymer. The other systems exhibited no visible changes in viscosity.

PDADMAC, HPC, and PVA were all observed to decrease the solubilization of oil at the optimal salinity of C₈₋₁₀E3.5, SDHS, and C₁₂₋₁₃ alkyl ethoxy sulfate systems. For the systems with weak charge interactions, this result was expected. For the systems with strong charge interactions, the opposite trend was expected. Possible reasons why the systems with strong charge interactions did not act as predicted include structural incompatibility, competition for water molecules at the interfaces, competition for open area at the interface due to relatively large polymer size and decrease in salt concentration due to the PDADMAC and HPC inducing a hydrophobic shift.

The NAC model was shown to provide a relatively good estimation for droplet radii, as most experimental droplet radii were within 10 nm of the model. For all systems, it was seen that the NAC model provided better size predictions for samples of an HLD value above zero than below zero due to assumptions included in NAC and lack of solubilization abilities for the polymer in oil.

Surfactant head group area in the palisade layer was generally observed to decrease with increasing EACN for a given PDADMAC or HPC concentration as expected. Surfactant head

group area also decreased with the addition of PDADMAC to C₈₋₁₀E3.5 and SDHS systems as expected, considering PDADMAC acted as a cation causing solutions to become hydrophobic.

The addition of HPC to C₈₋₁₀E3.5 and SDHS systems caused an initial decrease followed by an increase in head group area. This is speculated to be due to HPC tail groups interacting less with the surfactant tail groups at higher polymer concentrations due to association. The NAC model should not be taken to be always accurate due to ξ , surfactant head group area and L being dependent on each other and the many assumptions included in the model.

5.2. Future Work

Future work should consist of a more in-depth analysis of the systems characterized in this work. A broader range of polymer concentrations and oils would be beneficial to study so that trends in K and C_c values could be tested for consistency and more accurate f(P) functions for the HLD equation could be developed.

A quantitative study of the rheology of the systems would provide valuable information regarding the relationship between viscosity increase and polymer-surfactant interaction strength. It would also provide more information regarding the polymer-surfactant interactions, allowing for a better explanation in solubilization trends.

The exact cause for the decrease in solubilization abilities for systems with strong polymer-surfactant charge interactions should be determined through further analysis. Discrepancies in the general trends of system solubilization abilities with the addition of polymer existed in this work and should be ensured valid.

Utilization of a transmission electron microscopy technique would also be very beneficial in confirming the emulsion drop size data obtained from DLS tests. Given this extra information,

a better understanding of how and if the polymer is interacting with the surfactant could be obtained.

The NAC model parameters could be studied in depth so that all predictions from the model would be more accurate. In particular, the relationship between L , head group area, and ξ for common surfactant systems would be very beneficial. It would also be interesting to experiment with different surfactant concentrations and observe effects on NAC drop size predictions.

Finally, the findings from this work could be applied more firmly to the oil and gas, drug delivery, or other formulation industry. Because each industry has differing needs and specifications, one could experiment with controlling HLD value, viscosity, solubility and drop size using the addition of water-soluble polymers to fit a given need.

Appendices

Appendix A: Plots Determining f(P) Function for HLD Equation

$$f(P) = \text{slope} * \ln[\text{Polymer}]$$

Figure 35: C₈₋₁₀E3.5 & PDADMAC f(P)

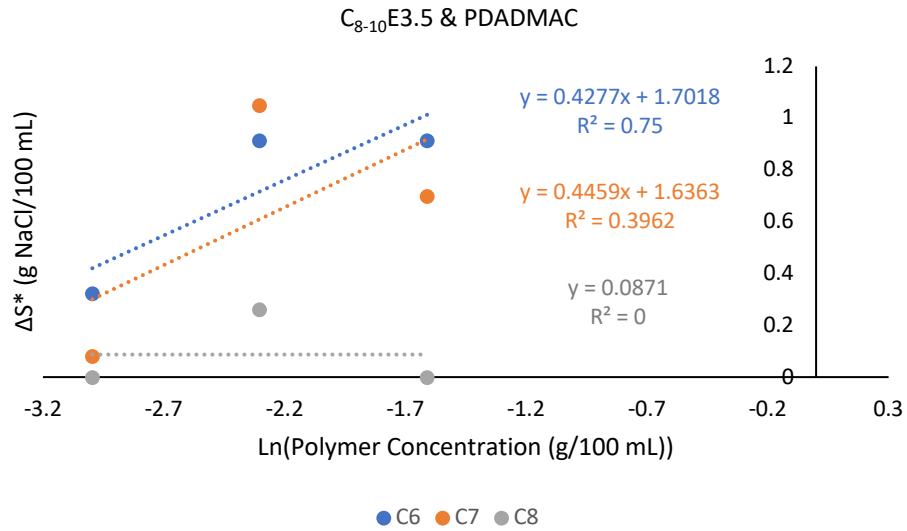


Figure 36: SDHS & PDADMAC f(P)

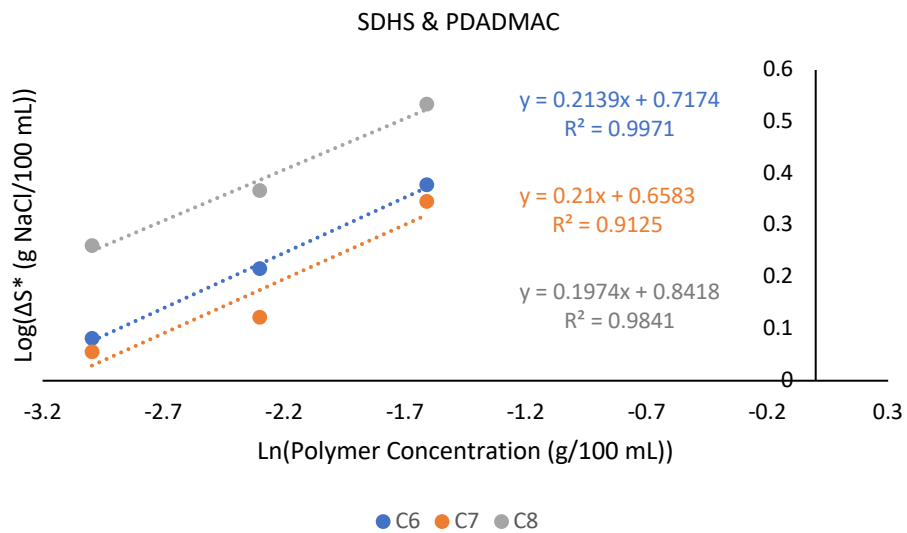


Figure 37: C₈₋₁₀E3.5 & HPC f(P)

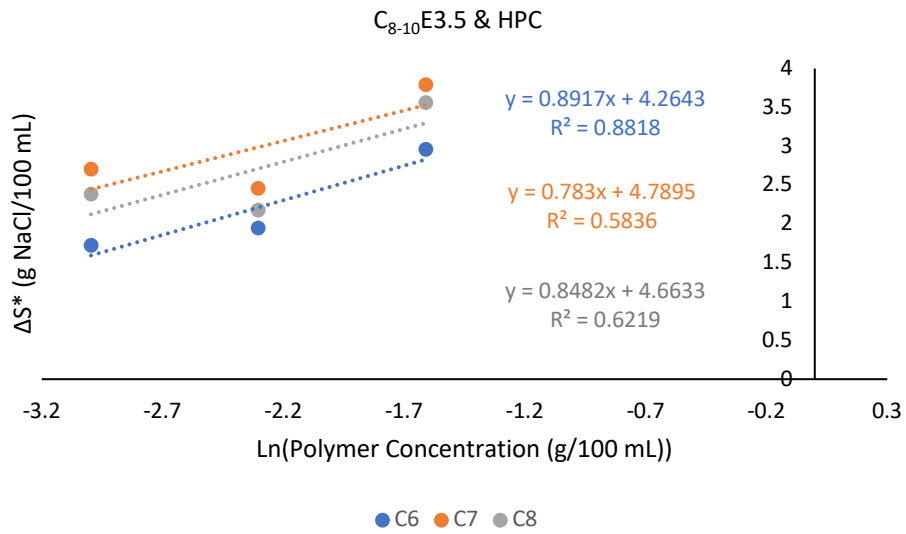


Figure 38: SDHS & HPC f(P)

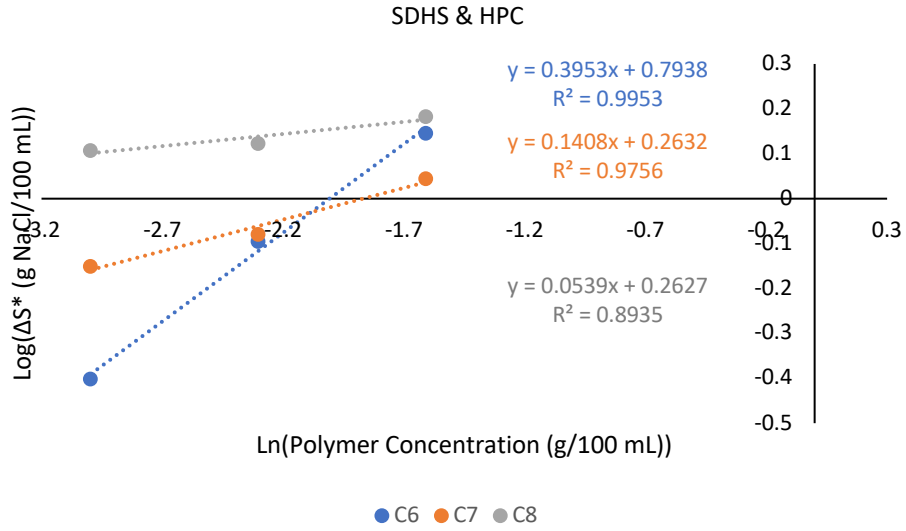
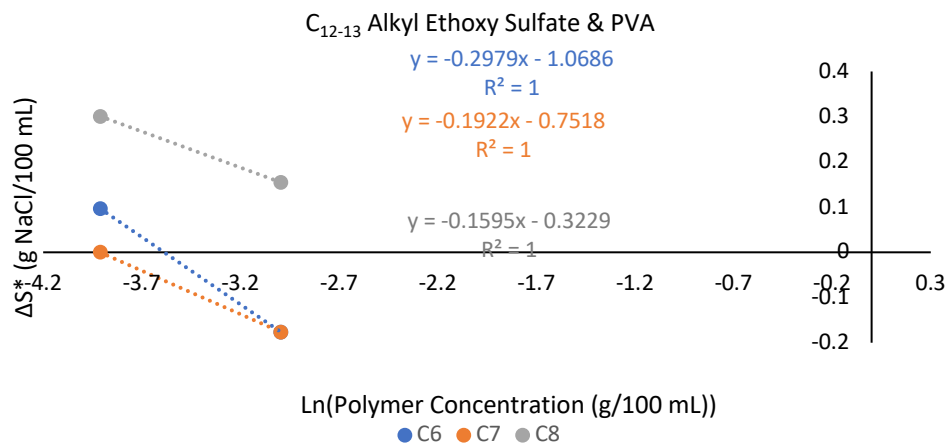


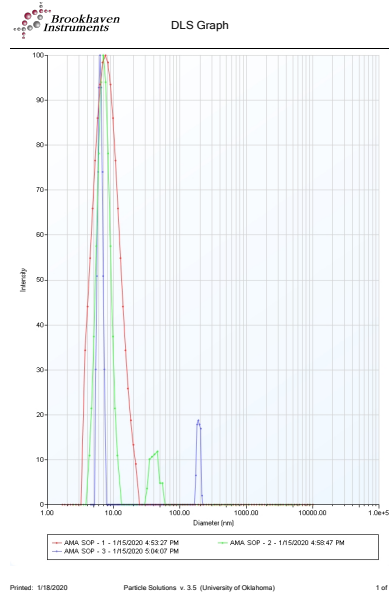
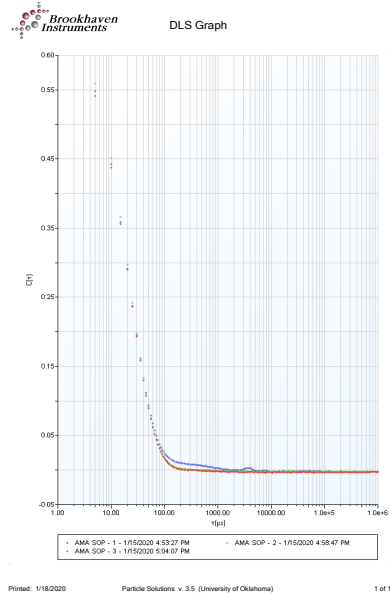
Figure 39: C₁₂₋₁₃ Alkyl Ethoxy Sulfate & PVA f(P)



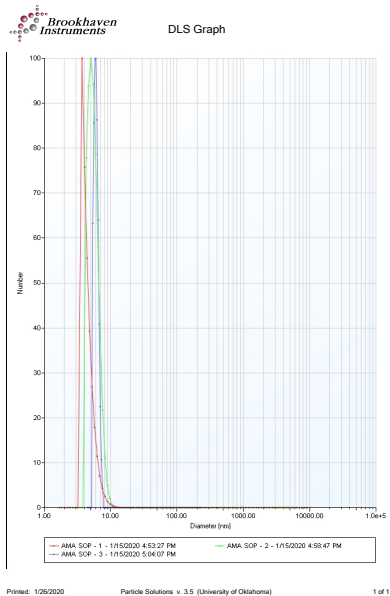
Appendix B: Sample DLS Graphs (PD = Polydispersity, CR = Count Rate (kcp))

B.1. SDHS Reference Systems

Figures 40-42: C6 Reference: 2 g NaCl/100 mL DI water PD = 0.138, CR = 399.6	
Correlation Graph	MSD Intensity Graph



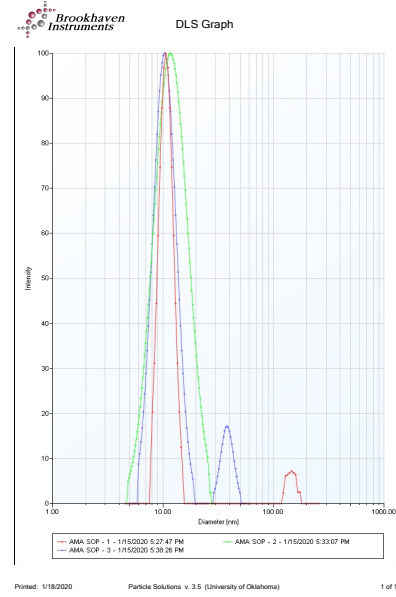
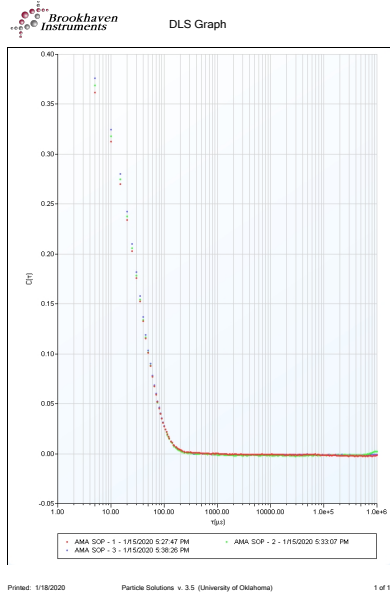
MSD Number Graph



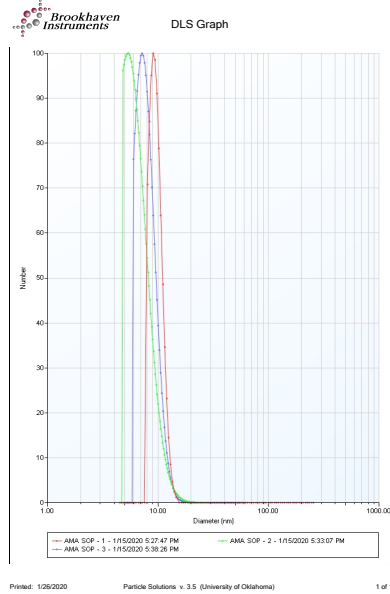
Figures 43-45: C6 Reference: 3 g NaCl/100 mL DI water PD = 0.121, CR = 503

Correlation Graph

MSD Intensity Graph



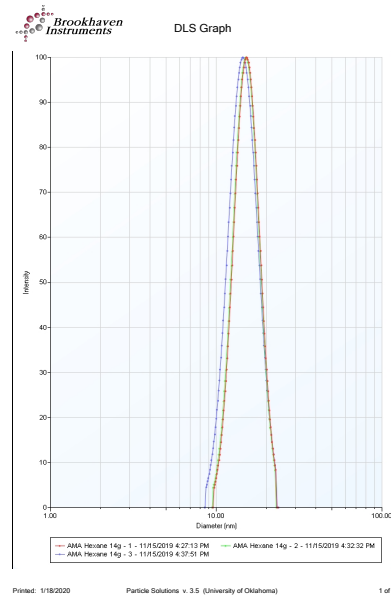
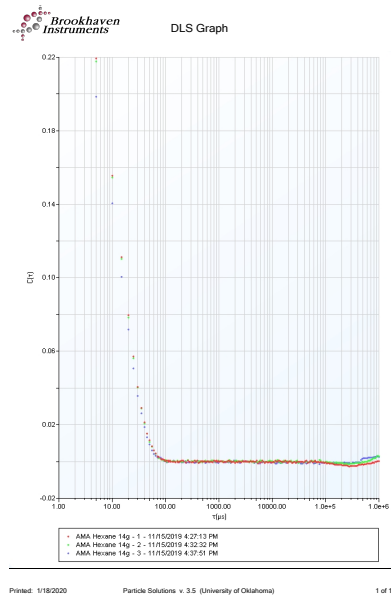
MSD Number Graph



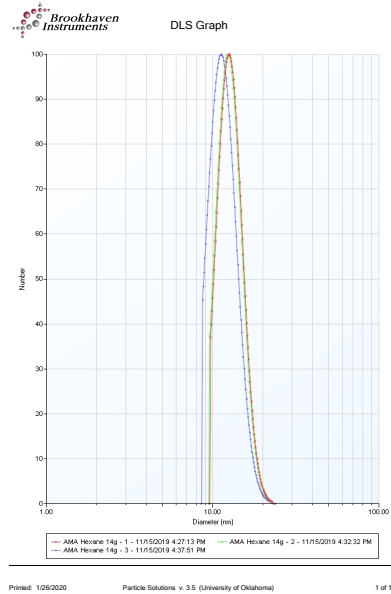
Figures 46-48: C6 Reference: 14 g NaCl/100 mL DI water PD = 0.028, CR = 103.3

Correlation Graph

MSD Intensity Graph



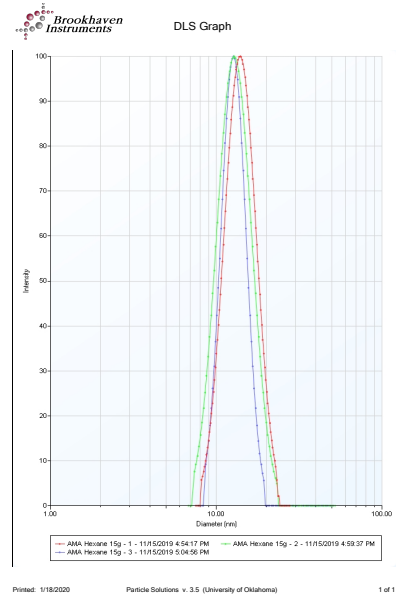
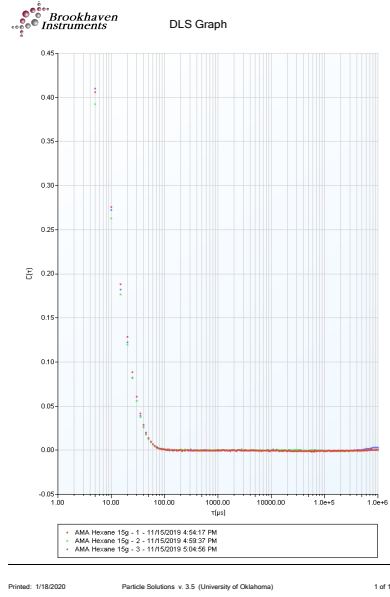
MSD Number Graph



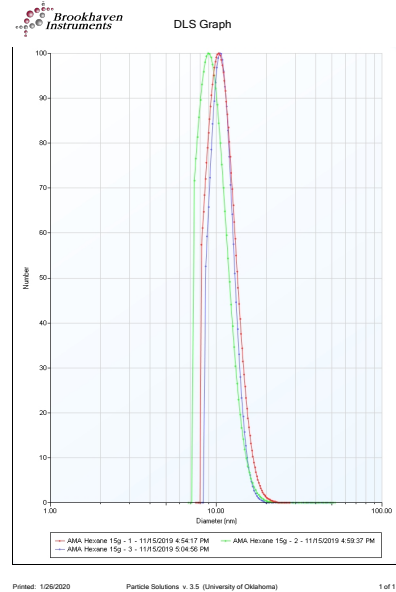
Figures 49-51: C6 Reference: 15 g NaCl/100 mL DI water PD = 0.066, CR = 140.7

Correlation Graph

MSD Intensity Graph



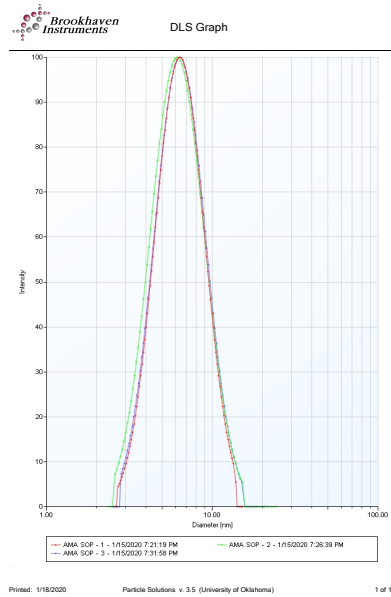
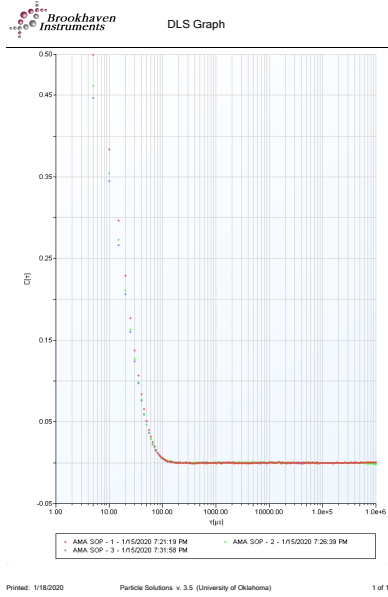
MSD Number Graph



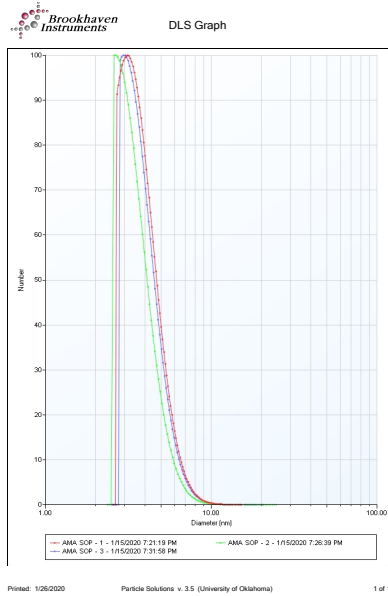
Figures 52-54: C7 Reference: 2 g NaCl/100 mL DI water PD = 0.082, CR = 269.6

Correlation Graph

MSD Intensity Graph



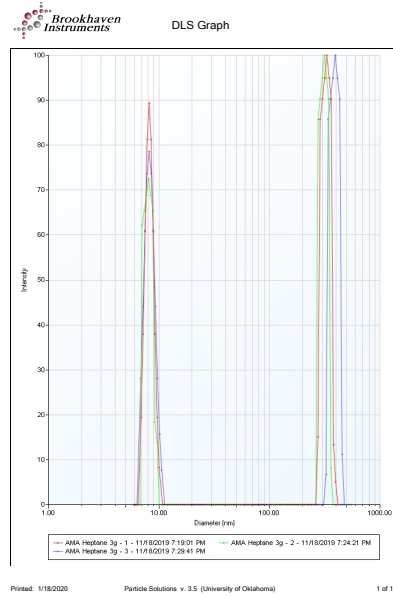
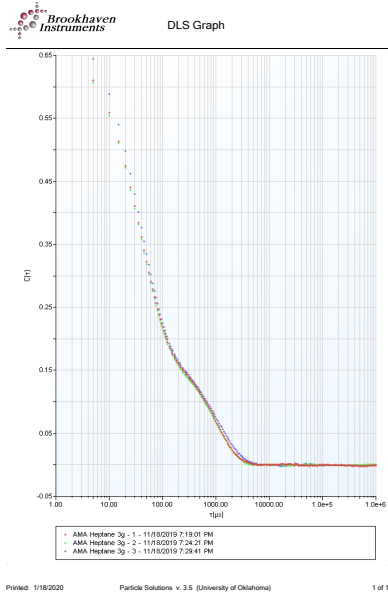
MSD Number Graph



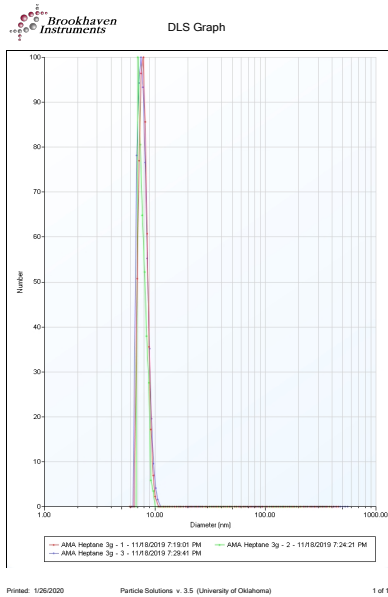
Figures 55-57: C7 Reference: 3 g NaCl/100 mL DI water PD = 0.234, CR = 473.3

Correlation Graph

MSD Intensity Graph



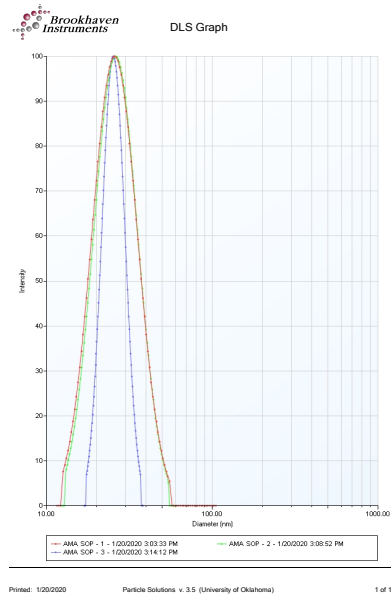
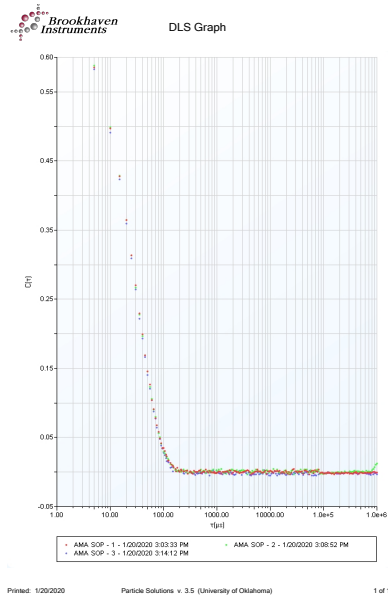
MSD Number Graph



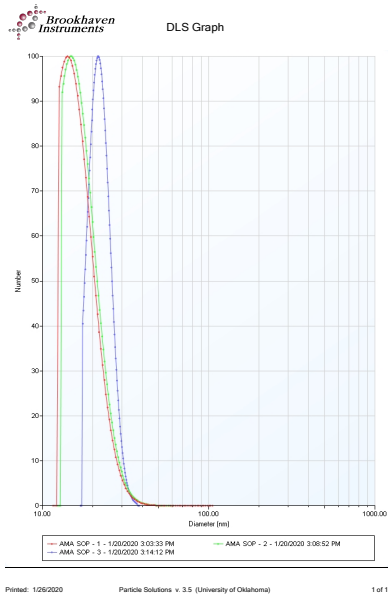
Figures 58-60: C7 Reference: 15 g NaCl/100 mL DI water PD = 0.033, CR = 22

Correlation Graph

MSD Intensity Graph



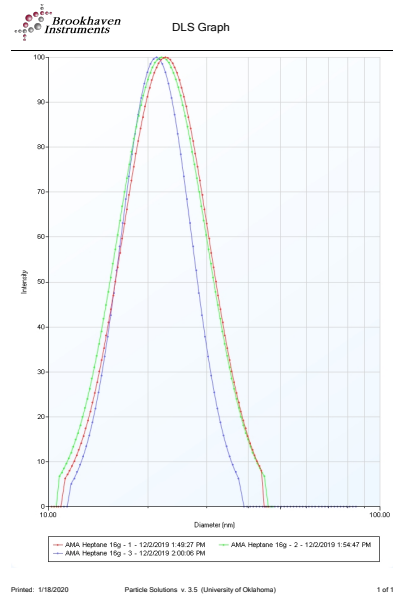
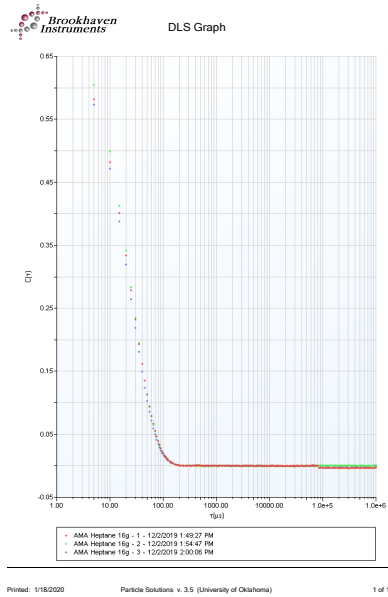
MSD Number Graph



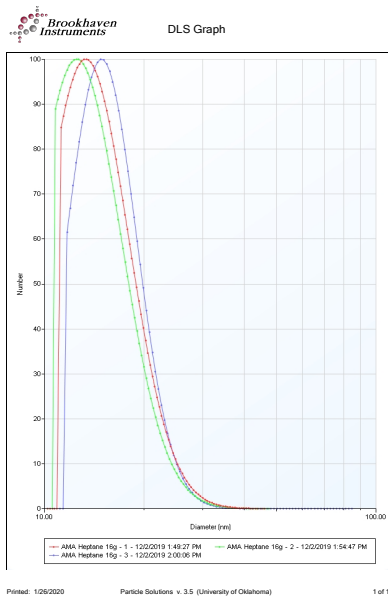
Figures 61-63: C7 Reference: 16 g NaCl/100 mL DI water PD = 0.059, CR = 209.4

Correlation Graph

MSD Intensity Graph



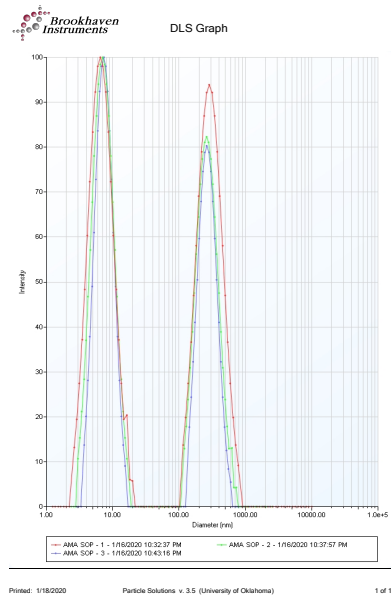
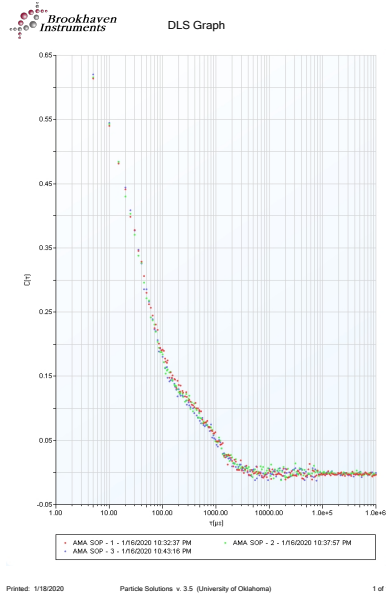
MSD Number Graph



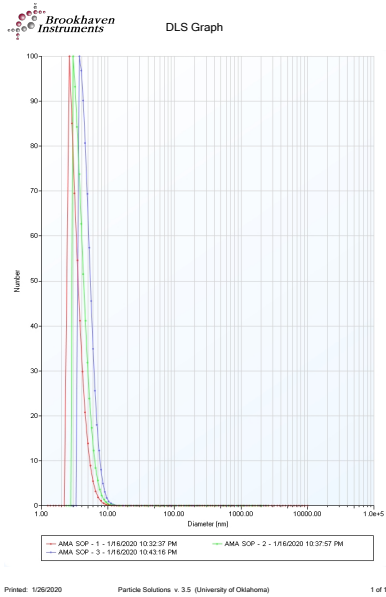
Figures 64-66: C8 Reference: 3 g NaCl/100 mL DI water PD = 0.372, CR = 92.14

Correlation Graph

MSD Intensity Graph



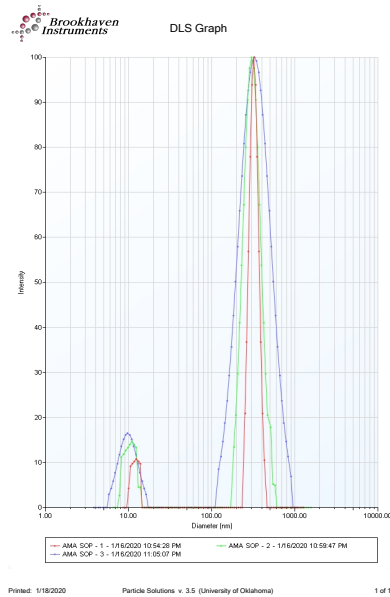
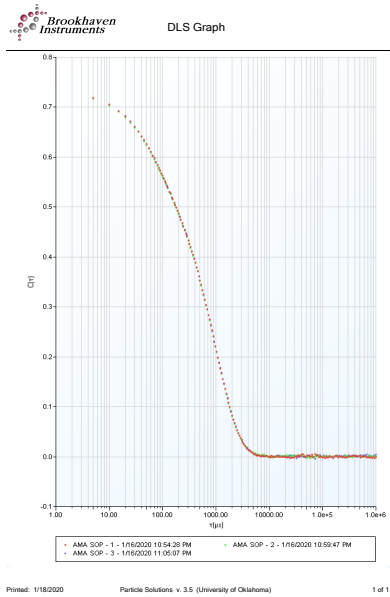
MSD Number Graph



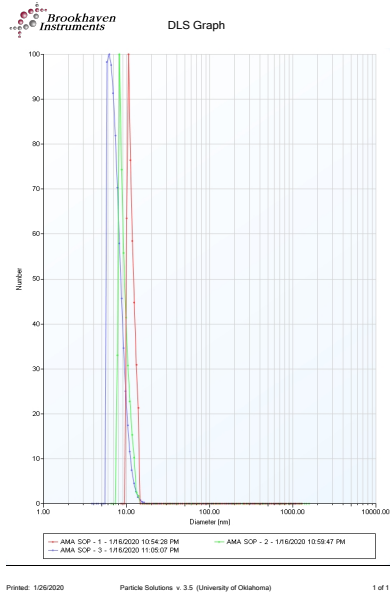
Figures 67-69: C8 Reference: 4 g NaCl/100 mL DI water PD = 0.313, CR = 63.1

Correlation Graph

MSD Intensity Graph



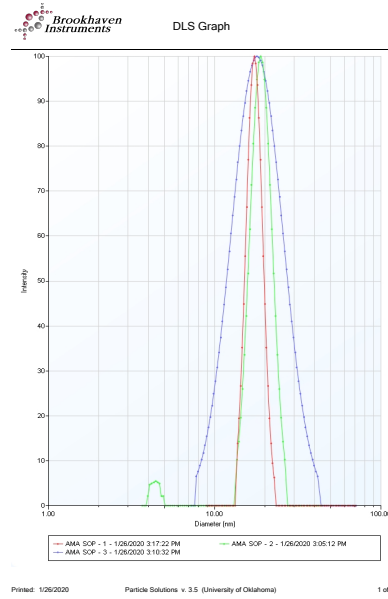
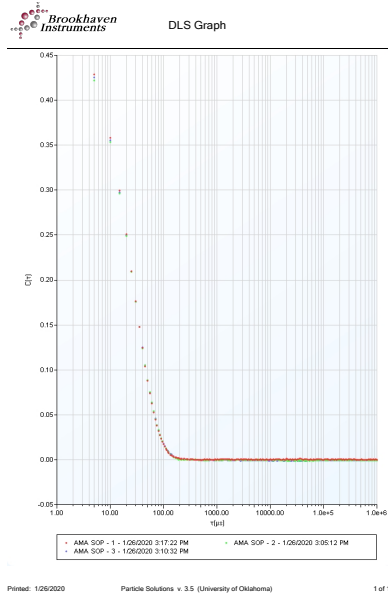
MSD Number Graph



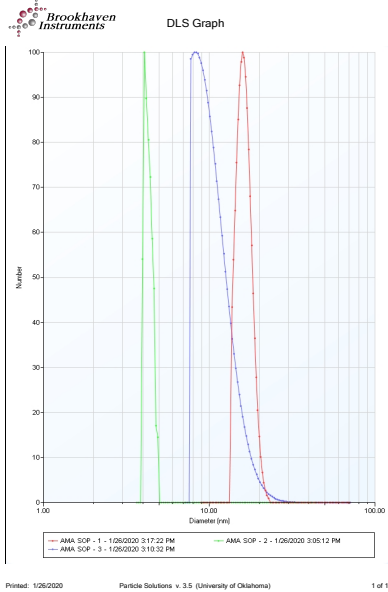
Figures 70-72: C8 Reference: 17 g NaCl/100 mL DI water PD = 0.076, CR = 144.7

Correlation Graph

MSD Intensity Graph



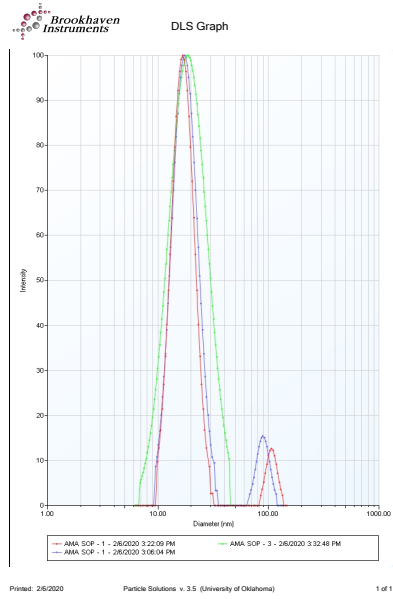
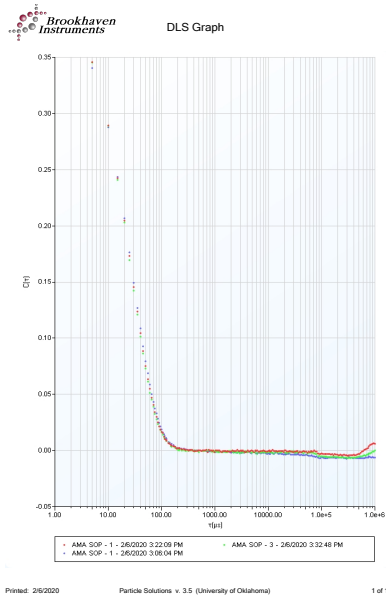
MSD Number Graph



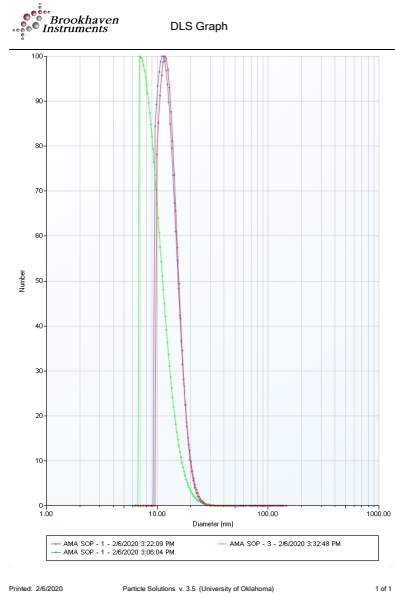
Figures 73-75: C8 Reference: 18 g NaCl/100 mL DI water PD = 0.129, CR = 80.7

Correlation Graph

MSD Intensity Graph



MSD Number Graph

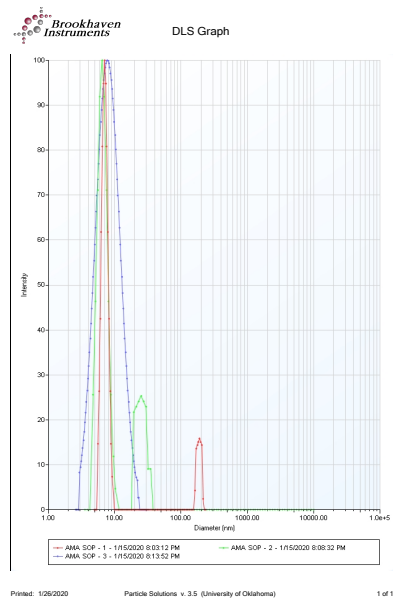
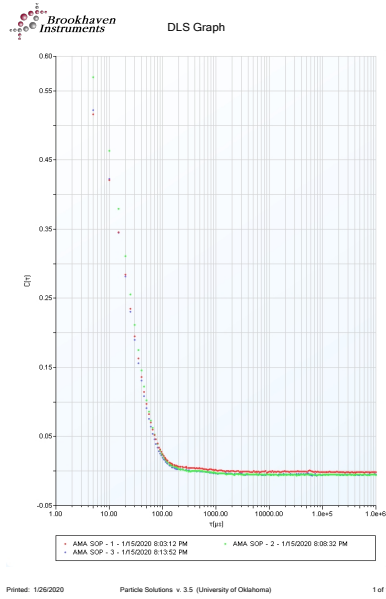


B.2. SDHS & PDADMAC Systems

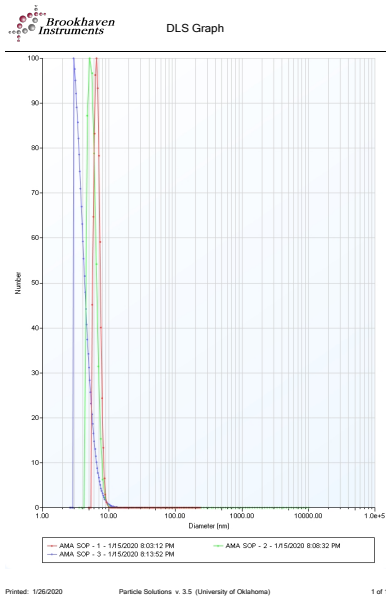
Figures 76-78: C6 0.05 g PDADMAC/100 mL: 2 g NaCl/100 mL DI water PD = 0.141, CR = 112.6

Correlation Graph

MSD Intensity Graph



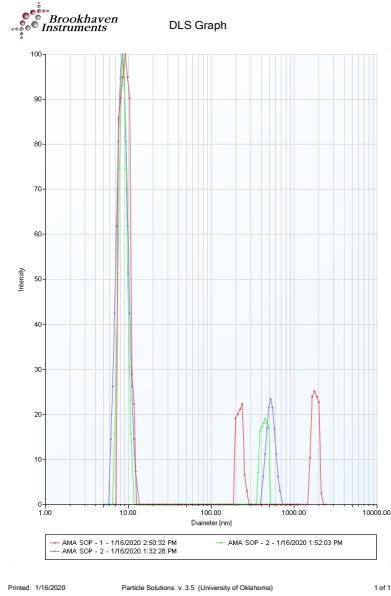
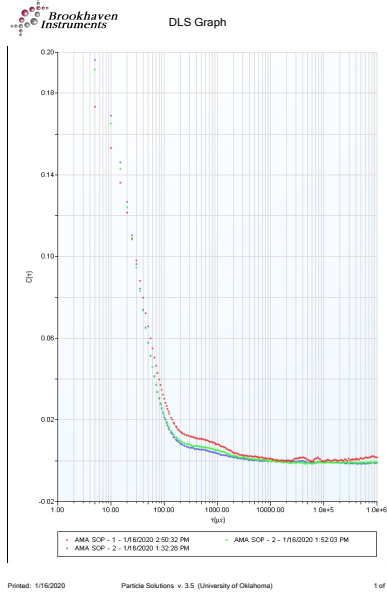
MSD Number Graph



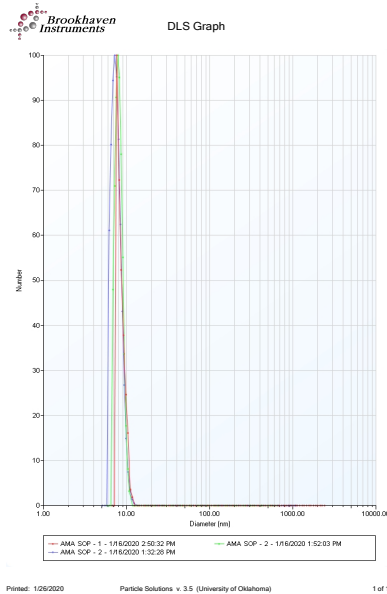
Figures 79-81: C6 0.05 g PDADMAC/100 mL: 3 g NaCl/100 mL DI water PD = 0.121, CR = 508.5

Correlation Graph

MSD Intensity Graph



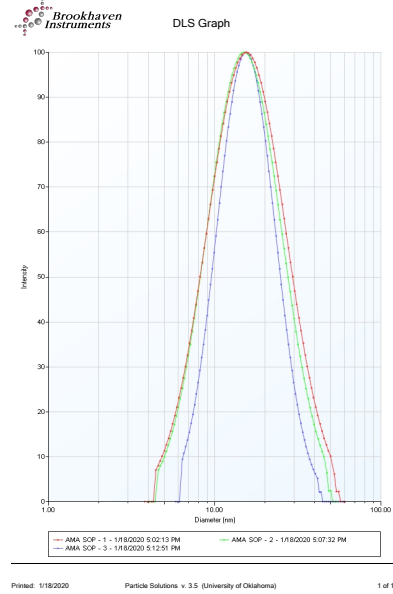
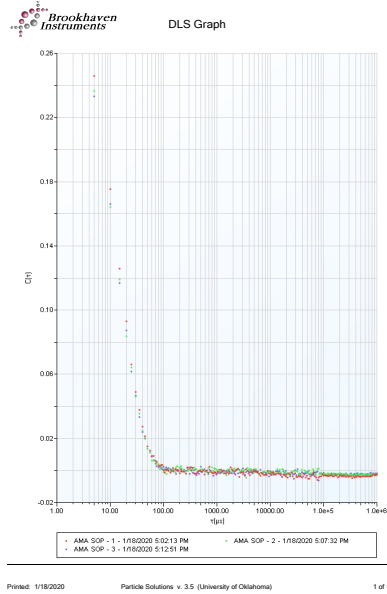
MSD Number Graph



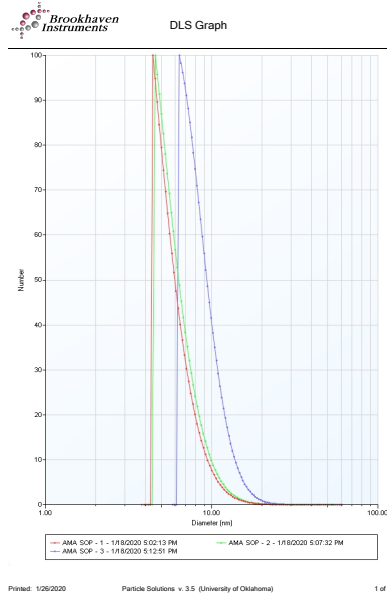
Figures 82-84: C6 0.05 g PDADMAC/100 mL: 14 g NaCl/100 mL DI water, PD = 0.141, CR = 26.5

Correlation Graph

MSD Intensity Graph



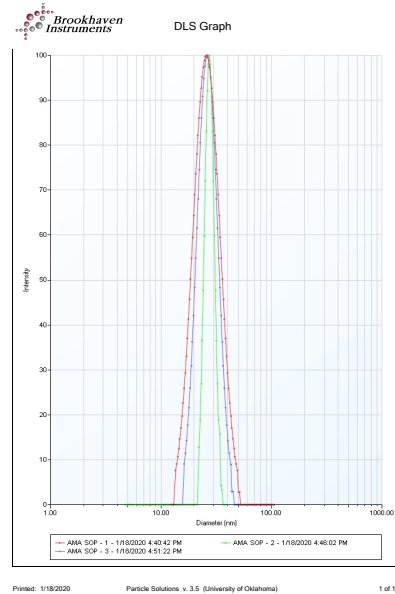
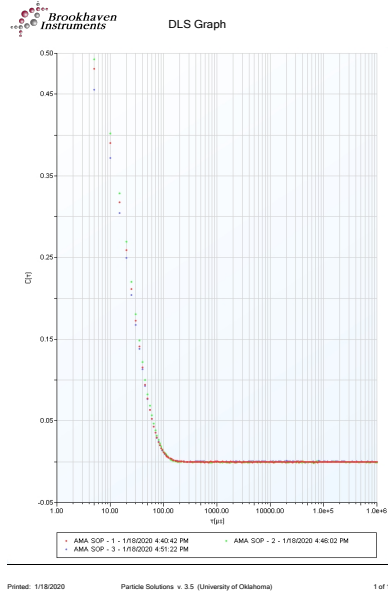
MSD Number Graph



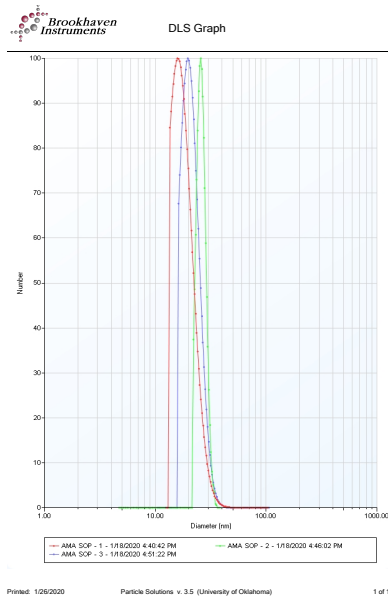
**Figures 85-87: C6 0.05 g PDADMAC/100 mL: 15 g NaCl/100 mL DI water PD = 0.056,
CR = 252.3**

Correlation Graph

MSD Intensity Graph



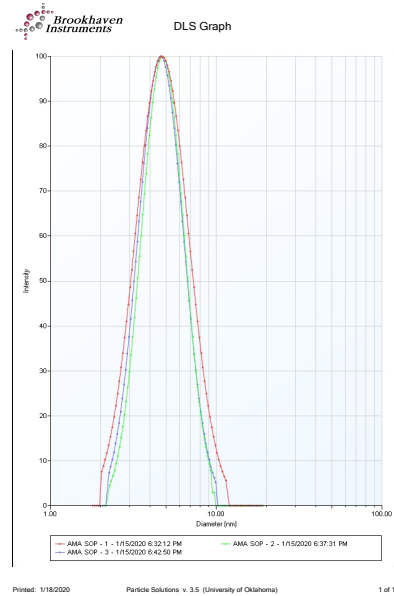
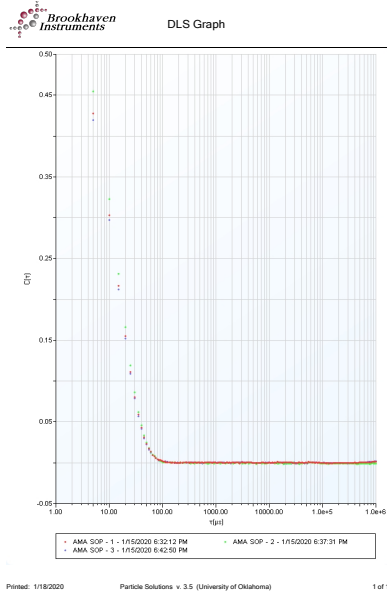
MSD Number Graph



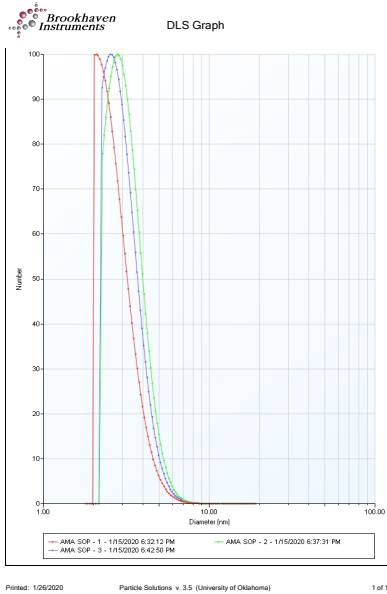
Figures 88-90: C6 0.1 g PDADMAC/100 mL: 1 g NaCl/100 mL DI water PD = 0.088, CR = 126.1

Correlation Graph

MSD Intensity Graph



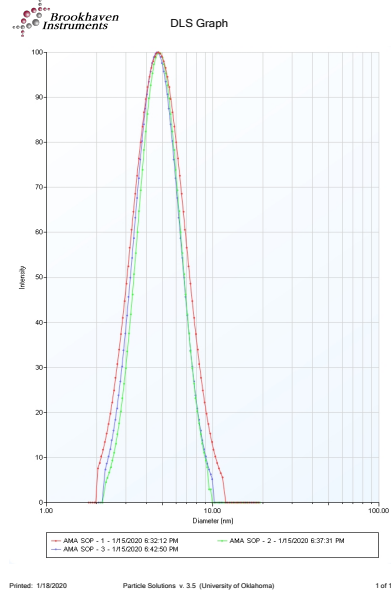
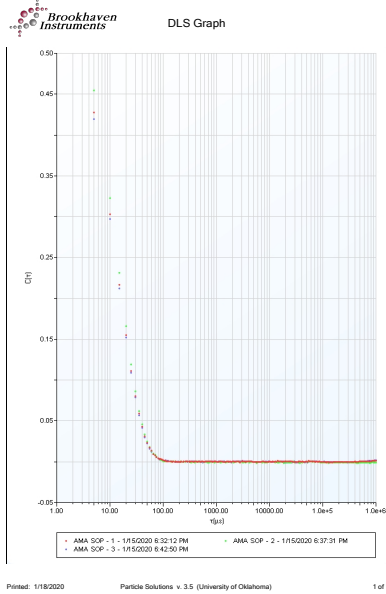
MSD Number Graph



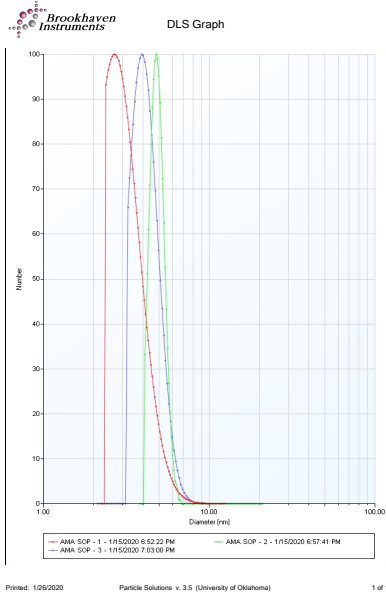
Figures 91-93: C6 0.1 g PDADMAC/100 mL: 2 g NaCl/100 mL DI water PD = 0.049, CR = 165.2

Correlation Graph

MSD Intensity Graph



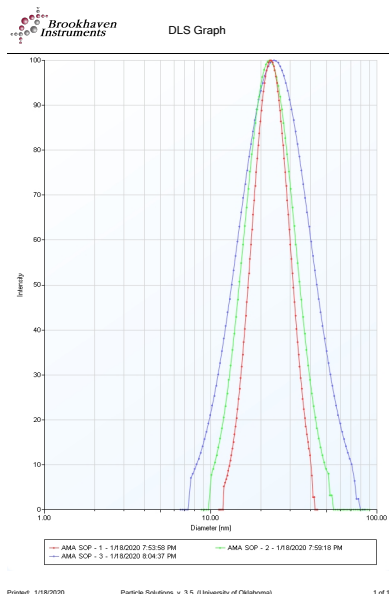
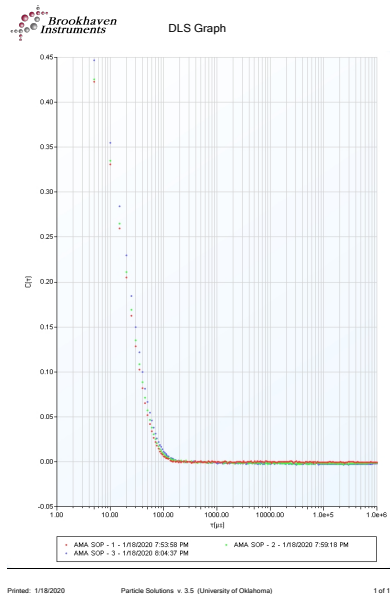
MSD Number Graph



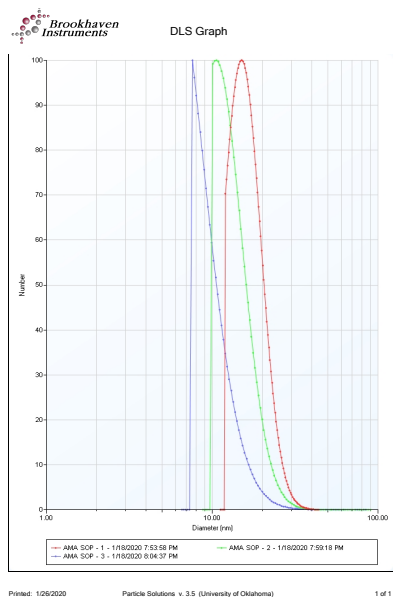
Figures 94-96: C6 0.1 g PDADMAC/100 mL: 13 g NaCl/100 mL DI water PD = 0.109, CR = 87.8

Correlation Graph

MSD Intensity Graph



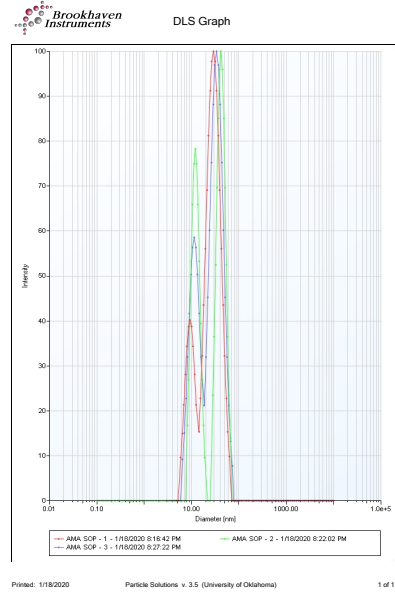
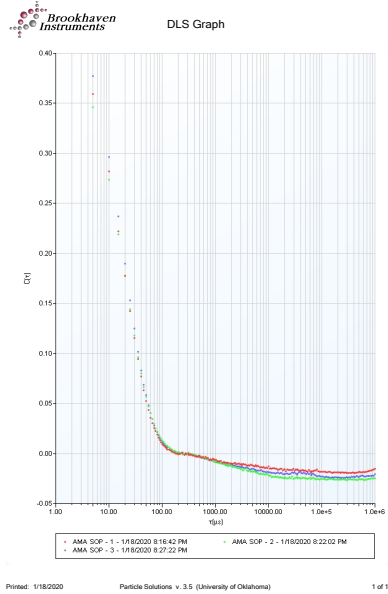
MSD Number Graph



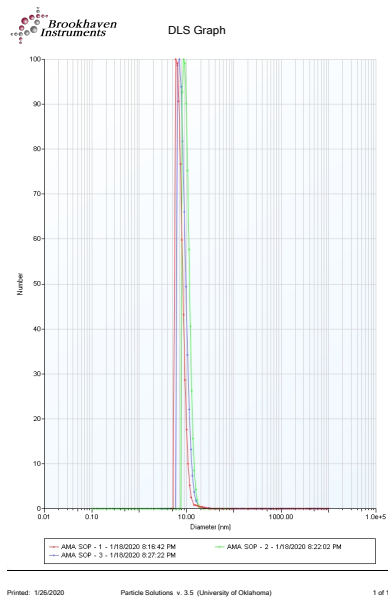
Figures 97-99: C6 0.1 g PDADMAC/100 mL: 14 g NaCl/100 mL DI water PD = 0.185, CR = 72.72

Correlation Graph

MSD Intensity Graph



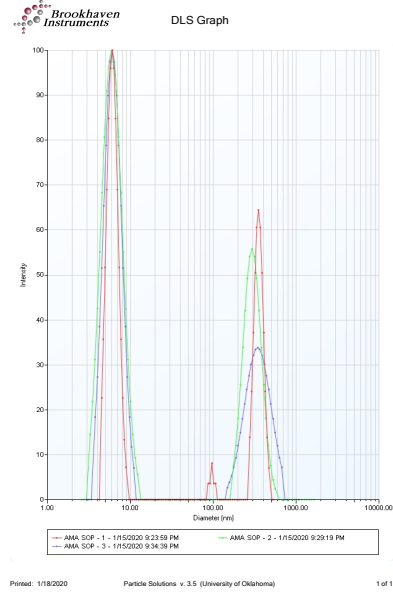
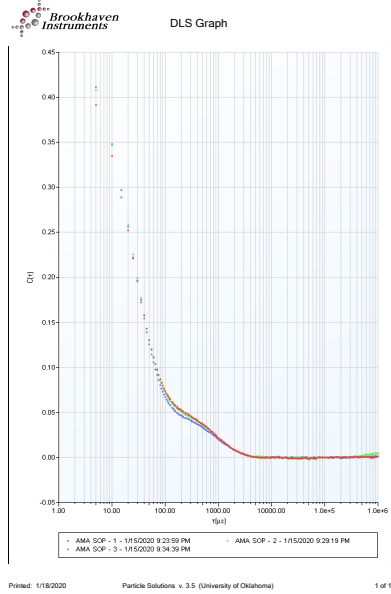
MSD Number Graph



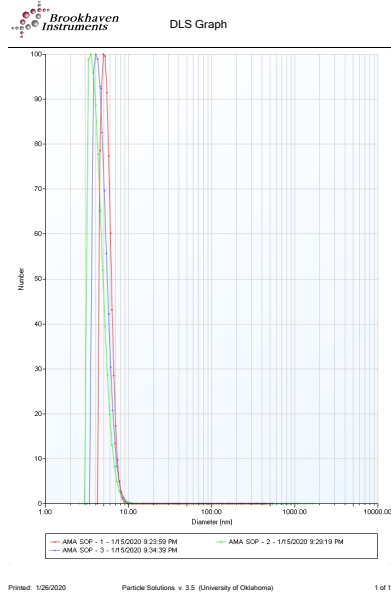
**Figures 100-102: C6 0.2g PDADMAC/100 mL: 2 g NaCl/100 mL DI water PD = 0.242,
CR = 262.7**

Correlation Graph

MSD Intensity Graph



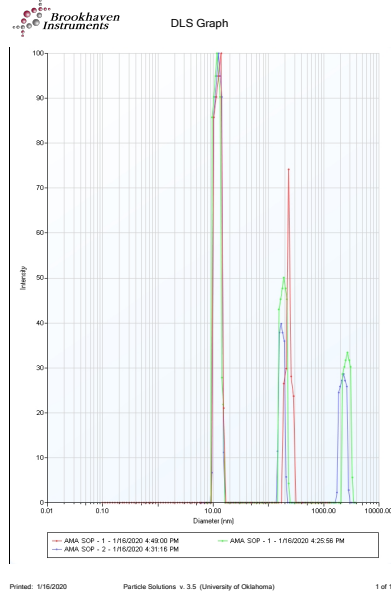
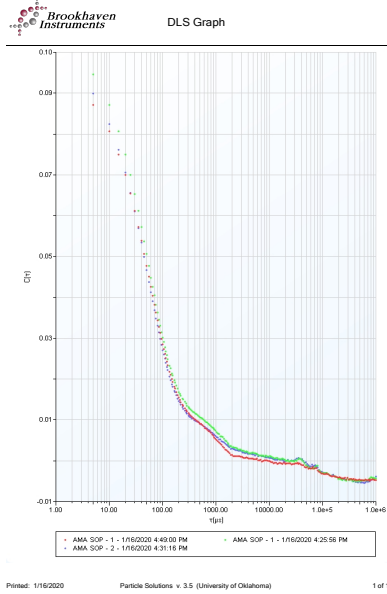
MSD Number Graph



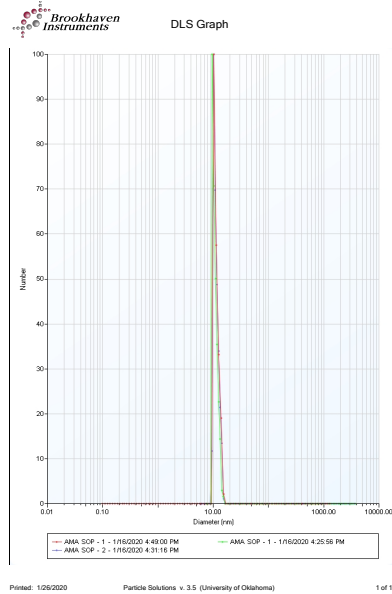
Figures 103-105: C6 0.2 PDADMAC/100 mL: 3 g NaCl/100 mL DI water PD = 0.147, CR = 477.7

Correlation Graph

MSD Intensity Graph



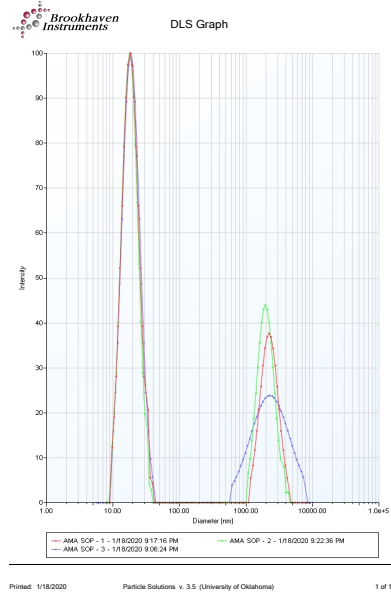
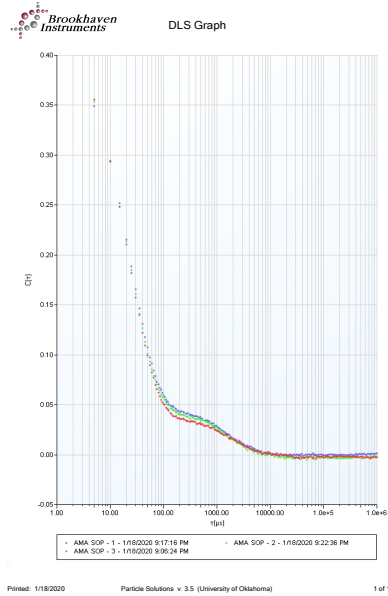
MSD Number Graph



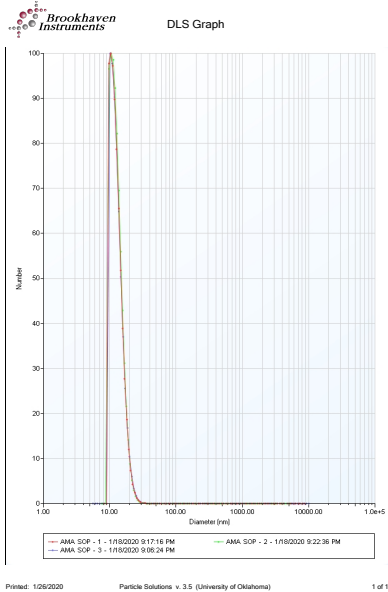
**Figures 106-108: C6 0.2 g PDADMAC/100 mL: 13 g NaCl/100 mL DI water PD = 0.236,
CR = 55.9**

Correlation Graph

MSD Intensity Graph

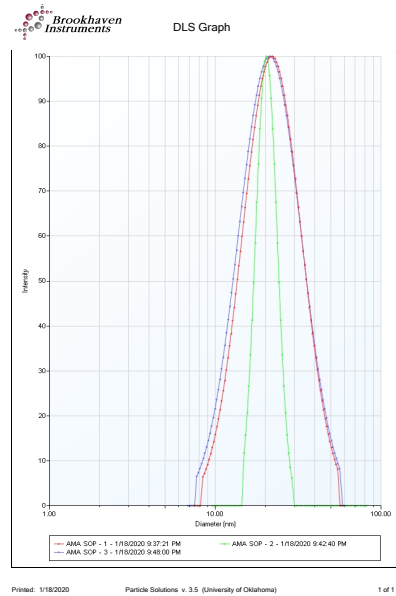
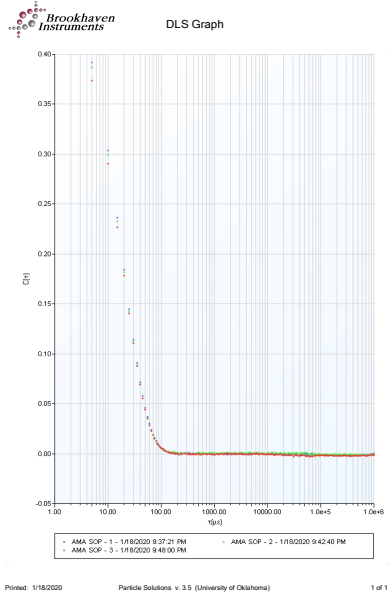


MSD Number Graph

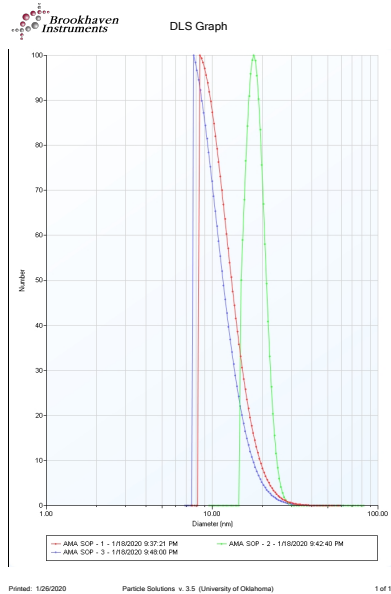


**Figures 109-111: C6 0.2 g PDADMAC/100 mL: 14 g NaCl/100 mL DI water PD = 0.112,
CR = 109.8**

Correlation Graph	MSD Intensity Graph
-------------------	---------------------

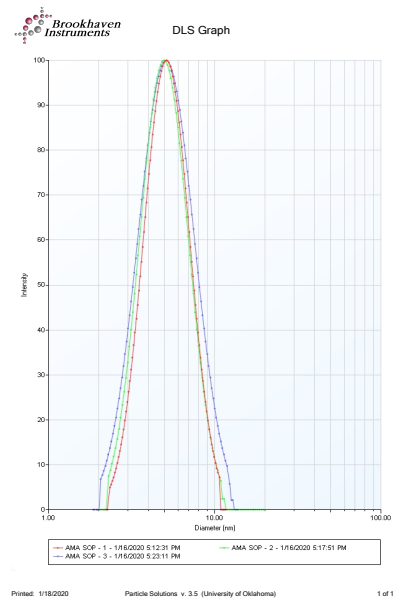
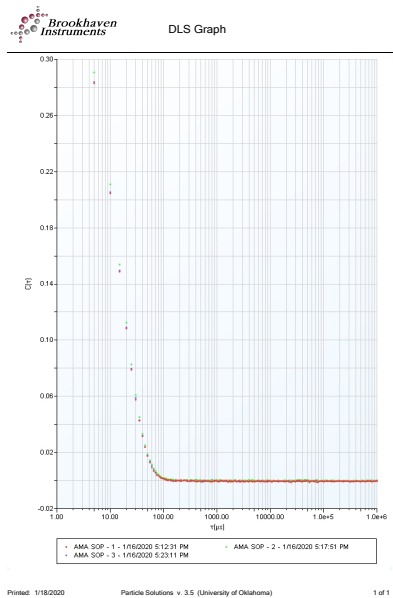


MSD Number Graph

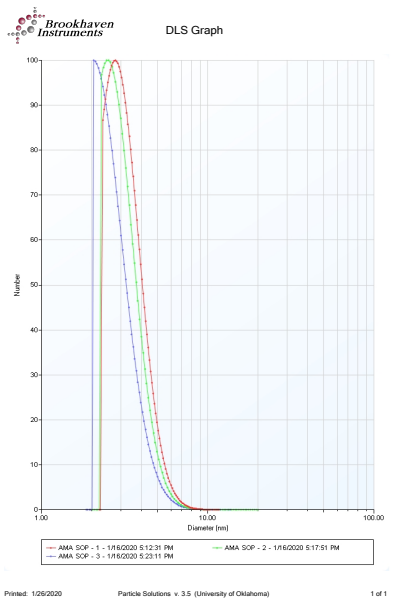


Figures 112-114: C7 0.05 g PDADMAC/100 mL: 2 g NaCl/100 mL DI water PD = 0.086, CR = 158.6

Correlation Graph	MSD Intensity Graph
-------------------	---------------------



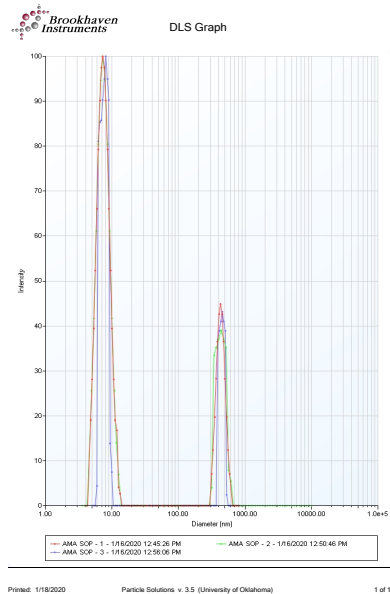
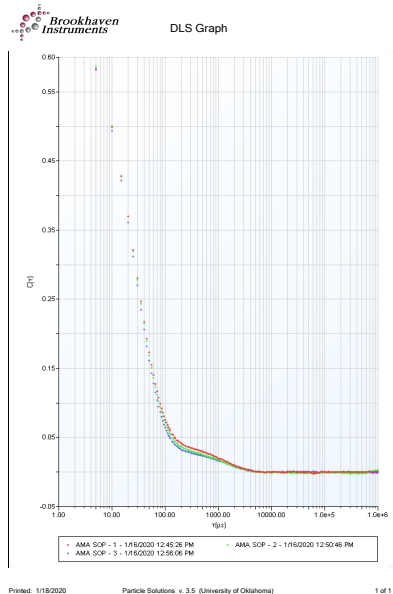
MSD Number Graph



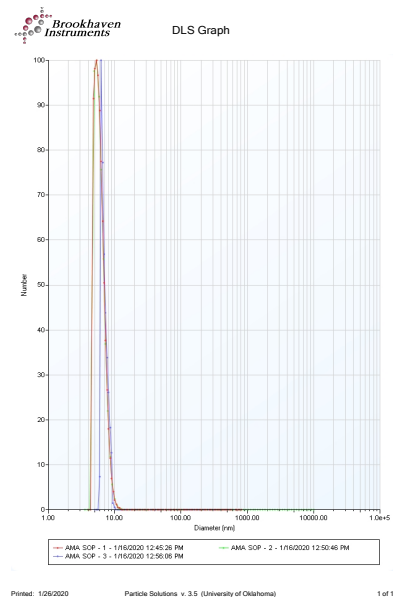
**Figures 115-117: C7 0.05 g PDADMAC/100 mL: 3 g NaCl/100 mL DI water PD = 0.172,
CR = 476.4**

Correlation Graph

MSD Intensity Graph



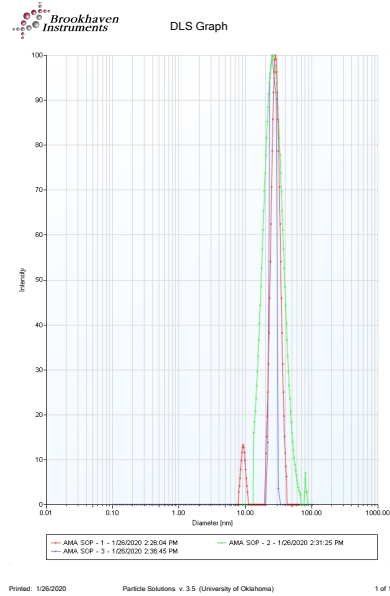
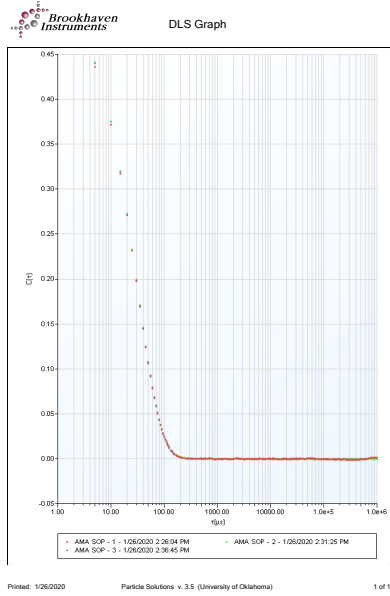
MSD Number Graph



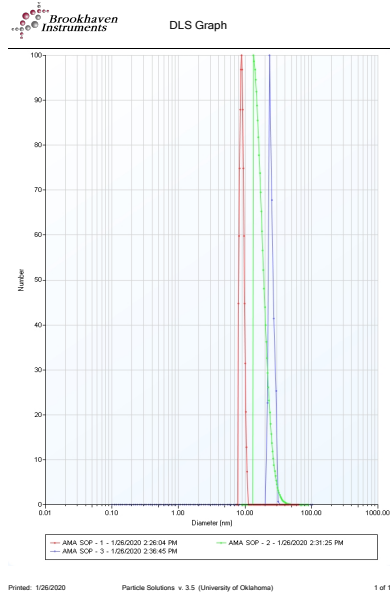
**Figures 118-120: C7 0.05 g PDADMAC/100 mL: 15 g NaCl/100 mL DI water PD = 0.074,
CR = 437.7**

Correlation Graph

MSD Intensity Graph



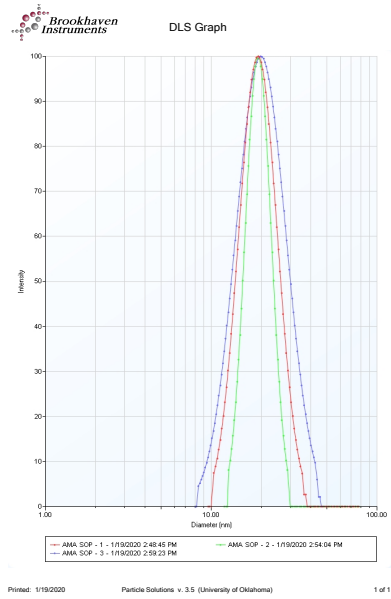
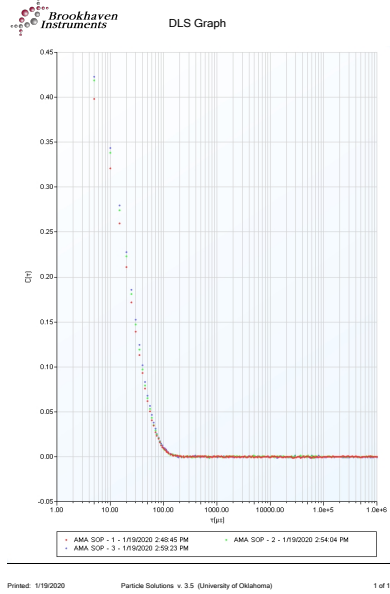
MSD Number Graph



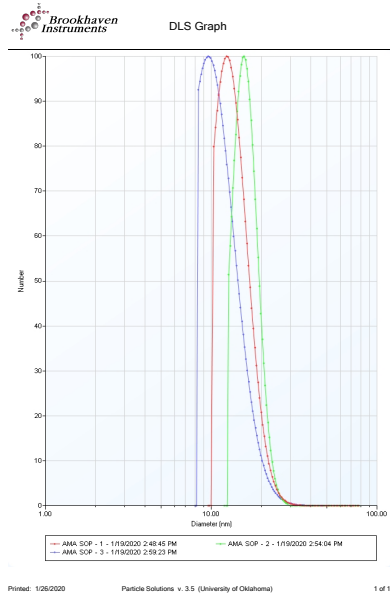
Figures 121-123: C7 0.05 g PDADMAC/100 mL: 16 g NaCl/100 mL DI water PD = 0.065, CR = 97.5

Correlation Graph

MSD Intensity Graph



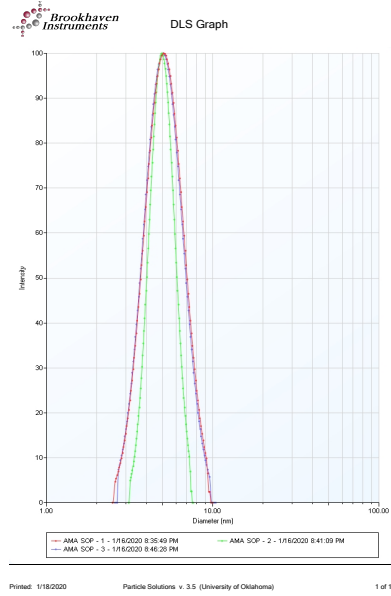
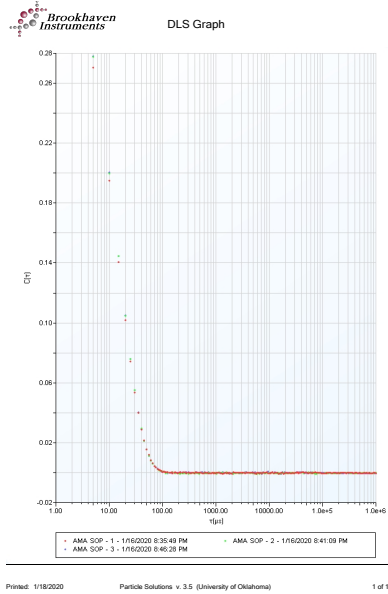
MSD Number Graph



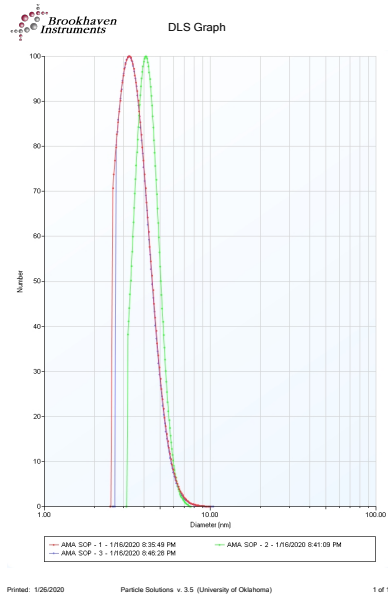
Figures 124-126: C7 0.1 g PDADMAC/100 mL: 2 g NaCl/100 mL DI water PD = 0.038, CR = 157.2

Correlation Graph

MSD Intensity Graph



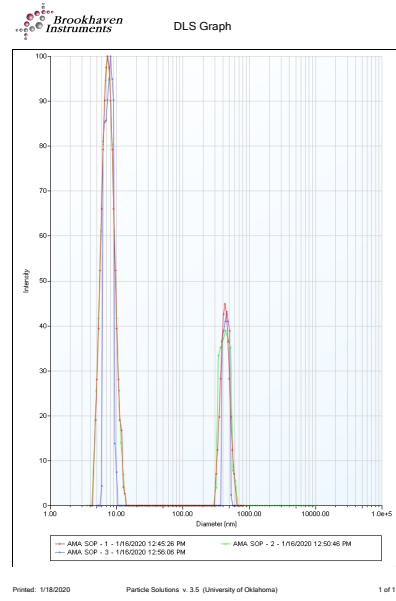
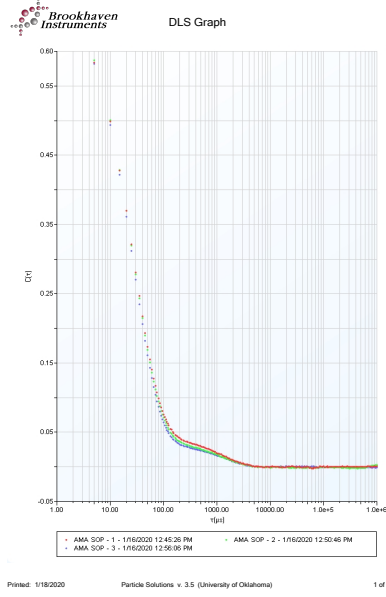
MSD Number Graph



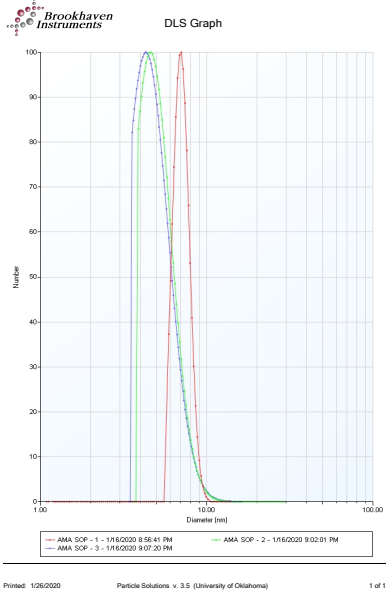
Figures 127-129: C7 0.1 g PDADMAC/100 mL: 3 g NaCl/100 mL DI water PD = 0.063,
CR = 247

Correlation Graph

MSD Intensity Graph



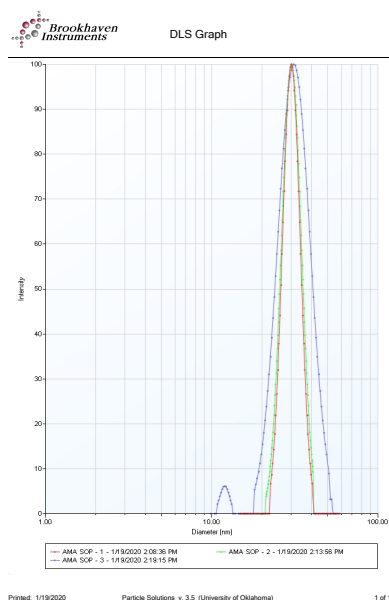
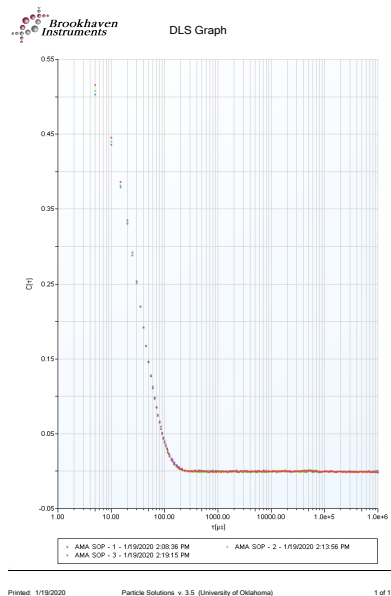
MSD Number Graph



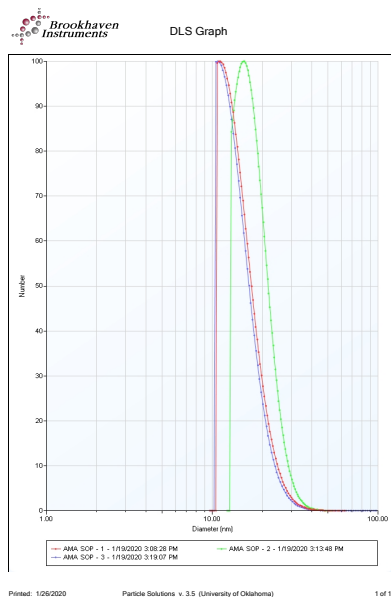
Figures 130-132: C7 0.1 g PDADMAC/100 mL: 15 g NaCl/100 mL DI water PD = 0.083, CR = 109.8

Correlation Graph

MSD Intensity Graph



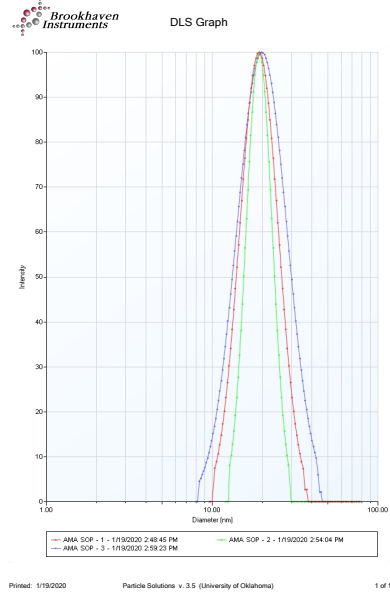
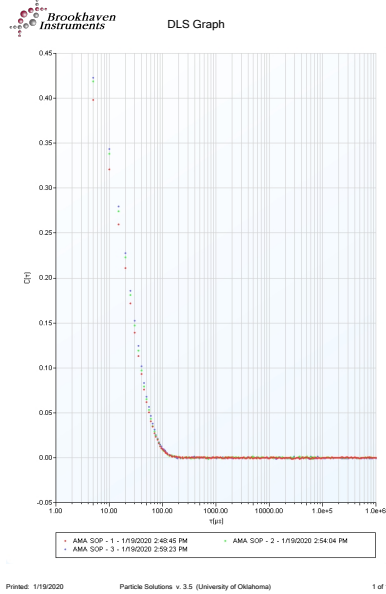
MSD Number Graph



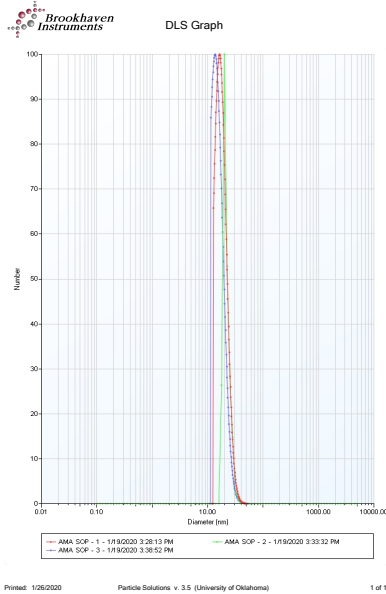
**Figures 133-135: C7 0.1 g PDADMAC/100 mL: 16 g NaCl/100 mL DI water PD = 0.061,
CR = 138.5**

Correlation Graph

MSD Intensity Graph



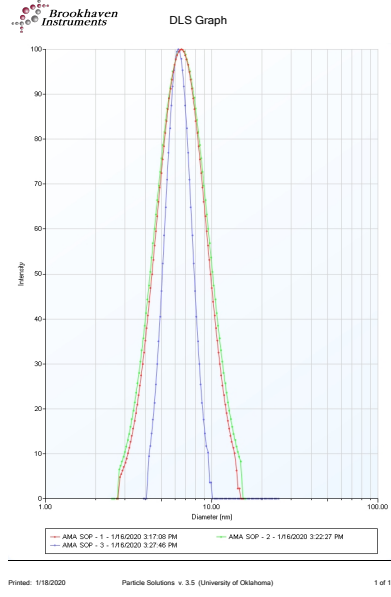
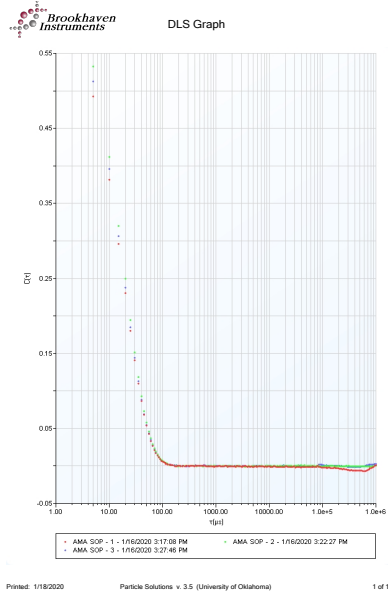
MSD Number Graph



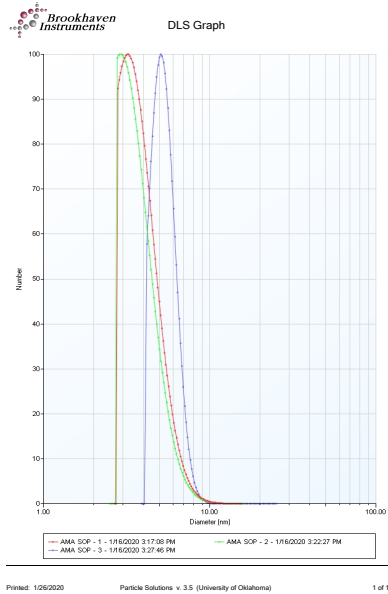
**Figures 136-138: C7 0.2 g PDADMAC/100 mL: 2 g NaCl/100 mL DI water PD = 0.083,
CR = 237.8**

Correlation Graph

MSD Intensity Graph



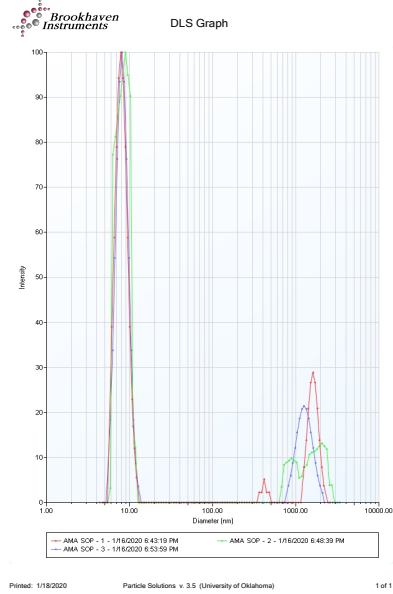
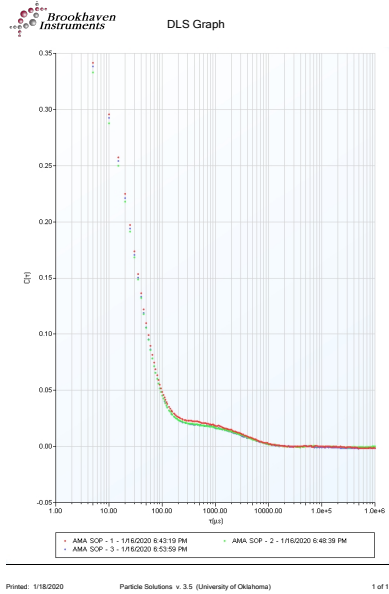
MSD Number Graph



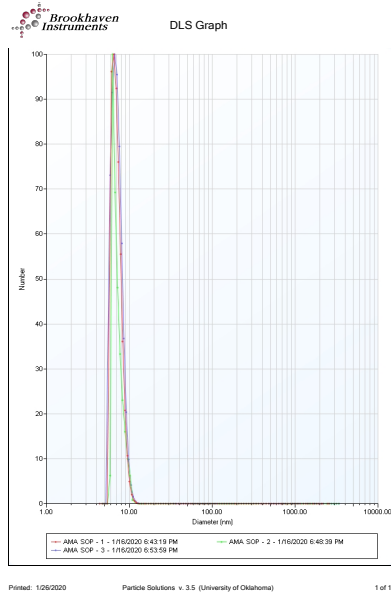
**Figures 139-141: C7 0.2 g PDADMAC/100 mL: 3 g NaCl/100 mL DI water PD = 0.173,
CR = 517.8**

Correlation Graph

MSD Intensity Graph



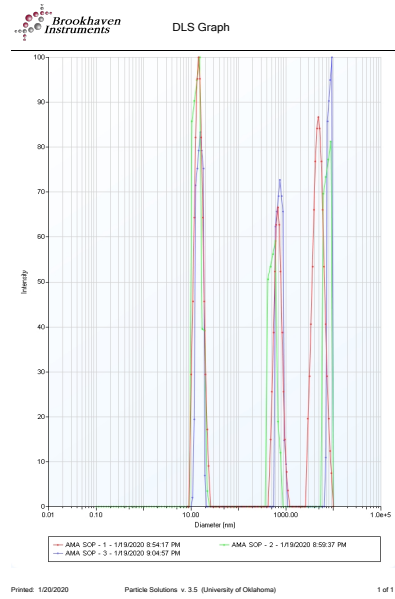
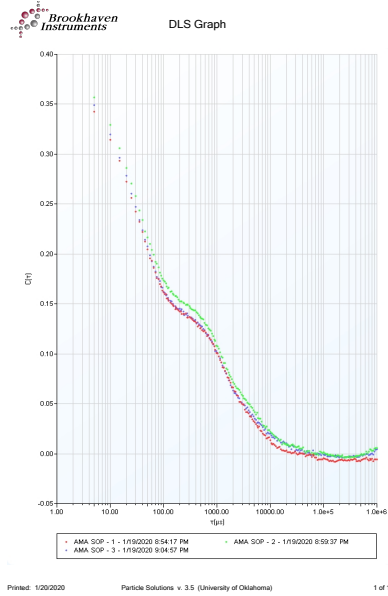
MSD Number Graph



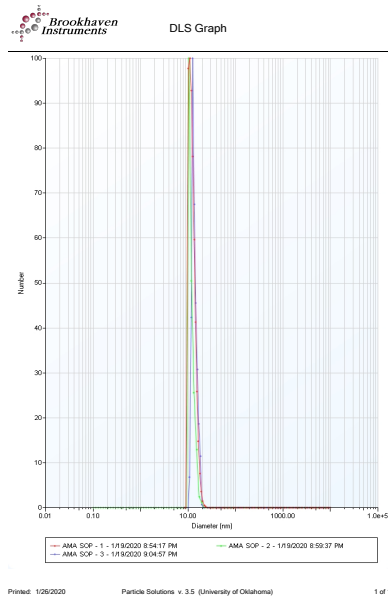
**Figures 142-144: C7 0.2 g PDADMAC/100 mL: 15 g NaCl/100 mL DI water PD = 0.272,
CR = 40**

Correlation Graph

MSD Intensity Graph

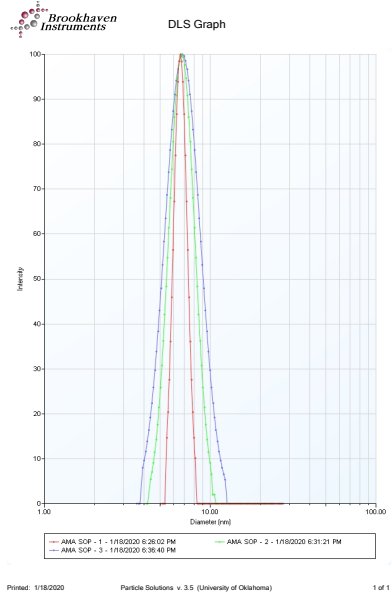
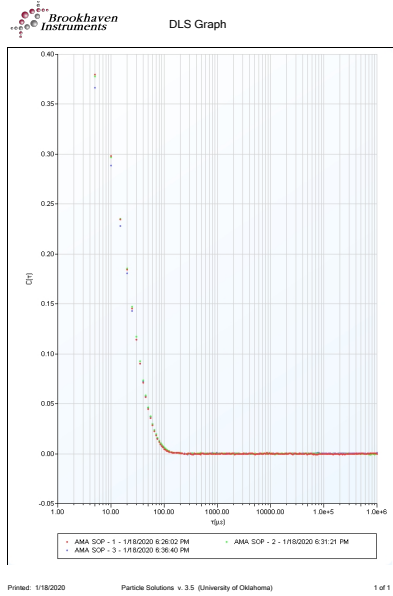


MSD Number Graph

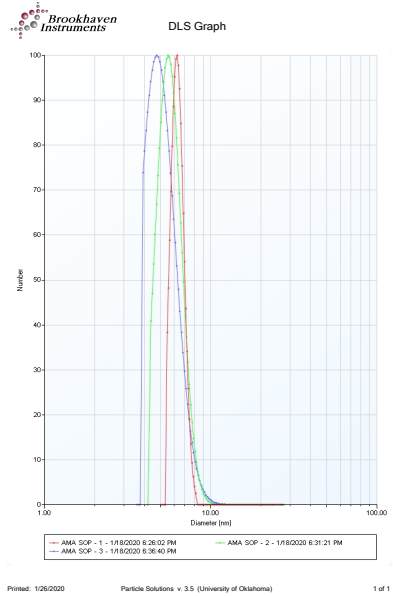


**Figures 145-147: C8 0.05 g PDADMAC/100 mL: 3 g NaCl/100 mL DI water PD = 0.074,
CR = 201.8**

Correlation Graph	MSD Intensity Graph
-------------------	---------------------



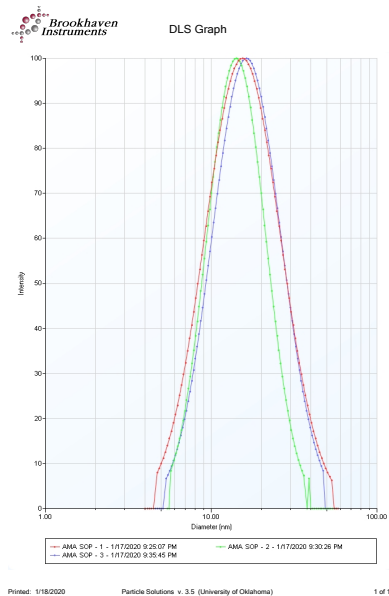
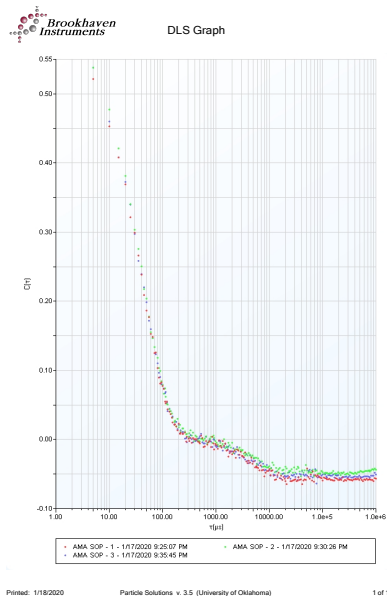
MSD Number Graph



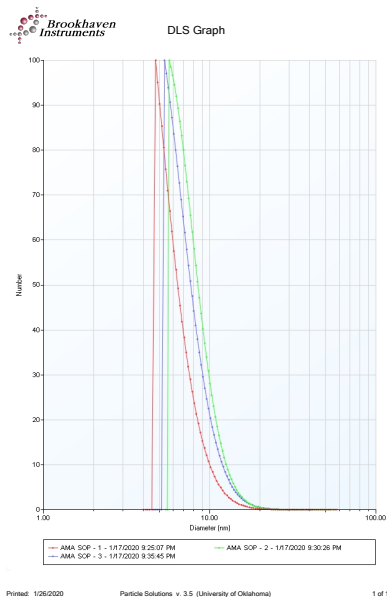
**Figures 148-150: C8 0.05 g PDADMAC/100 mL: 4 g NaCl/100 mL DI water PD = 0.211,
CR = 8.2**

Correlation Graph

MSD Intensity Graph



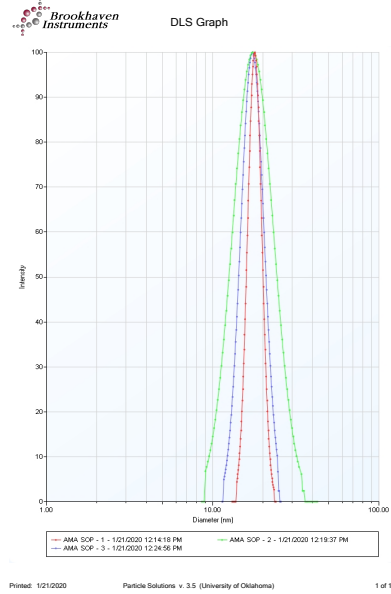
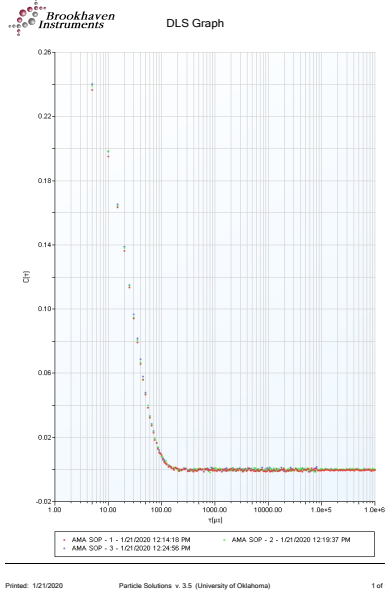
MSD Number Graph



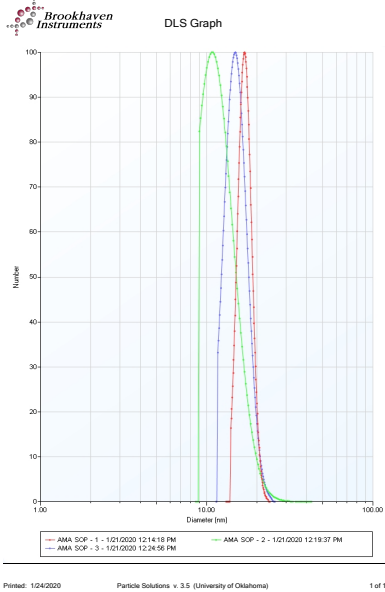
**Figures 151-153: C8 0.05 g PDADMAC/100 mL: 16 g NaCl/100 mL DI water PD = 0.034,
CR = 57.3**

Correlation Graph

MSD Intensity Graph



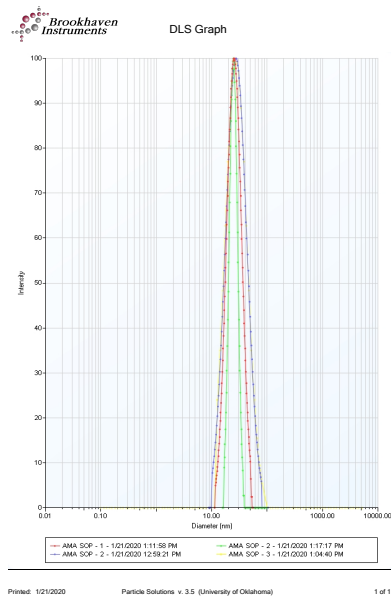
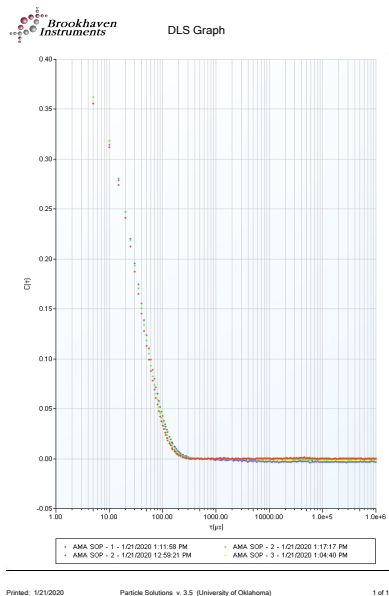
MSD Number Graph



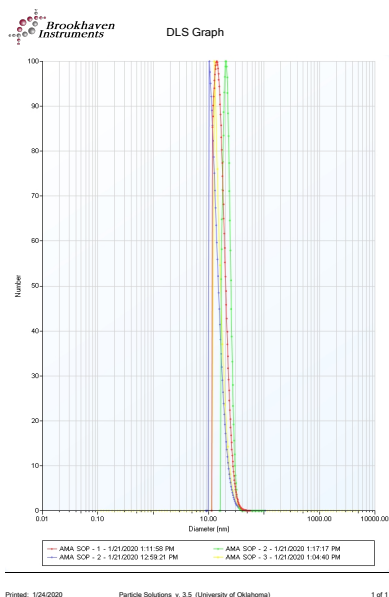
**Figures 154-156: C8 0.05 g PDADMAC/100 mL: 17 g NaCl/100 mL DI water PD = 0.11,
CR = 134**

Correlation Graph

MSD Intensity Graph



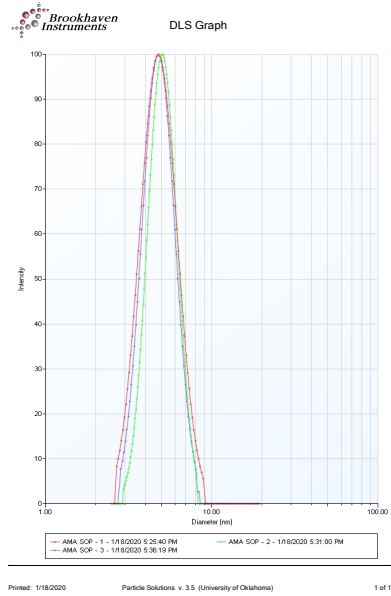
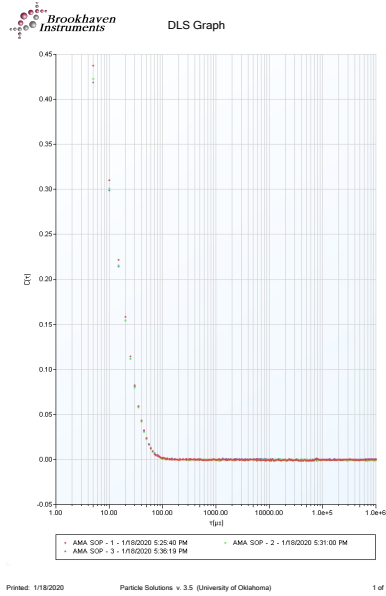
MSD Number Graph



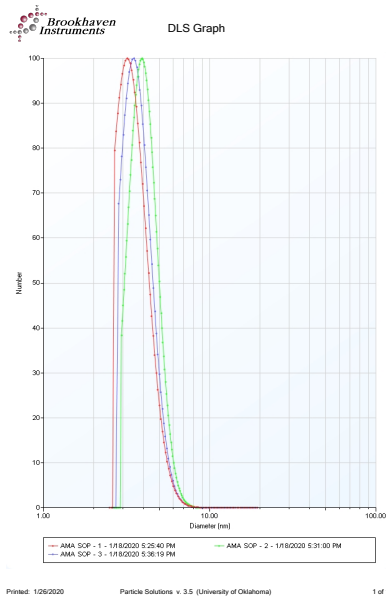
**Figures 157-159: C8 0.1 g PDADMAC/100 mL: 2 g NaCl/100 mL DI water PD = 0.071,
CR = 100.6**

Correlation Graph

MSD Intensity Graph



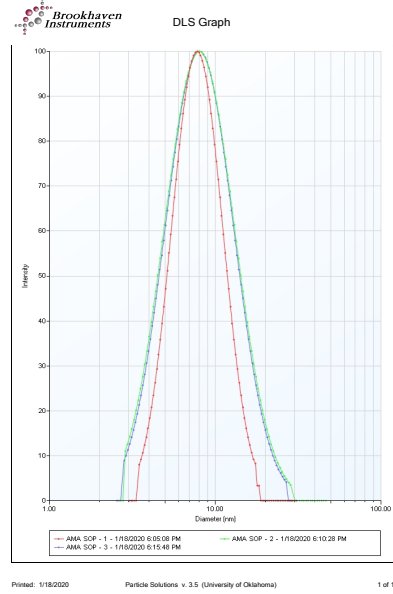
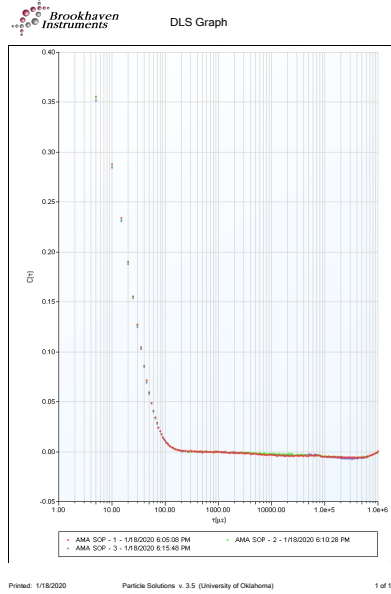
MSD Number Graph



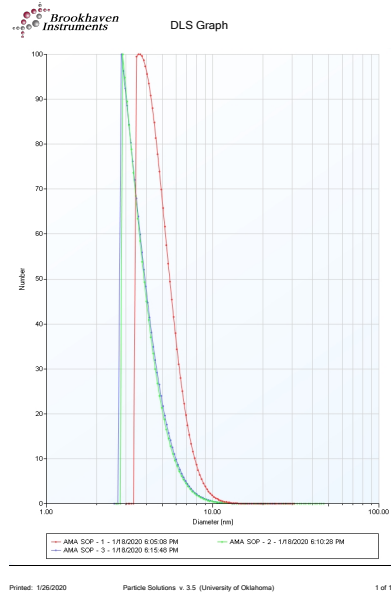
**Figures 160-162: C8 0.1 g PDADMAC/100 mL: 3 g NaCl/100 mL DI water PD = 0.137,
CR = 262.5**

Correlation Graph

MSD Intensity Graph



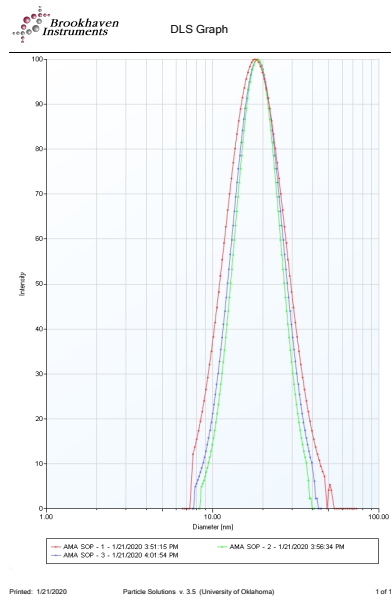
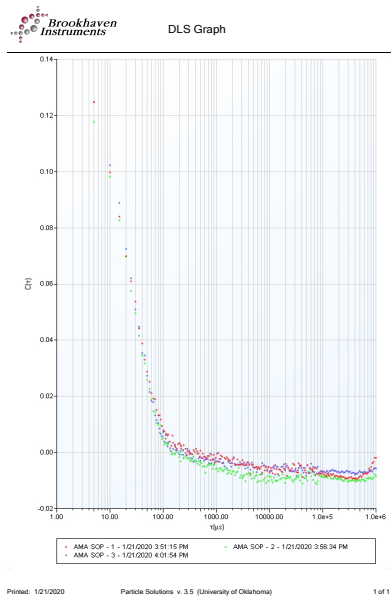
MSD Number Graph



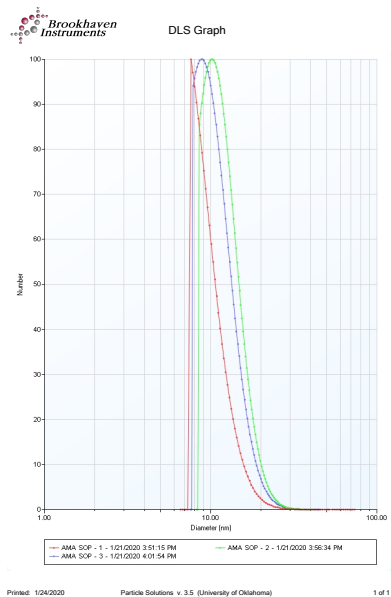
**Figures 163-165: C8 0.1 g PDADMAC/100 mL: 16 g NaCl/100 mL DI water PD = 0.147,
CR = 30.2**

Correlation Graph

MSD Intensity Graph



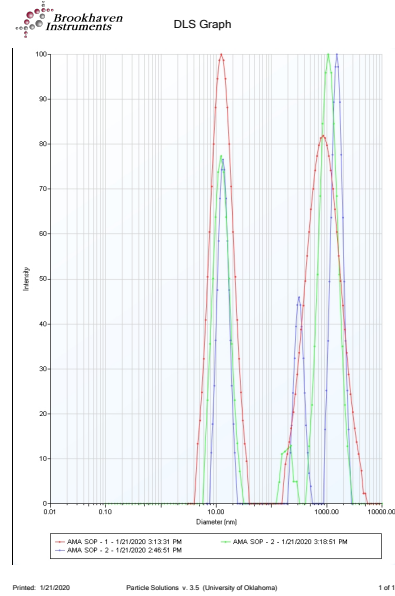
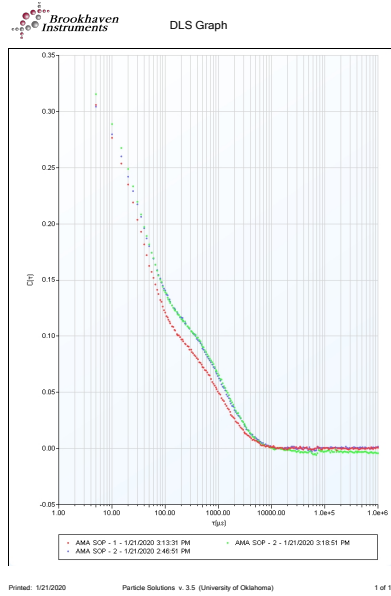
MSD Number Graph



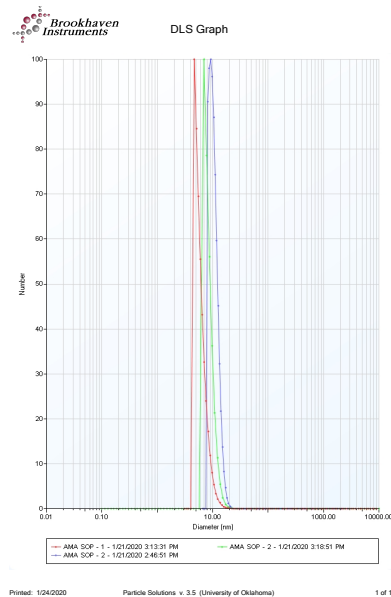
**Figures 166-168: C8 0.1 g PDADMAC/100 mL: 17 g NaCl/100 mL DI water PD = 0.354,
CR = 57.4**

Correlation Graph

MSD Intensity Graph



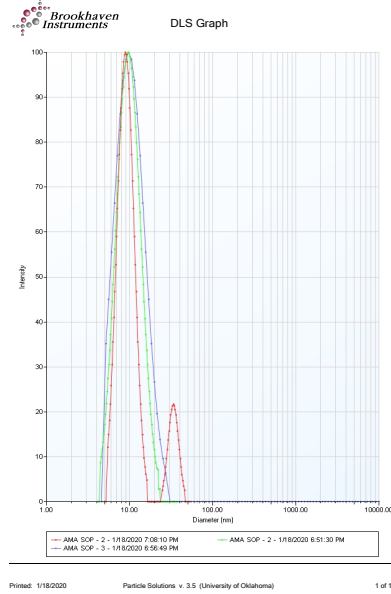
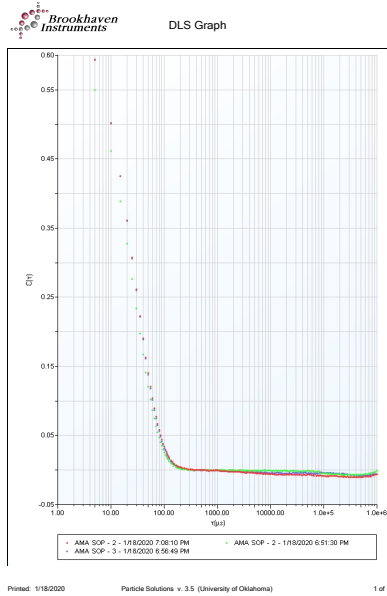
MSD Number Graph



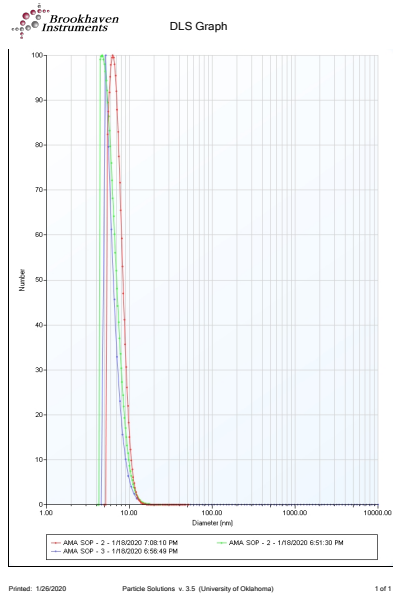
**Figures 169-171: C8 0.2 g PDADMAC/100 mL: 3 g NaCl/100 mL DI water PD = 0.115,
CR = 352.1**

Correlation Graph

MSD Intensity Graph



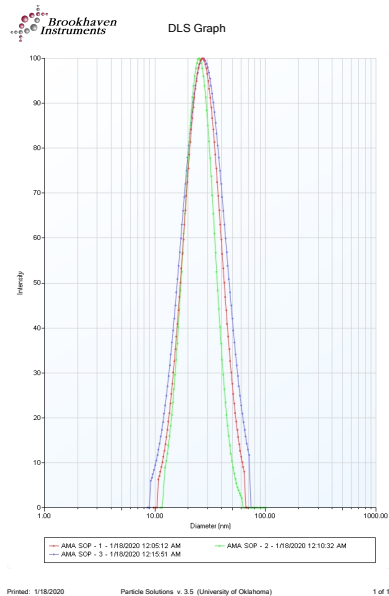
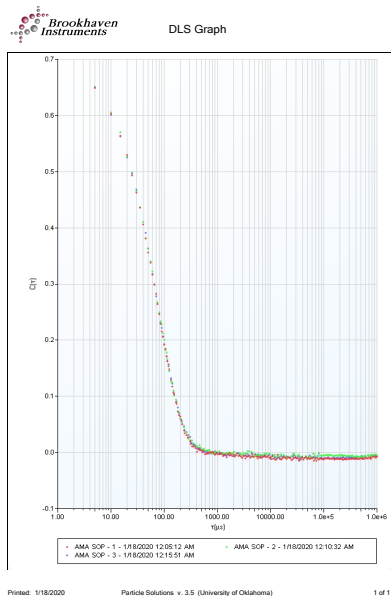
MSD Number Graph



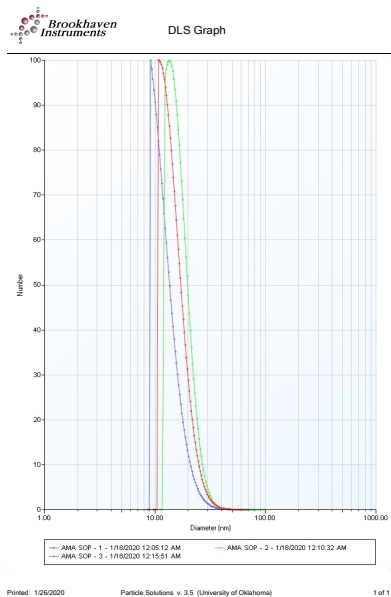
**Figures 172-174: C8 0.2 g PDADMAC/100 mL: 4 g NaCl/100 mL DI water PD = 0.151,
CR = 17.6**

Correlation Graph

MSD Intensity Graph



MSD Number Graph

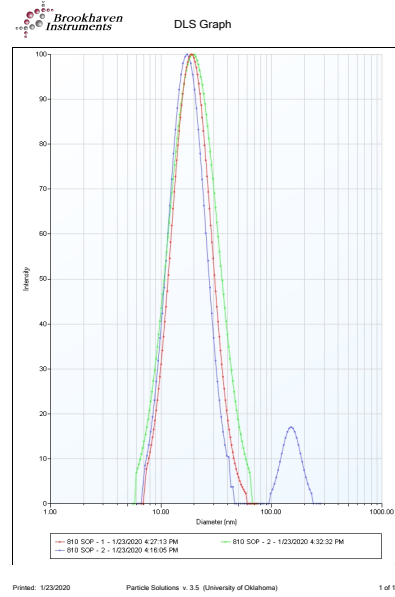
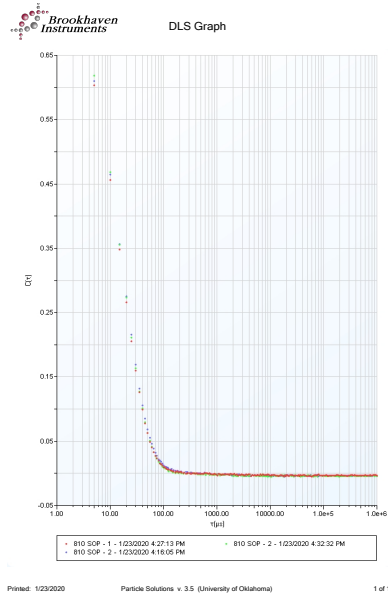


B.3. C₈₋₁₀E3.5 Reference Systems

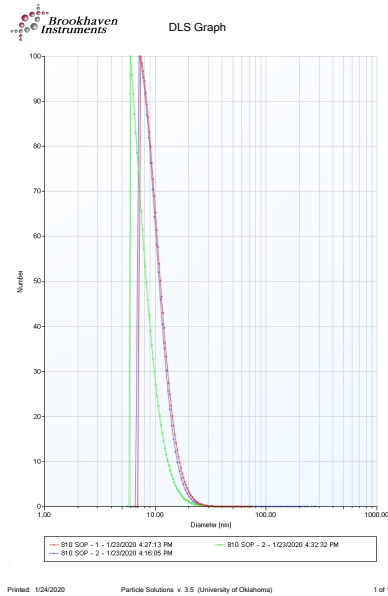
Figures 175-177: C6 Reference: 11 g NaCl/100 ml DI water PD = 0.166, CR = 56

Correlation Graph

MSD Intensity Graph



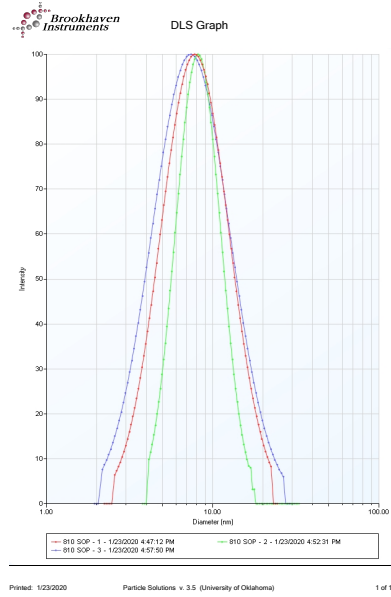
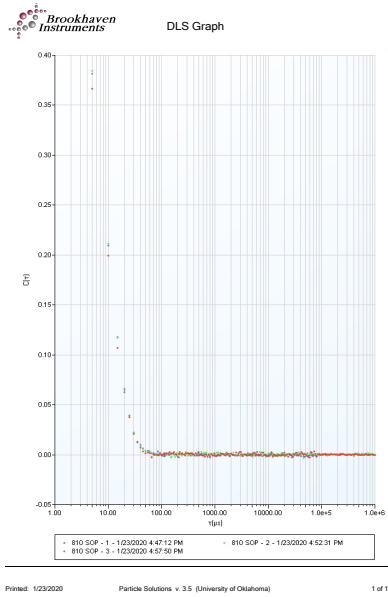
MSD Number Graph



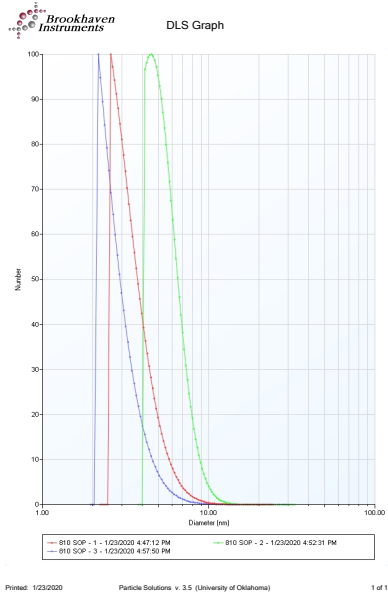
Figures 178-180: C6 Reference: 12 g NaCl/100 ml DI water PD = 0.13, CR = 28.2

Correlation Graph

MSD Intensity Graph



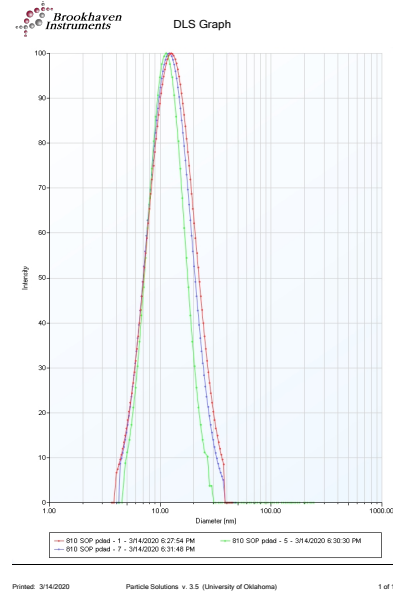
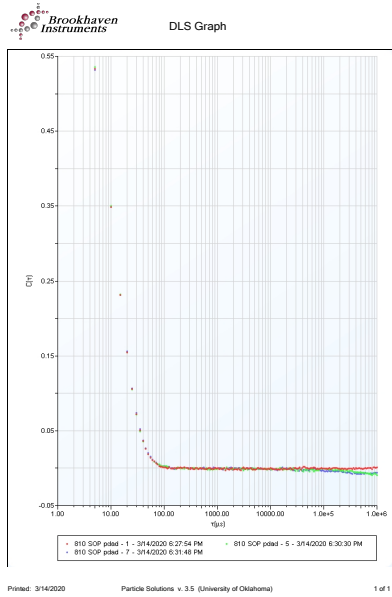
MSD Number Graph



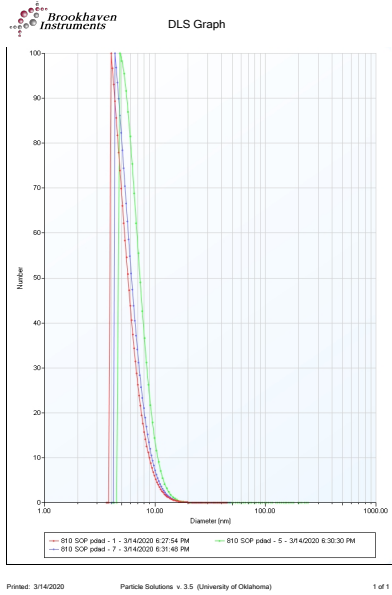
Figures 181-183: C6 Reference: 13 g NaCl/100 ml DI water PD = 0.148, CR = 489.9

Correlation Graph

MSD Intensity Graph



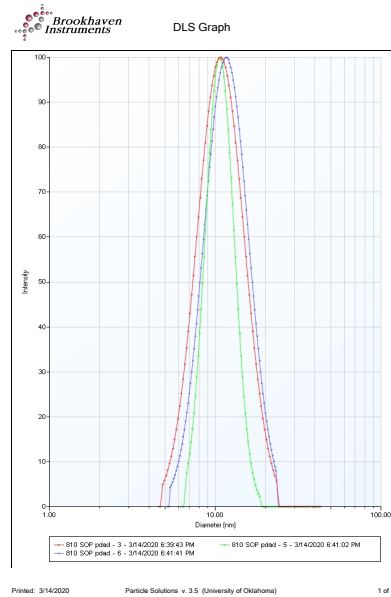
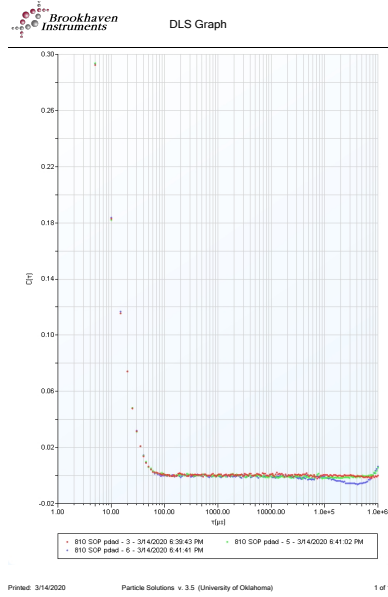
MSD Number Graph



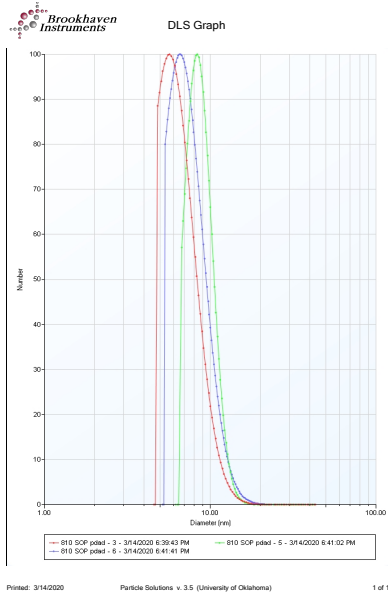
Figures 184-186: C6 Reference: 14 g NaCl/100 ml DI water PD = 0.109, CR = 448.7

Correlation Graph

MSD Intensity Graph



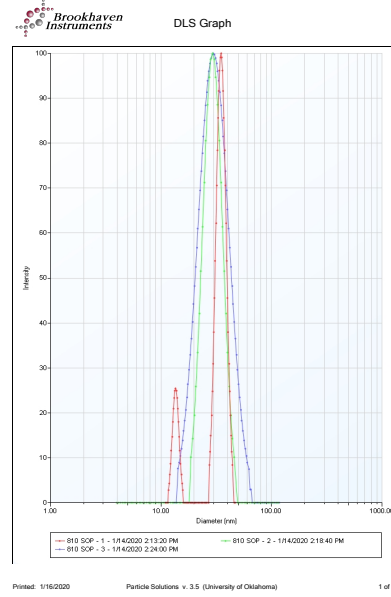
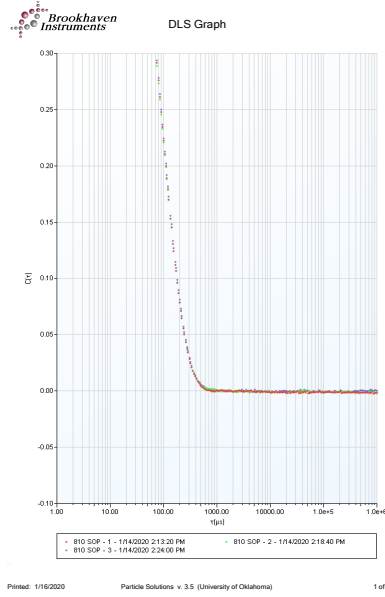
MSD Number Graph



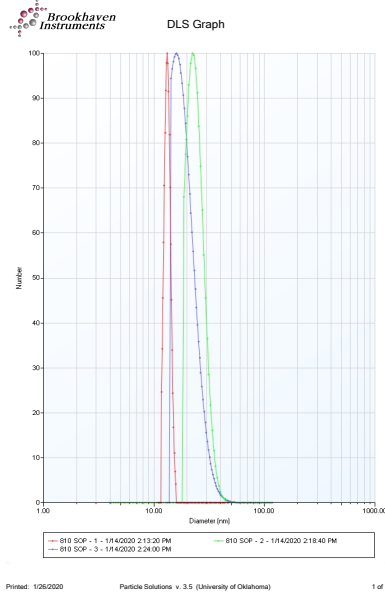
Figures 187-189: C7 Reference: 0 g NaCl/100 ml DI water PD = 0.117, CR = 503.1

Correlation Graph

MSD Intensity Graph



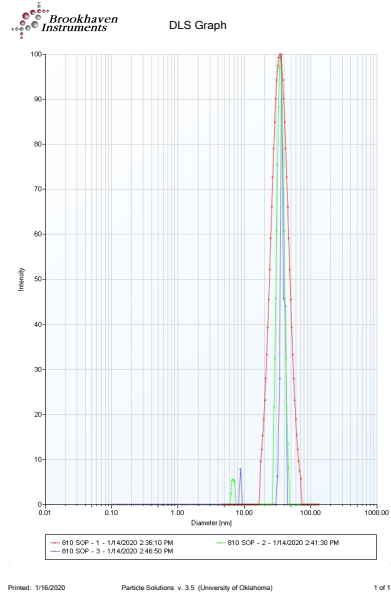
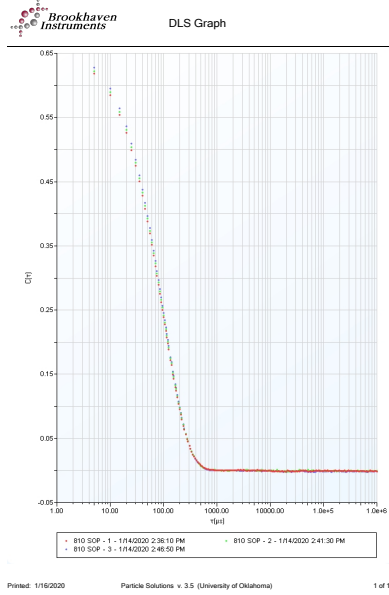
MSD Number Graph



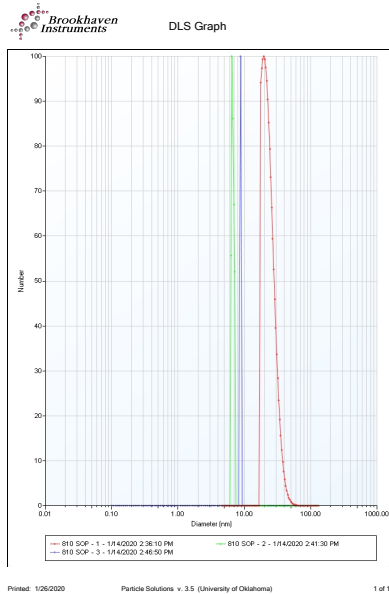
Figures 190-192: C7 Reference: 0.5 g NaCl/100 ml DI water PD = 0.118, CR = 576.2

Correlation Graph

MSD Intensity Graph



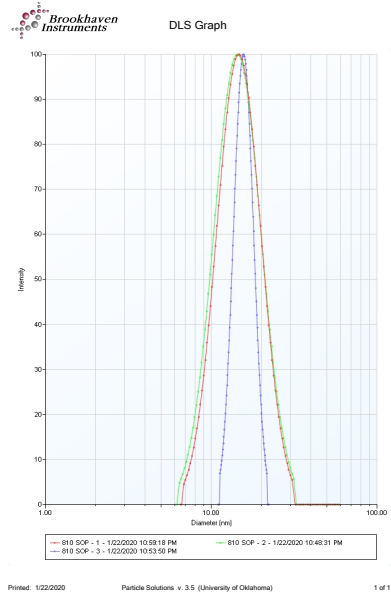
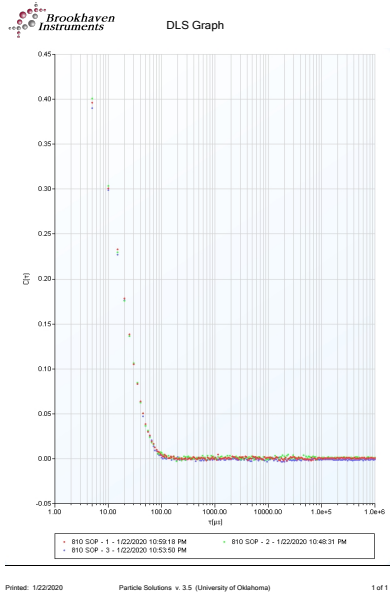
MSD Number Graph



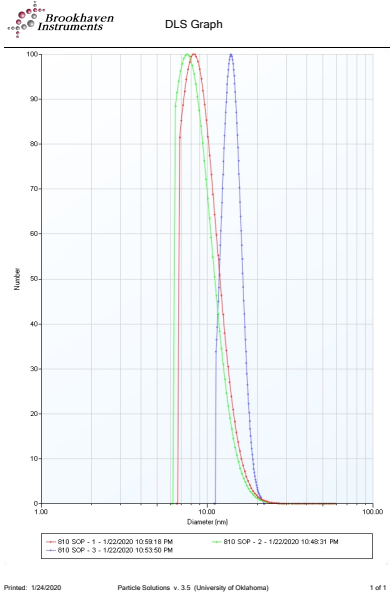
Figures 193-195: C7 Reference: 14 g NaCl/100 ml DI water PD = 0.1, CR = 26.4

Correlation Graph

MSD Intensity Graph



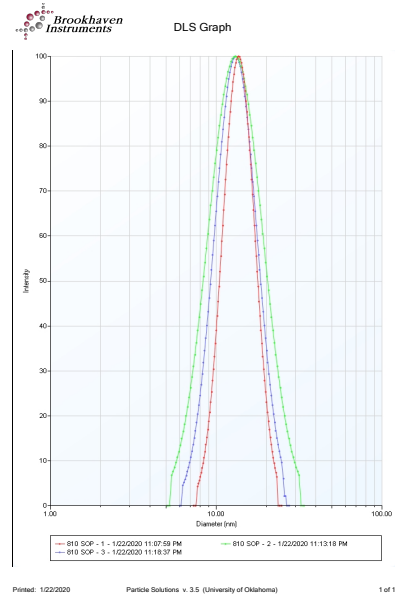
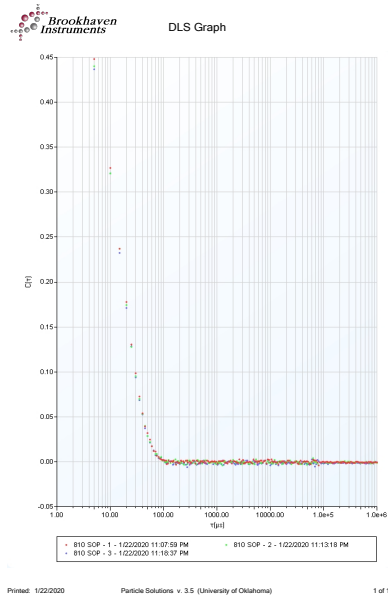
MSD Number Graph



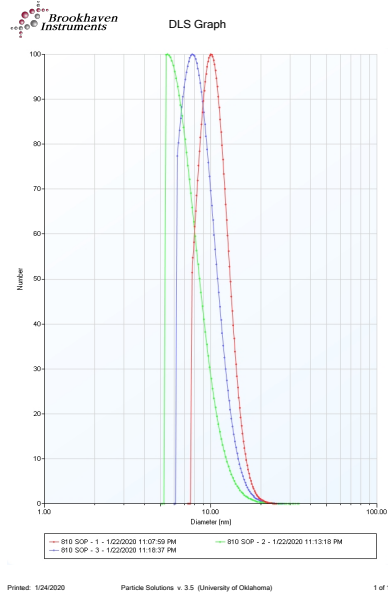
Figures 196-198: C7 Reference: 15 g NaCl/100 ml DI water PD = 0.063, CR = 23.1

Correlation Graph

MSD Intensity Graph



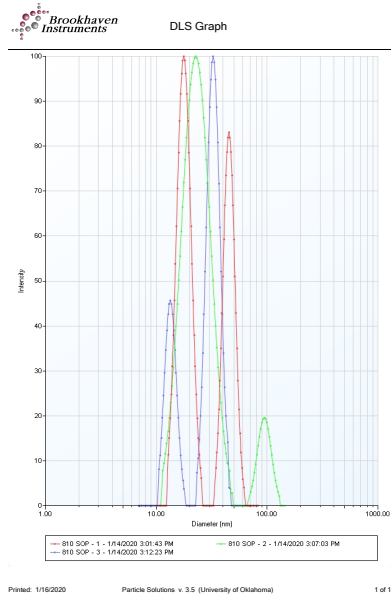
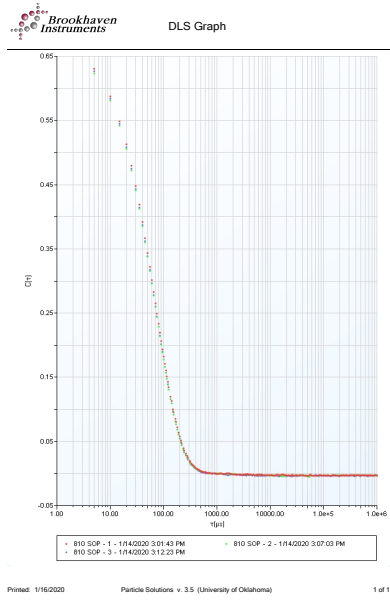
MSD Number Graph



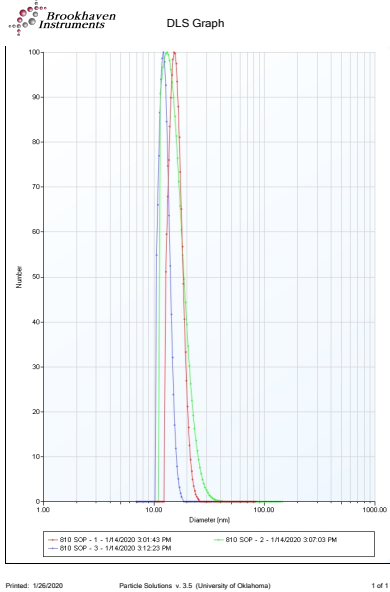
Figures 199-201: C8 Reference: 0.5 g NaCl/100 ml DI water PD = 0.152, CR = 452.9

Correlation Graph

MSD Intensity Graph



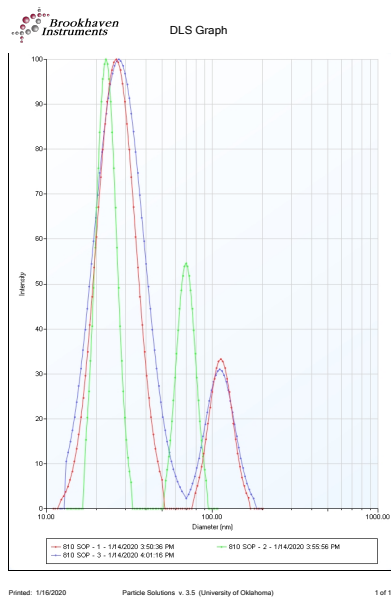
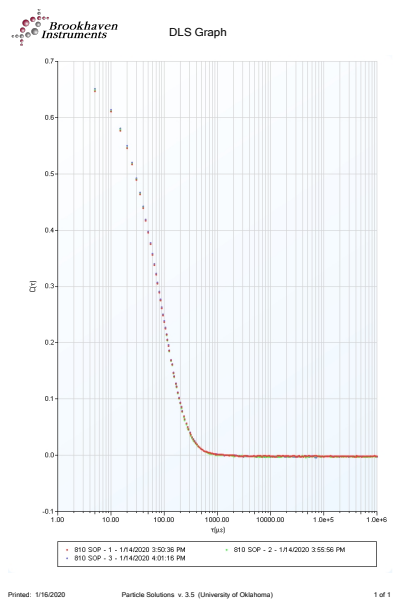
MSD Number Graph



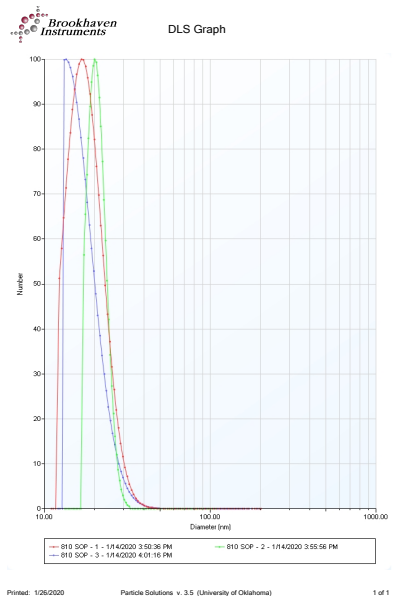
Figures 202-204: C8 Reference: 1 g NaCl/100 ml DI water PD = 0.186, CR = 408

Correlation Graph

MSD Intensity Graph



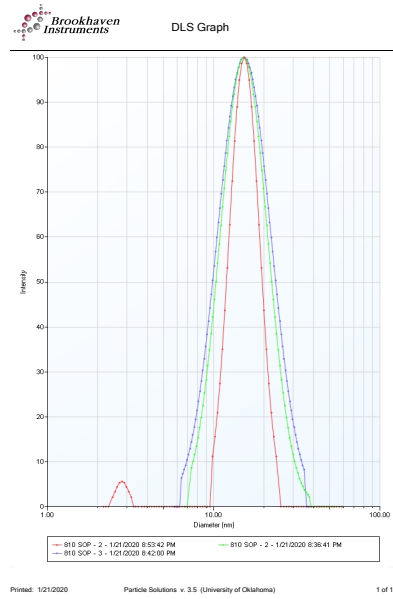
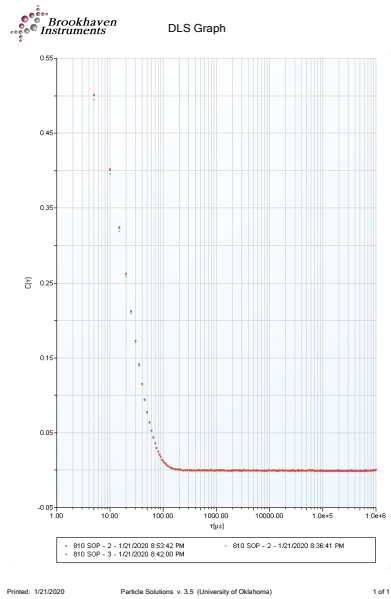
MSD Number Graph



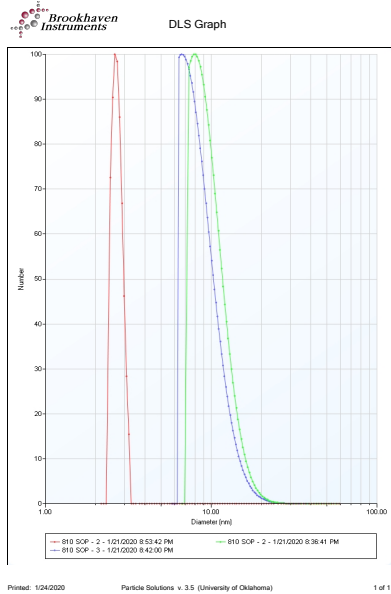
Figures 205-207: C8 Reference: 16 g NaCl/100 ml DI water PD = 0.096, CR = 147.1

Correlation Graph

MSD Intensity Graph



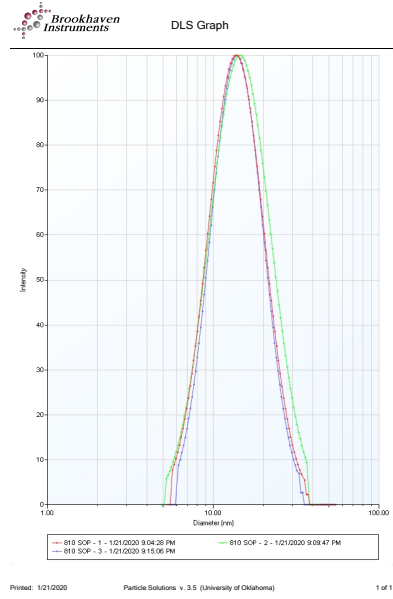
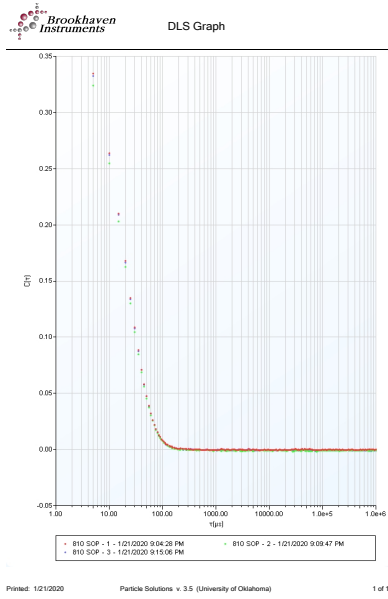
MSD Number Graph



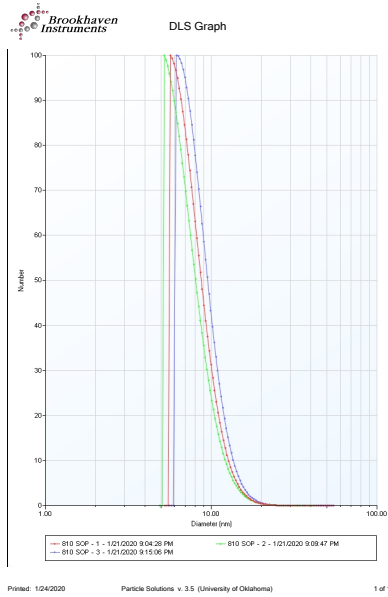
Figures 208-210: C8 Reference: 17 g NaCl/100 ml DI water PD = 0.131, CR =139.2

Correlation Graph

MSD Intensity Graph



MSD Number Graph



Appendix C: DLS Sample Examples

C₈₋₁₀E3.5, 0.05 g PDADMAC/100 mL, C₇, 0 g NaCl/100 mL

Figures 205 and 206 display examples of DLS samples. The aqueous phase of C₈₋₁₀E 3.5 Type I samples was often blue colored as shown in Figure 205. These solutions had to be diluted to make solutions clear to slightly hazy, resembling Figure 206 in order to obtain valid DLS data. This is true because the Stokes-Einstein equation applies to infinitely dilute solutions, and if the sample is too concentrated, the measured size of your particles will be inaccurate due to multiple scattering or viscosity effects (Farrell & Brousseau).

Figure 211: C₈₋₁₀E3.5 Type I aqueous phase sample

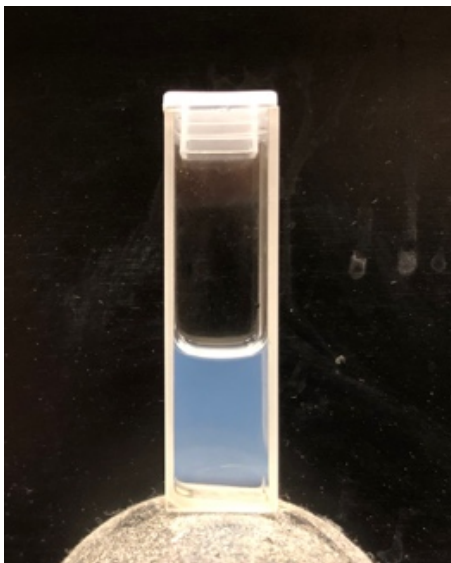
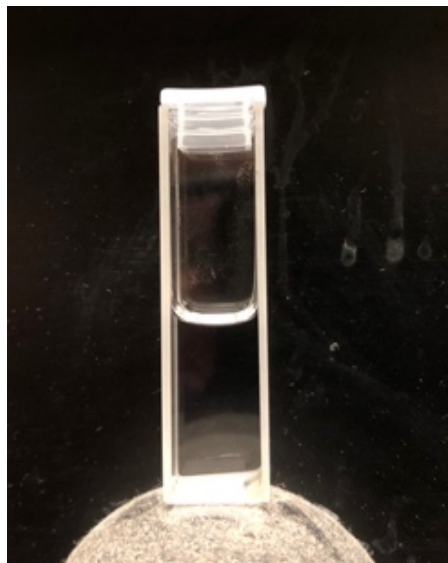


Figure 212: C₈₋₁₀E3.5 Type II oil phase sample



References

- 1) Acosta, E. J.; Yuan, J. S.; Bhakta, A. S. The Characteristic Curvature of Ionic Surfactants. *Journal of Surfactants and Detergents* **2008**, *11* (2), 145–158.
- 2) Acosta, E.; Szekeres, E.; Sabatini, D. A.; Harwell, J. H. Net-Average Curvature Model for Solubilization and Supersolubilization in Surfactant Microemulsions. *Langmuir* **2003**, *19* (1), 186–195.
- 3) Akima, H.; A New Method of Interpolation and Smooth Curve Fitting Based on Local Procedures," *J.ACM*, vol. 17, no. 4, pp. 589-602, 1970
- 4) Alhalaweh, A.; Ali, H. R. H.; Velaga, S. P. Effects of Polymer and Surfactant on the Dissolution and Transformation Profiles of Cocrystals in Aqueous Media. *Crystal Growth & Design* **2013**, *14* (2), 643–648.
- 5) Brackman, J. C.; Engberts, J. B. F. N. Polymer–Micelle Interactions: Physical Organic Aspects. *Chem. Soc. Rev.* **1993**, *22* (2), 85–92.
- 6) Broze, G. Handbook of Detergents, Part A. *Surfactant Science* **1999**.
- 7) Dhouib, A.; Hamad Naïma; Hassaïri Ilem; Sayadi, S. Degradation of Anionic Surfactants by *Citrobacter Braakii*. *Process Biochemistry* **2003**, *38* (8), 1245–1250.
- 8) Farrell, E.; Brousseau, J.-L. Guide for DLS sample preparation.
- 9) Gelardi, G.; Mantellato, S.; Marchon, D.; Palacios, M.; Eberhardt, A.; Flatt, R. Chemistry of Chemical Admixtures. *Science and Technology of Concrete Admixtures* **2016**, 149–218.
- 10) Goddard, E. D. In *Interactions of Surfactants with Polymers and Proteins*; Ananthapadmanabhan, K. P., Ed.; CRC Press, 2018.
- 11) Goddard, E. D.; Ananthapadmanabhan, K. P. In *Polymer-Surfactant Systems*; Kwak, J. C. T., Ed.; CRC Press: Boca Raton, FL, 1998; pp 21–31.
- 12) Goodwin, J. W. *Colloids and interfaces with surfactants and polymers*; John Wiley and Sons, Ltd: Chichester, 2009.
- 13) Hammond, C. E.; Acosta, E. J. On the Characteristic Curvature of Alkyl-Polypropylene Oxide Sulfate Extended Surfactants. *Journal of Surfactants and Detergents* **2011**, *15* (2), 157–165.
- 14) Hiemenz, P. C.; Rajagopalan, R. In *Principles of colloid and surface chemistry*; M. Dekker: New York, NY, 1986.

- 15) Huh, C. Interfacial Tensions and Solubilizing Ability of a Microemulsion Phase That Coexists with Oil and Brine. *Journal of Colloid and Interface Science* **1979**, 71 (2), 408–426.
- 16) Ikeda, S.; Ozeki, S.; Tsunoda, M.-A. Micelle Molecular Weight of Dodecyldimethylammonium Chloride in Aqueous Solutions, and the Transition of Micelle Shape in Concentrated NaCl Solutions. *Journal of Colloid and Interface Science* **1980**, 73 (1), 27–37.
- 17) Kadajji, V. G.; Betageri, G. V. Water Soluble Polymers for Pharmaceutical Applications. *Polymers* **2011**, 3 (4), 1972–2009.
- 18) Kiran, S. K.; Acosta, E. J. HLD–NAC and the Formation and Stability of Emulsions Near the Phase Inversion Point. *Industrial & Engineering Chemistry Research* **2015**, 54 (25), 6467–6479.
- 19) Klovenski, M. Hydrogen Peroxide and Water Interaction with Carbon Nitride. thesis, 2020.
- 20) Lindman, B.; Thalberg, K. In *Interactions of Surfactants with Polymers and Proteins*; Goddard, E. D., Ananthapadmanabhan, K. P., Eds.; CRC Press, 2018.
- 21) Llenado, R. A.; Neubecker, T. A. Surfactants. *Analytical Chemistry* **1983**, 55 (5), 93–102.
- 22) Nagarajan, R. Surfactant-Polymer Interactions. *New Horizons: Detergents for the New Millennium Conference Invited Papers* **2001**.
- 23) Saito, S. Solubilization Properties of Nonionic Surfactant-Polymeric Acid Complexes. *Colloid and Polymer Science* **1979**, 257 (3), 266–272.
- 24) Salager, J.-L.; Antón, R. E.; Sabatini, D. A.; Harwell, J. H.; Acosta, E. J.; Tolosa, L. I. Enhancing Solubilization in Microemulsions—State of the Art and Current Trends. *Journal of Surfactants and Detergents* **2005**, 8 (1), 3–21.
- 25) Salager, J.; Morgan, J.; Schechter, R.; Wade, W.; Vasquez, E. Optimum Formulation of Surfactant/Water/Oil Systems for Minimum Interfacial Tension or Phase Behavior. *Society of Petroleum Engineers Journal* **1979**, 19 (02), 107–115.
- 26) Shapiro, J. Understanding Surfactants: A Guide. <https://www.ipcol.com/blog/an-easy-guide-to-understanding-surfactants/> (accessed Apr 3, 2020).
- 27) Tadros, T. F. *Introduction to surfactants*; De Gruyter: Berlin, Germany, 2014.
- 28) Tanford, C. The Hydrophobic Effect: Formation of Micelles and Biological Membranes. *Journal of Polymer Science: Polymer Letters Edition* **1980**, 18 (10), 687–687.

- 29) Tehrani-Bagha, A.; Holmberg, K. Solubilization of Hydrophobic Dyes in Surfactant Solutions. *Materials* **2013**, *6* (2), 580–608.
- 30) Velásquez, J.; Scorzza, C.; Vejar, F.; Forgiarini, A. M.; Antón, R. E.; Salager, J.-L. Effect of Temperature and Other Variables on the Optimum Formulation of Anionic Extended Surfactant–Alkane–Brine Systems. *Journal of Surfactants and Detergents* **2009**, *13* (1), 69–73.
- 31) Warren, M. T. Understanding the Specific Ion Effects and Interfacially Active Solutes Using the Colligative Properties of Microemulsions. dissertation, 2020.
- 32) Will, R.; Loechner, U.; Yokose, K. Water-Soluble Synthetic Polymers. *Hydrocolloids* **2007**.
- 33) Witthayapanyanon, A.; Harwell, J. H.; Sabatini, D. A. Hydrophilic–Lipophilic Deviation (HLD) Method for Characterizing Conventional and Extended Surfactants. *Journal of Colloid and Interface Science* **2008**, *325* (1), 259–266.
- 34) Zhang, H.; Deng, L.; Sun, P.; Que, F.; Weiss, J. Solubilization of Octane in Cationic Surfactant–Anionic Polymer Complexes: Effect of Ionic Strength. *Journal of Colloid and Interface Science* **2016**, *461*, 88–95.
- 35) Zhang, H.; Deng, L.; Zeeb, B.; Weiss, J. Solubilization of Octane in Cationic Surfactant–Anionic Polymer Complexes: Effect of Polymer Concentration and Temperature. *Journal of Colloid and Interface Science* **2015**, *450*, 332–338. (a)
- 36) Zhang, H.; Zeeb, B.; Salminen, H.; Weiss, J. Isothermal Titration Calorimetric Analysis on Solubilization of an Octane Oil-in-Water Emulsion in Surfactant Micelles and Surfactant–Anionic Polymer Complexes. *Journal of Colloid and Interface Science* **2015**, *452*, 1. (b)